

12-2015

Design, Fabrication, and Testing of a 3D Printer Based Microfluidic System

Carlton A. McMullen
University of Arkansas, Fayetteville

Follow this and additional works at: <https://scholarworks.uark.edu/etd>



Part of the [Computer-Aided Engineering and Design Commons](#), and the [Manufacturing Commons](#)

Citation

McMullen, C. A. (2015). Design, Fabrication, and Testing of a 3D Printer Based Microfluidic System. *Graduate Theses and Dissertations* Retrieved from <https://scholarworks.uark.edu/etd/1964>

This Thesis is brought to you for free and open access by ScholarWorks@UARK. It has been accepted for inclusion in Graduate Theses and Dissertations by an authorized administrator of ScholarWorks@UARK. For more information, please contact scholar@uark.edu, uarepos@uark.edu.

Design, Fabrication, and Testing of a 3D Printer Based Microfluidic System

A thesis submitted in partial fulfillment
of the requirement for the degree of
Master of Science in Mechanical Engineering

by

Carlton McMullen
University of Arkansas at Little Rock
Bachelor of Science in Systems Engineering – Mechanical Systems, 2012

December 2015
University of Arkansas

This thesis is approved for recommendation to the Graduate Council.

Dr. Steve Tung
Thesis Director

Dr. Uchechukwu Wejinya
Committee Member

Dr. Po-Hao Huang
Committee Member

Abstract

A pneumatically actuated PDMS based microfluidic devices were designed and fabricated by soft-lithography. Two types of molds were fabricated out of different material for this experiment. The first mold, (device 1), was fabricated from a sheet of Polymethyl methacrylate (PMMA) material, similar to Plexiglas. The device features were micro-engraved onto the face of the material. The second mold, (device 2), was fabricated from the use of fused deposition modeling (FDM) 3D printing. The pumping efficiency of the PDMS devices was analyzed through the characterization of the micro-pumps flowrate with respect to the pumps driving pressure and the actuation frequency. Tested at a driving pressure of 10psi, the flowrate for device 1 peaked at 75 μ L/min with a 7Hz actuation frequency before failing, while device 2 peaked at 498 μ L/min with a 15Hz actuation frequency.

Using the techniques of rapid prototyping and fused deposition modelling a pneumatically actuated 3D printer based micro-pump and micro-mixer are fabricated. The devices were fabricated using a thermoplastic elastomer (TPE) material as an alternative material to the present polydimethylsiloxane (PDMS). The micro-pump's fluid flow output was analyzed through the characterization of the micro-pumps flowrate with respect to the pumps driving pressure and the actuation frequency. Testing showed that a maximum flowrate of 1120 μ L/min was achieved at an actuation frequency of 10Hz with an applied driving pressure of 40psi. A qualitative mixing performance was conducted with the micro-mixer. The diffusion of two dyes was tested under an active mix and non-active mix condition. Testing showed that the active mixing condition resulted in a complete diffusion as opposed to the non-mixing condition which partially diffused. As a proof of concept for biological testing, E. coli and E.coli anti-bodies were mixes to measure the capturing efficiency. The results showed that the active mixing resulted in about 50% capturing efficiency as opposed to the non-mixing which resulted in 33% capturing efficiency.

Acknowledgements

I would like to thank the University of Arkansas with an esteemed recognition to the Mechanical Engineering department for granting me the opportunity to continue and expand my education. This opportunity has allowed me to grow academically and professionally within the science, technology, engineering, and mathematics (STEM) field. I would like to extend a sincere appreciation to Dr. Steve Tung for allowing me to be a member of group, and also for his continuous guidance and support. Thank you for granting me the opportunity to travel to Shenyang, China where I received training at the Shenyang Institute of Automation. While there I was received with the utmost hospitality by the students, therefore I would also like to thank them.

I would like to thank my committee members Dr. Uche Wejinya and Dr. Adam Huang. Thank you again Dr. Wejinya for granting me my first grading position and the bits of advice when I first arrived. Dr. Yanbin Li and his group provided me with the opportunity to perform the biological test. I am grateful to have received the Benjamin Lever Fellowship during my years in the Program, therefore thank you Vickie Hartwell. To my colleagues and research peers Yao Ping, Zach Calloway, Zeina Salman, and Bo Ma I would like to thank you for the training, assistance and support that was provided. I would like to thank my family, friends, and loved ones for your never ending support and understanding which encouraged me to continue my journey through academia.

Table of Contents

Chapter 1:	Introduction.....	1
Chapter 2:	Design, Fabrication Methods and Materials.....	9
2.1	Microfluidic Device General Working Principles.....	9
2.1.1	Micro-Pump.....	9
2.1.2	Micro-Mixer.....	11
2.2	Fabrication of Microfluidic Devices.....	12
2.2.1	PDMS Device Using PMMA Mold.....	12
2.2.2	PDMS Device Using 3D Printed Mold.....	25
2.2.3	3D Printed Device Fabrication.....	30
2.3	Control System.....	39
2.3.1	Control System Components.....	39
2.3.2	LabVIEW Control System.....	40
2.3.3	Control System Integration.....	42
2.4	Hydrophobic and Hydrophilic Testing.....	45
2.5	PDMS Surface Modification.....	46
2.6	Bond TPE to Glass/TPE to ABS.....	47
Chapter 3:	Results and Discussion.....	49
3.1	PDMS Device Testing.....	49
3.1.1	Micro-Pump: Test Setup and Results.....	49
3.2	3D Printed Micro-Pump Testing.....	52
3.2.1	Test Setup and Results.....	55
3.2.2	Diaphragm Deflection Testing.....	55
3.3	3D Printed Micro-Mixer Testing.....	66
3.3.1	Test Setup and Results.....	66
3.3.2	Biological Testing.....	67
Chapter 4:	Conclusion.....	72
Chapter 5:	Future Work.....	73

5.1	Incorporation of Shut off Valve.....	73
5.2	Integrated Micro-Pump with Micro-Mixer.....	73
5.3	3D Printing Resolution.....	73
	References.....	74

List of Figures

Figure 1.1:	Non-Mechanical Electro-osmosis micro-pump diagram [1].....	2
Figure 1.2:	Mechanical micro-pump with actuating diaphragms. Image (a): Diaphragms at rest Image (b): Applied energy source converted to motion.....	3
Figure 1.3:	Graph showing the increase in published journals involving microfluidics with 3D printing [5].....	5
Figure 1.4:	Diagram of Stereo-lithography 3D Printing [20].....	6
Figure 1.5:	Diagram of Fused Deposition Modeling 3D Printing [21].....	7
Figure 2.1:	Pneumatically actuated peristaltic diaphragm deflecting into micro-channel causing fluid flow with arrows indicate bi-directional flow; Check-valve and check-valve assist preventing backflow.....	10
Figure 2.2:	Micro-mixer with pneumatically actuated diaphragms causing the mixing of two samples	12
Figure 2.3:	The multiple layers of a PDMS Microfluidic device assembly	13
Figure 2.4:	PMMA mold design of fluidic layer micro-channel.....	14
Figure 2.5:	PMMA mold design of control layer.....	15
Figure 2.6:	3D AutoCAD design of PMMA master mold.....	15
Figure 2.7:	Micro-engraving process flow of master mold.....	16
Figure 2.8:	Micro-engraved PMMA master mold of control layer.....	17
Figure 2.9:	Fluidic layer casting process.....	17
Figure 2.10:	Image a: Resulting engraved mold. Image b: Casted PDMS layer with holes cut out for inlets and outlet.....	18
Figure 2.11:	Control layer casting process.....	19
Figure 2.12:	PDMS thickness controlled as function of spin speed [23].....	20
Figure 2.13:	Casted PDMS control layer and mold.....	20
Figure 2.14:	Oxygen plasma chamber.....	21
Figure 2.15:	Process flow for bonding and assembling PDMS device.....	22
Figure 2.16:	Roll technique of PDMS layer to reduce trapped air and induce uniformed bonding.....	24
Figure 2.17:	3D CAD design of aligned layers with circles indicating where air inlet holes are punched.....	24

Figure 2.18:	Image (a): Completely fabricated microfluidic device. Image (b): Top view of fabricated device.....	25
Figure 2.19:	Process flow of 3D CAD design, 3D printer, and final master mold	26
Figure 2.20:	3D print mold design of fluidic layer micro-channel.....	27
Figure 2.21:	3D print mold design of control layer.....	27
Figure 2.22:	Process flow of Acetone vapor bath procedure.....	28
Figure 2.23:	Image (a): 3D printed master mold of fluid layer before AVB surface treatment Image (b): 3D printed master mold of fluid layer after AVB surface treatment.....	29
Figure 2.24:	Image (a): Completely fabricated microfluidic device. Image (b): Top view of fabricated device.....	30
Figure 2.25:	Image a: A cross-sectional view of a PDMS diaphragm assembly arranged parallel to the x-plane. (1) Illustrates the diaphragm at rest. (2) Illustrated the diaphragm deflected. Image b: A cross-sectional view of a TPE diaphragm assembly arranged perpendicular to the z-plane along the micro-channel wall. (1) Diaphragm is at rest. (2) Diaphragm is deflected.....	32
Figure 2.26:	Image a: Cross-sectional view of 3D CAD design micro-pump. Image b: Cross-sectional cut out of 3D printed micro-pump showing the sidewall diaphragm and air chamber. Image (c) shows the 3D CAD design of micro-channel with the diaphragms at rest. Image (d) shows the 3D CAD design of micro-channel with the diaphragms deflected.....	33
Figure 2.27:	3D model of 3D printed micro-pump. The orange lines indicate the location of the air inlet, and air-chamber aligned to the diaphragms.....	34
Figure 2.28:	Top view of 3D Printed Design of Micro-Pump.....	34
Figure 2.29:	Image a: Top down cross-sectional view of 3D CAD design micro-mixer. Image b: Top down cross-sectional cut out of 3D printed micro-pump showing the sidewall diaphragm, reservoir, and air chamber. Image (c) shows the 3D CAD design of micro-mixer with the diaphragms at rest. Image (d) shows the 3D CAD design of micro-mixer with the diaphragms deflected.....	35
Figure 2.30:	3D model of 3D printed micro-mixer. The organge lines indicate the location of the airchamber aligned to the diaphragms.....	36
Figure 2.31:	Top view of 3D Printed Device Design of Micro-Mixer.....	36
Figure 2.32:	Process flow of 3D CAD design, 3D printer, and final device	38
Figure 2.33:	Control System Process Flow.....	39

Figure 2.34:	Image (a): The 3-port solenoid valve with the connections to the micro-pump and the to the pressure source. Image (b): The analog signal converter that is connected to laptop with LabVIEW software, and solenoid valve connected to converter...	40
Figure 2.35:	Screen shot of a block diagram setup of LabVIEW.....	41
Figure 2.36:	Image (a): Top view of enclosure with valves positioned on plate secured with clams and tubing connection. Image (b) Side view of enclosure showing valves wired to signal converter. Image (c): Extruded ports used to stabilize air tubing. Image (d): Fully enclosed box with labeled valve ports.....	42
Figure 2.37:	Image (a): Cross-section view of clamp with corresponding dimensions. Image (b) Top view of clamp with corresponding dimensions. Image (c): 3D CAD design of clamp.....	43
Figure 2.38:	Schematic of the experimental setup layout describing the integrated connectivity for operating the PDMS and the 3D printed device.....	44
Figure 2.39:	Image (a): Hydrophobic test of PDMS with contact angle of about 115° Image (b): Hydrophilic test of NinjaFlex with contact angle of about 44°	46
Figure 3.1:	Image (a): Test fixture for the PDMS device with project enclosure and computer control system. Image (b): Close up of PDMS test fixture mounted on x-y stage with PTFE tubing connected to air inlets of device.....	51
Figure 3.2:	Flowrate of the micro-pump with respect to the diaphragm actuation frequency and driving pressure; Curve (a) (Device 1): 5Hz-7Hz; Curve (b) (Device 2): 5Hz-10Hz.....	52
Figure 3.3:	Test fixture for the micro-pump testing with the connected components.....	53
Figure 3.4:	Image (a): The initial position of the fluid at t=0. Image (b): The final position of the fluid at t=5s.....	54
Figure 3.5:	Flowrate of micro-pump with respect to the diaphragm's actuation frequency ranging from 10Hz-70Hz; Driving Pressures: Curve (a): 20Psi; Curve (b): 30Psi; Curve (c): 40Psi.....	55
Figure 3.6:	Diaphragm at 10Hz deflection frequency with 30psi pressure. Image (a) shows the diaphragm at rest "no deflection". Image (b) shows the diaphragm at maximum deflection with respect to the open valve. Image (c) shows the diaphragm at minimum deflection with respect to the closed valve.....	56
Figure 3.7:	This figure shows a sequence of tests with the diaphragm operating at a driving pressure of 30psi, with each image corresponding to its respective frequency. Each image represents the minimum deflection "at rest position" of the diaphragm's behavior at 10Hz-70Hz.....	57

Figure 3.8:	20Psi driving maximum and minimum deflection behavior and resulting stroke-length with respect to actuation frequency.....	58
Figure 3.9:	30Psi driving maximum and minimum deflection behavior and resulting stroke-length with respect to actuation frequency.....	59
Figure 3.10:	40Psi driving maximum and minimum deflection behavior and resulting stroke-length with respect to actuation frequency.....	59
Figure 3.11:	Stroke-length comparison for 20Psi-40Psi driving pressures per actuation frequency.....	60
Figure 3.12:	SolidWorks Diaphragm Deflection Simulation. Image (a): Maximum Deflection Image (b): Minimum Deflection.....	61
Figure 3.13:	Flat plate with clamped edges and applied uniform pressure.....	61
Figure 3.14:	Theoretical Flowrate results.....	63
Figure 3.15:	Normalized Theoretical and Experimental Flowrate comparative at 20psi.....	64
Figure 3.16:	Normalized Theoretical and Experimental Flowrate comparative at 30psi.....	64
Figure 3.17:	Normalized Theoretical and Experimental Flowrate comparative at 40psi.....	65
Figure 3.18:	Image (a): Inactive diaphragms, unassisted diffusion process with at varying times. Image (b): Active diaphragms assisted diffusion at varying times.....	67
Figure 3.19:	Process flow of mixing and E. coli cell capturing process.....	70
Figure 3.20:	Active and Inactive capturing efficiency for micro-mixer at varying operating frequencies and rotator-mixer.....	71

List of tables

Table 1: Minimum and Maximum Deflections and resulting Stroke-Volumes..... 62

List of Equation and Symbols

Eq. 3.1:	<i>Mass to Volume ratio</i> $\Delta m = \Delta V$	50
	<i>Mass</i> = m [mg]	
	<i>Volume</i> = V [μ L]	
Eq. 3.2:	<i>Volumetric Flowrate</i> $(Q) = \frac{\Delta V}{\Delta t}$	50
	<i>Volume</i> = v	
	<i>Time</i> = t	
Eq. 3.3:	<i>Volumetric Flowrate</i> $(Q) = V \cdot f$	51
	<i>Volume</i> = V	
	<i>Actuation Frequency</i> = f	
Eq. 3.4:	<i>Velocity</i> $(v) = \frac{\Delta x}{\Delta t}$	53
	<i>Distance</i> = x	
	<i>Time</i> = t	
Eq. 3.5:	<i>Volumetric Flowrate</i> $(Q) = v \cdot A$	53
	<i>Velocity</i> = v	
	<i>Cross sectional area</i> = A	
Eq. 3.6:	<i>Stroke Length</i> $(\Delta x) = x_{max} - x_{min}$	57
	<i>Maximum Deflection Point of Diaphragm</i> = x_{max}	
	<i>Minimum Deflection Point of Diaphragm</i> = x_{min}	
Eq. 3.7:	<i>Stroke Volume</i> $(\Delta V) = V_{max} - V_{min}$	62
	<i>Maximum Volume Displaced of Diaphragm</i> = V_{max}	
	<i>Minimum Volume Displaced of Diaphragm</i> = V_{min}	
Eq. 3.8:	<i>Actuation Frequency</i> $(f) = \frac{1}{s}$	62
Eq. 3.9:	<i>Theoretical Flowrate</i> $(\dot{V}) = \Delta V \cdot f$	62
	<i>Change in Volume</i> = ΔV	
	<i>Actuation Frequency</i> = f	

Eq. 3.10: *Capture Efficiency (CE %)* = $\frac{N_c}{N_o} \times 100$ 70

Number of Captured Cells = N_c

Number of Original Cells = N_o

Chapter 1. Introduction

As the growth in popularity for research and development of microfluidic devices increases, so shall there be an increase in research for optimizing alternative methods for fabricating the devices. Microfluidics deals with fluid flow on a miniaturized scale, normally in the range of micrometres (μm) and microliters (μL) [1, 2]. Microfluidic devices are on the subcategory of Lab on a chip (LOC) which is a subclass of micro-electro mechanical systems (MEMS) [3]. LOC devices are able to combine a miniature scaled version of various laboratory protocols onto a single chip [4, 5]. These devices can be applied in a multitude of laboratory applications. Some of these applications include sample preparation, separation, transport, bio-sensing and detection [1, 6]. The compelling growth for research towards miniaturization is to help reduce the expenses and the environmental impact of research [7, 8], and also to increase the speed of biological analysis. Because the devices operate on a scaled down laboratory protocol, they only require a small fluid sample size which means that there can be a reduction in the amount of reagents required [9]. The decreasing of the required reagents can lead to a reduction in cost of supplies by unit. Multiple factors come into play during the analysis process of the devices and this ranges from the diffusion distance of the fluid sample, the heating of the fluid sample, and the surface area to volume ratio. Because the fluid sample volume has been scaled down this shortens the diffusion area by sample volume, this reduction in volume can also apply to a reduced heating time. The device size can also increase the surface area to fluid sample volume ratio [10]. All of these factors operating on a scaled down level help with the increase in rapid detection. Within the healthcare field rapid detection can increase the chances for an early detection and a prevention of pathogen exposure [11].

The main component of the microfluidic device is the micro-pump which, through actuation, converts energy into motion [1]. Micro-pumps can be categorized into two types, one being a mechanical micro-pump which utilizes moving parts; the other being a non-mechanical micro-pump which has no moving parts [1]. The non-mechanical pump utilizes kinetic momentum, converted from a particular source of non-mechanical energy (i.e. electro-osmosis, or electro-wetting). For the electro-osmosis condition, an external potential charge is applied along the channel walls, and in response an electric field (AD or DC) pulls the electric conductive fluids along the channel (fig. 1.1).

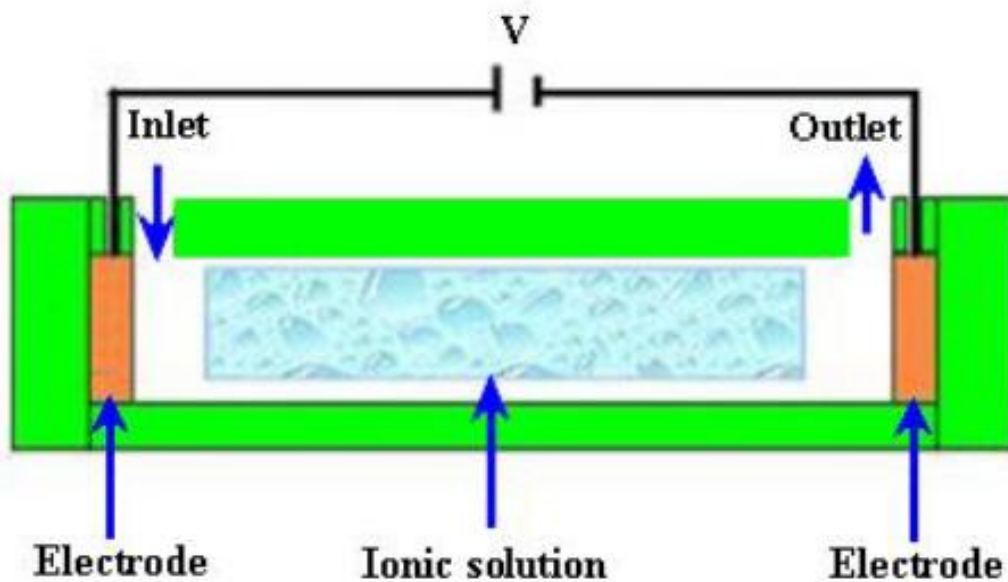


Figure 1.1. Non-Mechanical Electro-osmosis micro-pump diagram [1]

For the mechanical micro-pump the actuation of the diaphragm membrane, and the valve are what controls the fluid flow. This is achieved by the transfer of energy into motion from some particular source (i.e. electricity, heat, or air pressure). Through this actuation of the diaphragm or the valve,

the fluid in the micro-channel is displaced which creates a fluid flow [1]. The current research will be using a mechanical type micro-pump that utilizes compressed air/gas.

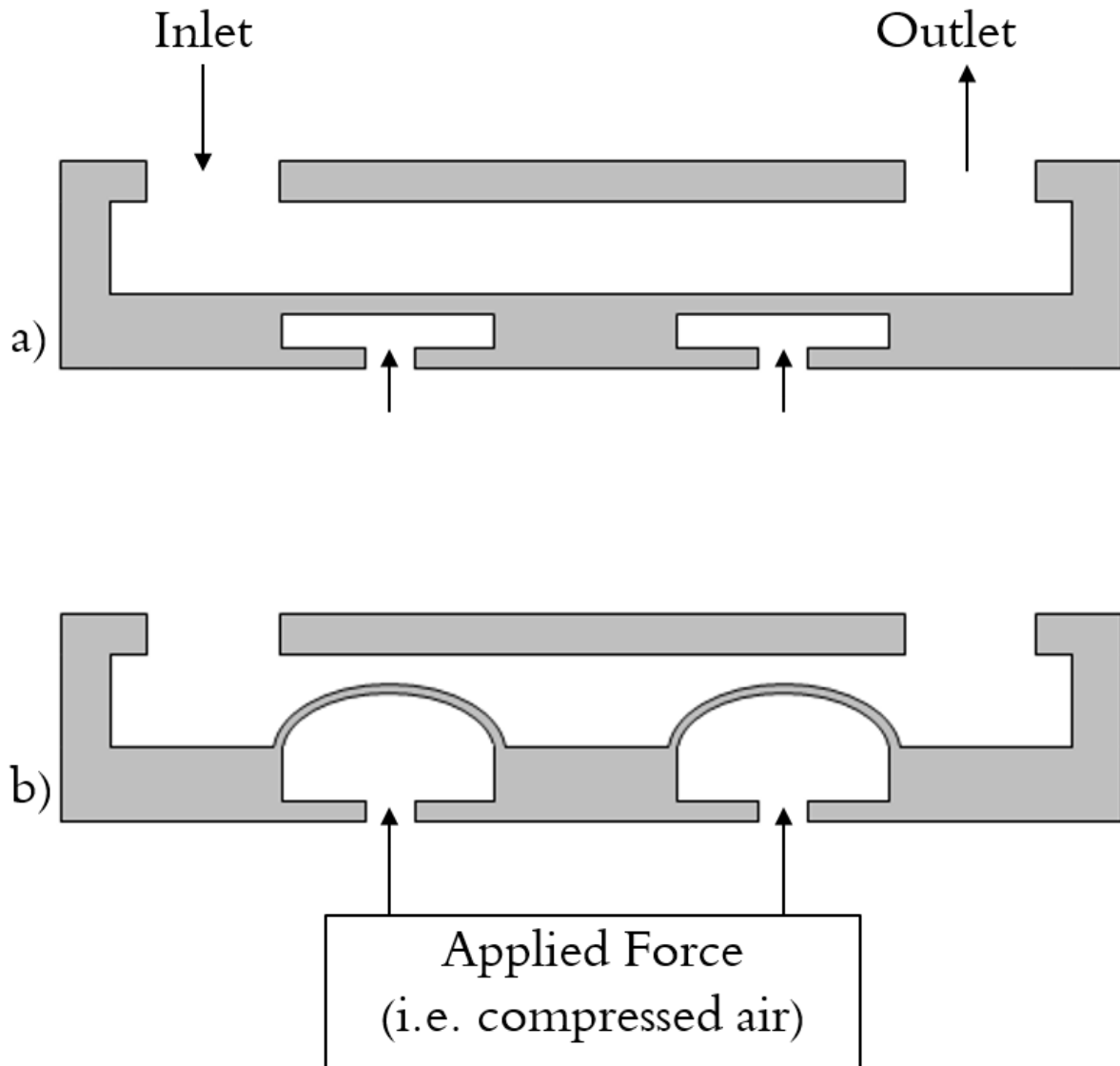


Figure 1.2: Mechanical micro-pump with actuating diaphragms. Image (a): Diaphragms at rest
Image (b): Applied force converted to motion

Multiple techniques can be used when fabricating a microfluidics device. Some of the popular methods include micro-machining, injection molding, in situ construction, and soft-lithography [2]. For production on a trivial scale the traditional method of fabrication for

microfluidic devices is with polydimethylsiloxane (PDMS) through the replica molding technique, soft-lithography [7]. Firstly, using 3D CAD, a master-mold is created with the desired micro-channel and diaphragm patterns. Once the patterns are created they are then molded onto a SU-8 master [7], or can be engraved onto a Polymethyl methacrylate (PMMA) sheet which is similar to Plexiglas. Next, the soft-lithography automation generally involves a polymer material as it is casted and cured on the master-mold. Once the multiple layers are cured they are assembled through a layer stacking, alignment, and bonding process [12]. Through the use of the multilayer stacking technique, people have been able to fabricate active microfluidic devices which contain valves and pumps [13]. The use of PDMS has become increasingly standard among many groups. This is mainly because it is inexpensive, transparent, and non-toxic (biocompatible). However this method can be very labor-intensive, and extremely difficult to fabricate. This is mainly due to the lengthy time consumption required for the fabrication process, misalignment of the device layers, and inefficient bonding. Typically each layer requires a separate patterned master-mold [14], which requires time to design and fabricate and if any changes are made more time is required per master-mold. In addition each layer requires bonding [14] along with proper alignment, and if either of these are performed incorrectly then the device will be faulty and unable to perform its duties properly. To add to the matter at hand this technique require a significant amount of space for the materials and equipment to perform the duties of fabrication [7].

As previously mentioned, the traditional fabrication method can be labor intensive do to the time and precision required for the mold design, and device fabrication process. According to **Figure 1.3**, in recent years the occurrence journals on 3D printing together with microfluidics has begun to show growth [5].

Published Items over 10 years (2005-2015)

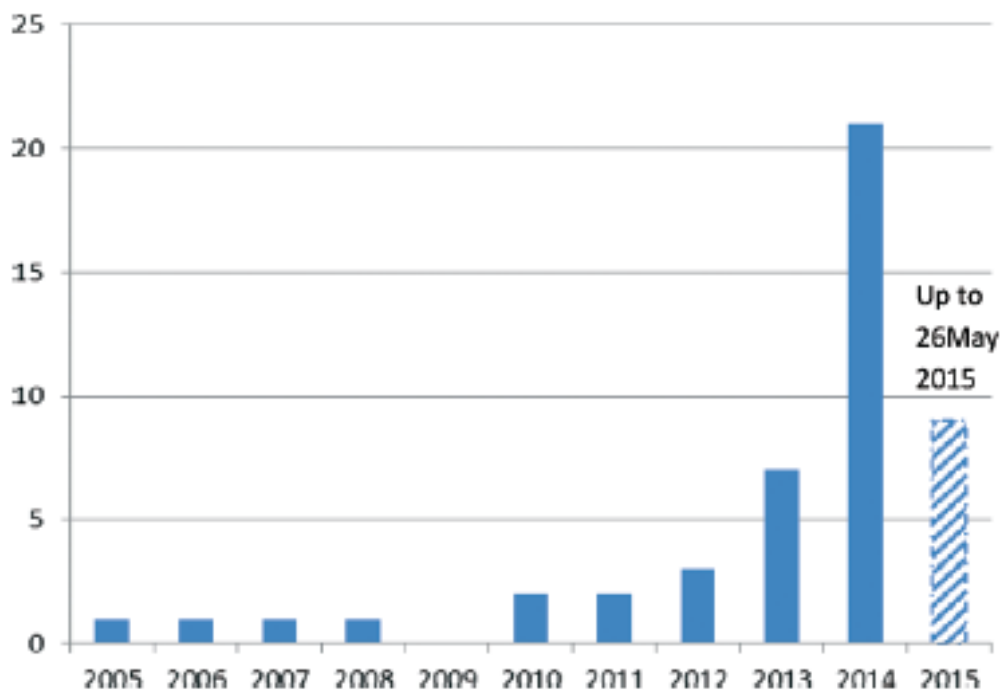


Figure 1.3: Graph showing the increase in published journals involving microfluidics with 3D printing [5]

Nevertheless 3D printing is not dependent on the use of a master-mold, or a micro-molding process [15, 16]. Instead, with the recent advancements of rapid prototyping technology, 3D-printing has shortened the fabrication process time as well as increased the production efficiency of microfluidic devices. 3D printing simply replicates directly from the 3D CAD design. To elaborate, the device is first modelled with any commercial 3D CAD software. The part is then saved and exported via the stereo-lithography (.STL) file format, where it is then transferred to the 3D printer software which corresponds with the 3D printer. In contrast to the PDMS soft-lithography process, 3D printing is completely alphanumeric which allows for unpretentious modifications, and can streamline the track to commercialization [17]. In addition it has created a completely assembly-free fabrication method that has eliminated “the manual alignment and

bonding steps” that would be required with its predecessor [14, 18], and has removed the requirement of a large amount of space that would be needed for equipment and assembly purposes.

Established in 1988 by Chuck Hall [19], SLA is an additive process which uses a trace and scan technique with a UV laser to cure a resin material over a selected area. Once that particular area is cured, the build-plate shifts down and this process is repeated until the feature and part is created [7] (fig. 1.4) [cite]. One major advantage with the SLA method is its high resolution output, which is a big factor to consider when designing and fabricating a microfluidics device which can deal with a range of micrometres (μm). Some disadvantages of this method are its high cost from the machine to the material used in the replication process, also the current limitation of material selection.

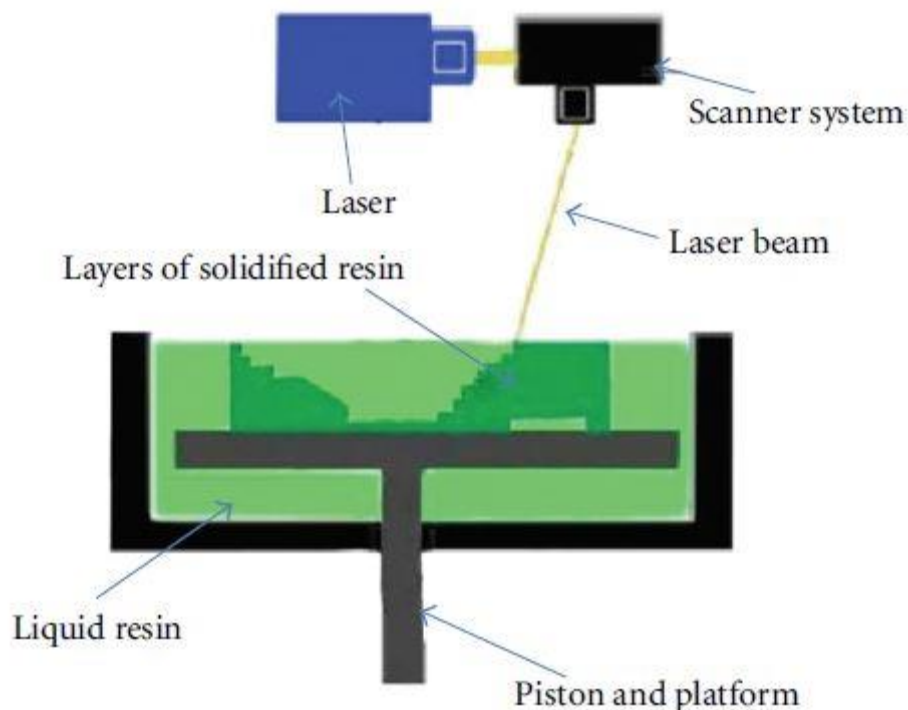


Figure 1.4: Diagram of Stereo-lithography 3D Printing [20]

Another form of the additive method is the FDM technique. The FDM technique heats a thermoplastic or elastomer material into a quasi-solid form as it comes into contact with a print head nozzle. The material is then extruded through the heated nozzle and deposited onto a build-plate. This extrusion process is repeated thereby creating a layering effect (fig. 1.5). Currently being the more inexpensive of the two as well as the most popular for 3D printing hobbyists, this method is based on the ideologies of thermal energy, surface chemistry, and layer manufacturing technology [21]. Some disadvantages of this method are its layer resolution in comparison to the SLA method, also sometime it can be difficult to remove the support material.

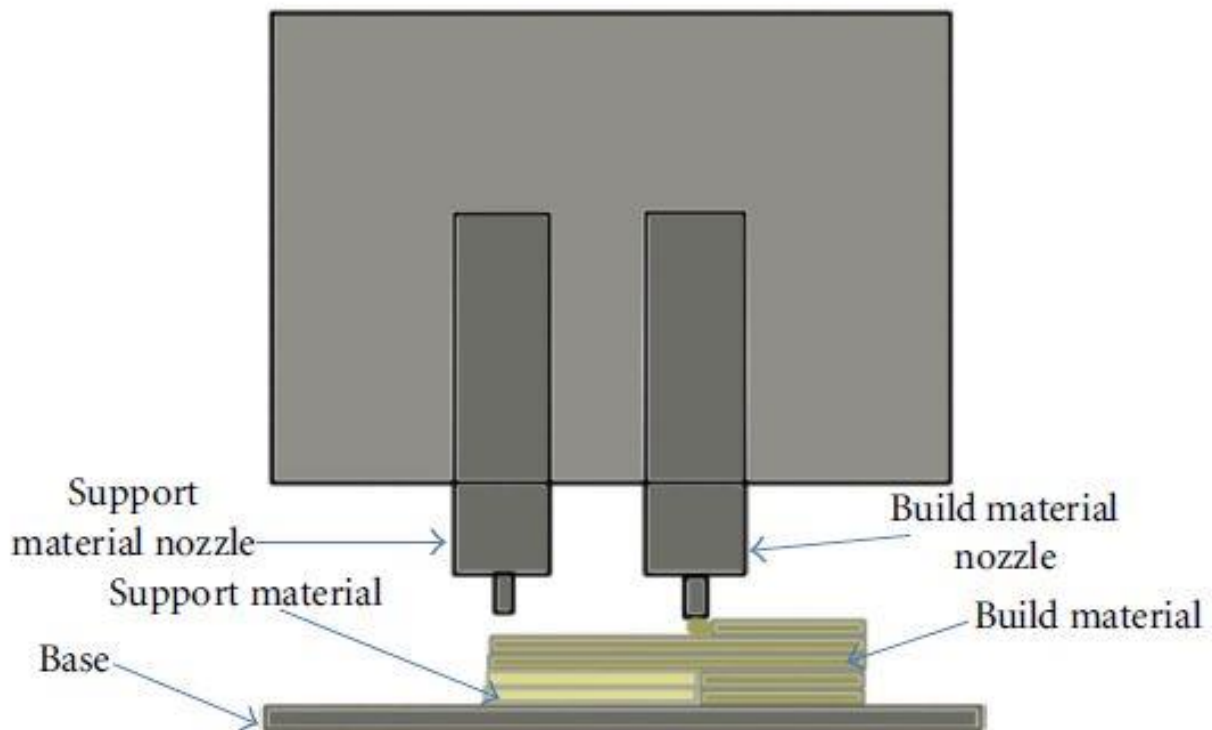


Figure 1.5: Diagram of Fused Deposition Modeling 3D Printing [21]

The use of 3D printing is growing more and more for industrial, commercial, and research purposes. When designing microfluidic device multiple factors come into play when utilizing 3D

printing fabrication techniques, some of these factors are the layer resolution, and the open source of material [7]. Many different techniques for 3D printing have been established and more are developing. Two widely used techniques of 3D printing are stereolithography (SLA) and Fused Deposition Modelling (FDM).

The primary goal of the project is to design, fabricate, and test a 3D printed microfluidic system for biological applications. The key objectives of the project were:

- PDMS microfluidic system fabricated from PMMA molds (existing design)
 - Fabricate a peristaltic microfluidic system with moving diaphragms
 - Develop integrated control box for automated actuation
 - Develop LabVIEW based control software
 - Conduct flowrate performance test
- PDMS microfluidic system fabricated from 3D printed molds (transition design)
 - Utilize FDM to fabricate ABS molds
 - Utilize acetone vapor bath to reduce surface roughness of molds
 - Fabricate microfluidic system
 - Conduct flowrate performance test
- 3D printed microfluidic system (new design)
 - Develop control parameters for consistent diaphragm fabrication
 - Redesign microfluidic system for 3D printing
 - Fabricate redesigned microfluidic system with integrated pumps, valves, and mixer
 - Conduct performance test
 - Compare experimental with numerical simulation results
 - Conduct E. Coli capture test in micro-mixer

Chapter 2. Design, Fabrication Methods and Materials

This chapter will discuss the working principles of the microfluidic devices components which are the micro-pump and the micro-mixer. The soft-lithography technique will be detailed which will include the micro-machining, micro-molding, and bonding methods that are utilized. The fused deposition modeling (FDM) 3D printing process will be explained along with the motivation of the material selection.

2.1 Microfluidic Device General Working Principles

This following section discusses the concept and the designs of the various components for the microfluidic devices.

2.1.1 Micro-pump

The critical part of the microfluidic device is the diaphragm, which is utilized as the pumping and mixing mechanism. The pumping is achieved with an actuation motion of the diaphragm as it deflects into the fluid channel thereby causing the fluid in the channel to displace. The micro-pumps for this study utilize the peristaltic pump working principle by which the diaphragms deflect creating wavelike sequence that push the fluid forward. In order to achieve the action of pumping, diaphragms are situated parallel to the fluid channel. The fluid channel refers to the micro-channel where the fluid is pumped. The device consists of two diaphragms side by side one small diaphragm acting as a backflow check-valve and the one large diaphragm acting as the driving pump, which derives from previous work on diaphragm geometry and orientation [22]. The check-valve has two primary functions. One function is to block the micro-channel to prevent fluid flow. The other is to ensure that the fluid flow is unidirectional. The

check-valve deflects a fraction of a second before the driving pump. This deflection prevents the bi-directional flow of the driving pump and cause the fluid to flow in one direction. Figure 2.1 demonstrates the fluid displacement and the bi-directional flow that is caused by the peristaltic diaphragm deflection. It also illustrates the check valve and the check valve assist which prevents the back flow of the driving pump diaphragm

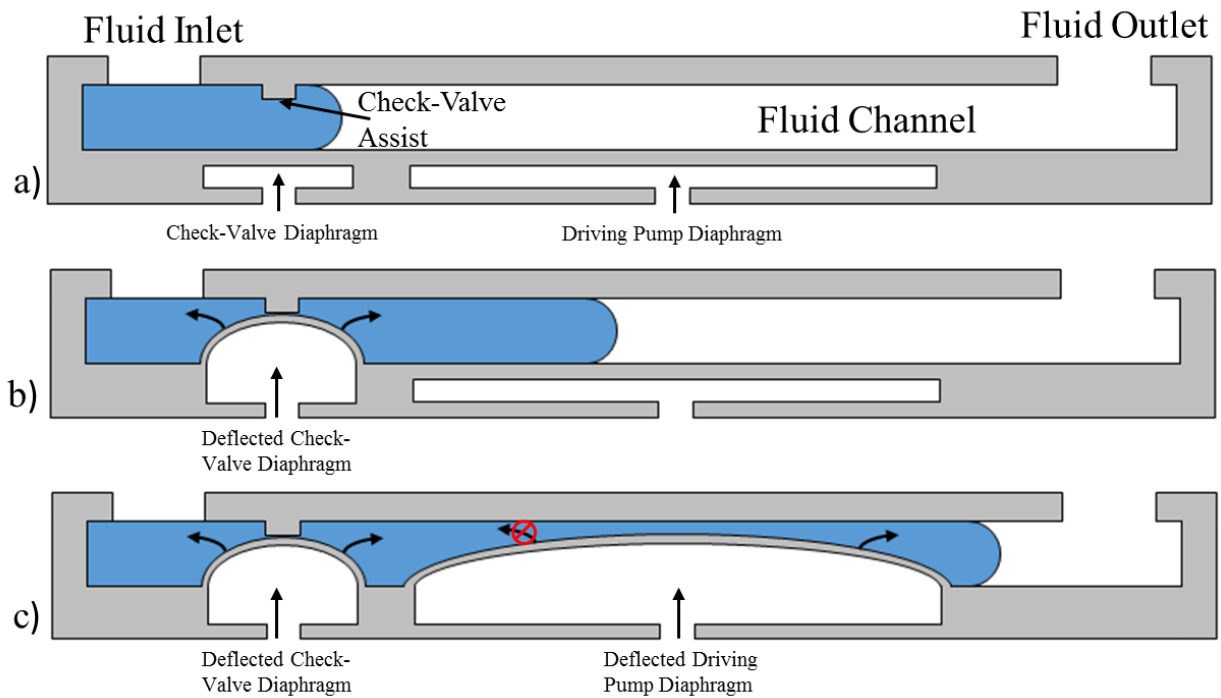


Figure 2.1: Pneumatically actuated peristaltic diaphragm deflecting into micro-channel causing fluid flow with arrows indicate bi-directional flow; Check-valve and check-valve assist preventing backflow

The diaphragms are operated pneumatically with air/gas pressure. Each diaphragms can operate via a single air inlet, which can split into two channels which lead to the respected air chamber. The thin wall of the air chambers function as diaphragms which deflect once the air chambers are filled with compressed air/gas. When the compressed air/gas is introduced through the air inlet, it causes the diaphragms to deflect. However the smallest diaphragm with the smallest air chamber will deflect first because of it lower volume capacity. This action causes the two diaphragms to

have a sequential deflection, similar to that of a peristaltic motion. When the smaller diaphragm deflects first, this prevents fluid from being displaced in a backward direction. This combined actuation motion of the two diaphragms causes the fluid in the fluid channel to be displaced in a forward direction. The oscillation frequency of the diaphragms are controlled via a solenoid valve, which controls the compressed air/gas flow which is fed into the air inlet of the micro-pump.

2.1.2 Micro-mixer

The micro-mixer operates, with the use of diaphragms, on the same working actuation oscillation principle as the micro-pump. The diaphragms, which are situated around the walls or at the base of the mixer-reservoir, sequentially deflecting in and out of the fluid reservoir. The conceptual idea is for the diaphragms to agitate the fluid which induces convective mixing of the fluid. The diaphragms are operated pneumatically with air/gas pressure. The diaphragms are operated via a single air inlet which leads to the air chamber of the corresponding diaphragm. The oscillation frequency of the mixer diaphragms are controlled via a solenoid valve, which controls the compressed air/gas flow which is fed into the air inlet of the micro-pump. Figure 2.2 illustrates the mixing concept of the micro-mixer. Image a) shows the micro-mixer with samples 1 and 2 in an undiffused state. Image b) and image c) shows the diaphragms deflecting causing the samples to diffuse. Image d) shows the mixer with the sample 1 and sample 2 fully mixed.

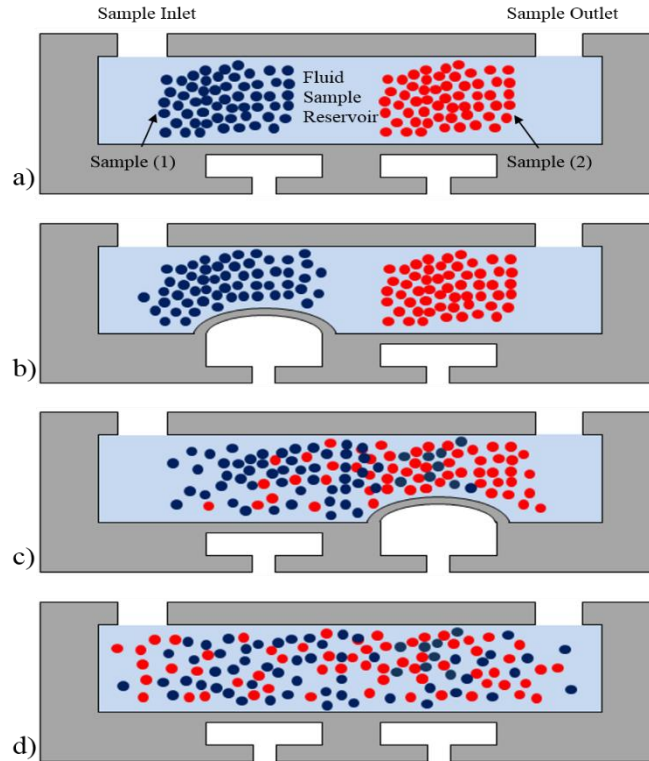


Figure 2.2: Micro-mixer with pneumatically actuated diaphragms causing the mixing of two samples

2.2 Fabrication of Microfluidic Devices

2.2.1 PDMS Device Using PMMA Mold

The technique utilized for this fabrication process is a soft lithography application. The process involves a casting process of a polymer material onto a micro-mold. The parts are casted separately, therefore involve an assembly process. This assembly process involves an alignment and stacking process. The parts are joined together with a bonding technique. The materials that are most commonly used for soft lithography are polymers, silicon, and glass.

Fabrication Material - The material selected for the fabrication process of this microfluidic device is PMMA (Poly methyl methacrylate), Sylgard 184 Silicone Elastomer Base and Curing Agent from Dow Corning Corporation (Midland, MI), because of its Young's Modulus = 1.84

MPa. This allows for flexibility, which is utilized for the diaphragm actuation. Plain glass slides (75x38 mm, 1 mm thick, Electron Microscopy Sciences, Hatfield, PA).

Device Specifications - The PDMS based microfluidic devices are comprised of the micro-pump and the micro-mixer integrated onto one chip. Figure 2.3 shows that the device is comprised of two layers of PDMS and one glass slide layer. The PDMS layer are categorized as the fluidic layer and the control layer. The fluidic layer is the thick layer of PDMS, which consists of the micro-channel that holds the liquid sample and permits the transfer from the inlet to the outlet. The control layer is the thin layer of PDMS, which houses the diaphragms that are used to control the fluid flow within the micro-channel as well as the liquid agitation within the mixing reservoir. Two of the micro-channels act as the vessels for the fluid inlets which is directed towards the mixing reservoir that is situated in the center of the device. A third micro-channel, which acts as the vessel for the fluid outlet, is directed from the mixing reservoir towards the fluid outlet.

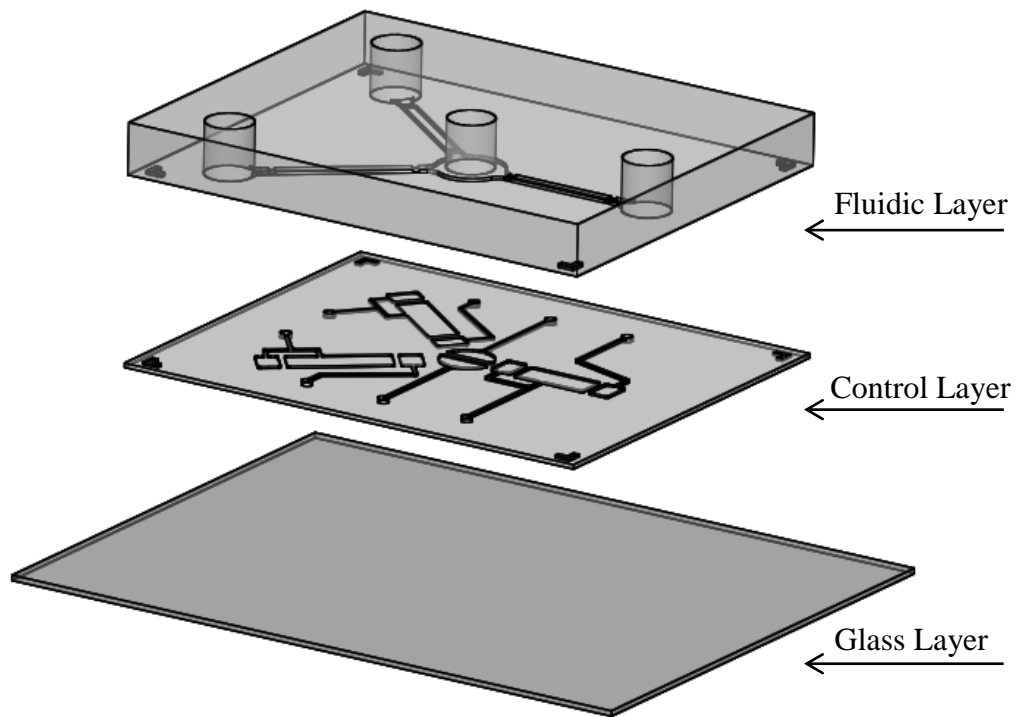


Figure 2.3: The multiple layers of a PDMS Microfluidic device assembly

The mold for the device is design using a 3D CAD software, for the experiment SolidWirks was used. The fluidic layer mold has a channels height of 0.3mm and width of 1.2mm. It also has a check valve assist with a height of 0.1mm. The check valve assist is to help ensure that the channel is closed when the diaphragm is used as a shut off valve. The features for the control layer mold have a height of 0.2mm. Figure 2.4 shows the proposed design of the fluidic layer which consists of three micro-channels and a reservoir. Figure 2.5 shows the proposed design of the control layer.

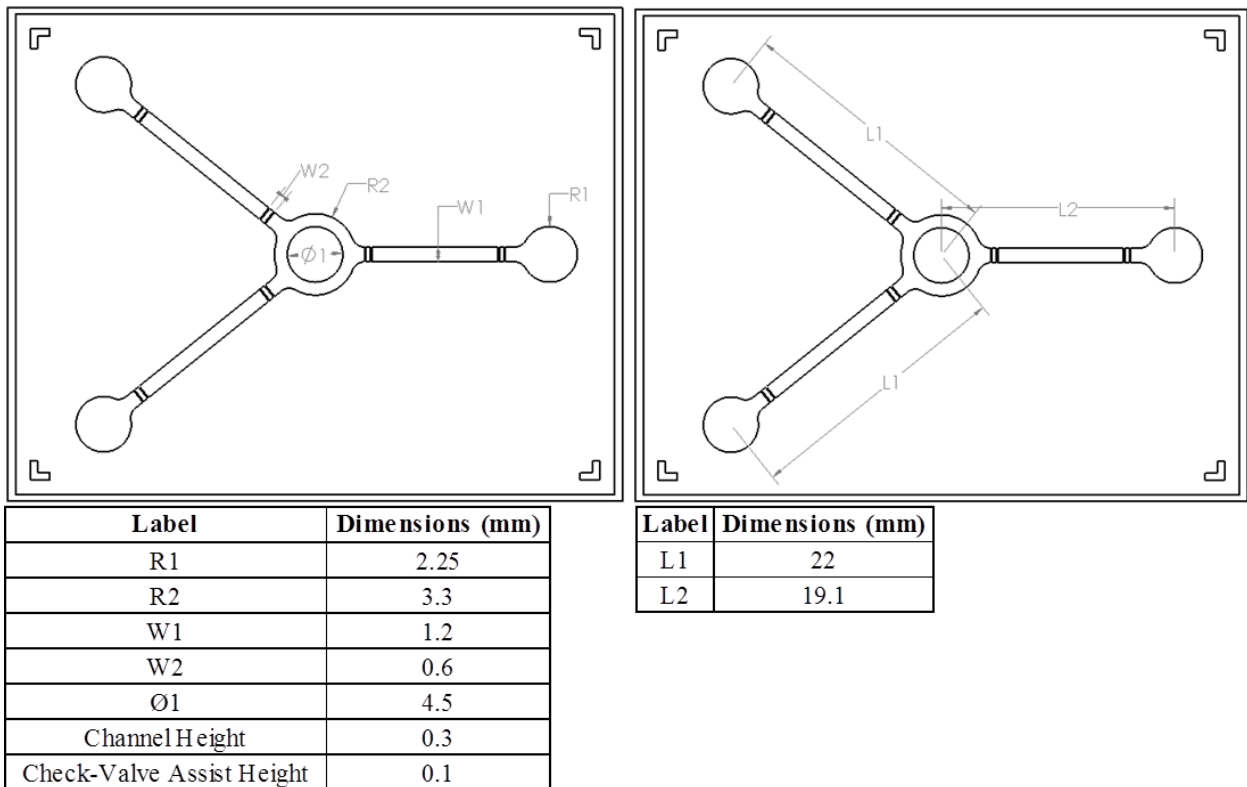


Figure 2.4: PMMA mold design of fluidic layer micro-channel

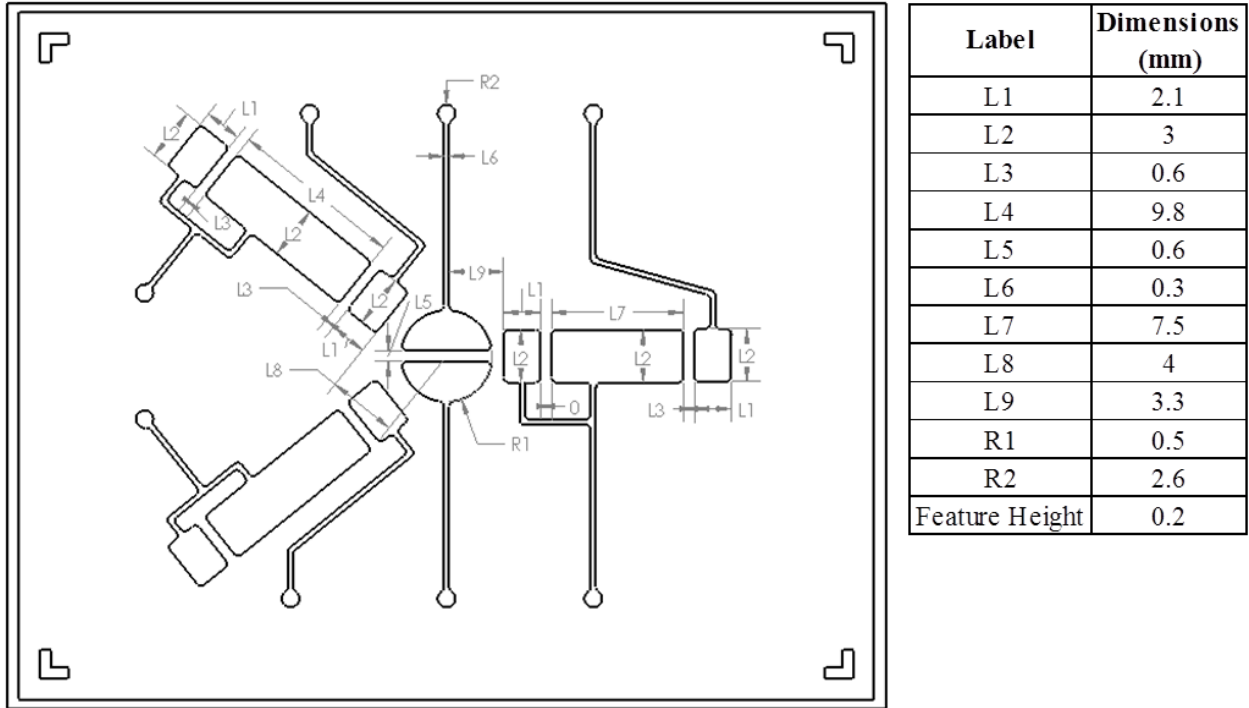


Figure 2.5: PMMA mold design of control layer

PMMA Mold Engraving - The PMMA material was selected for the advantages of it being cheap and that it is easy to micro-engraving the features onto the surface. Once the mold is designed using the 3D CAD software, it is then transferred to the software which is used for the micro-milling machine. At this point the software is set with all the appropriate parameters which correspond to the mold design. Figure 2.6 shows a completed 3D CAD design of the microfluidic device's control layer.

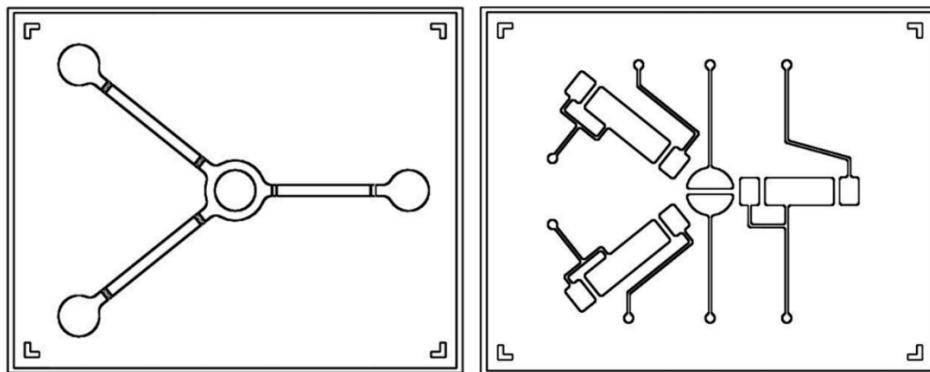


Figure 2.6: 3D AutoCAD designs of PMMA master mold

With the use of micro engraving, the master molds designs were cut into the surface of the PMMA sheet. The process flow for the fabrication process is shown in Figure 2.7. Figure 2.8 shows a resulting PMMA master mold of a control layer after the Micro-engraving process.

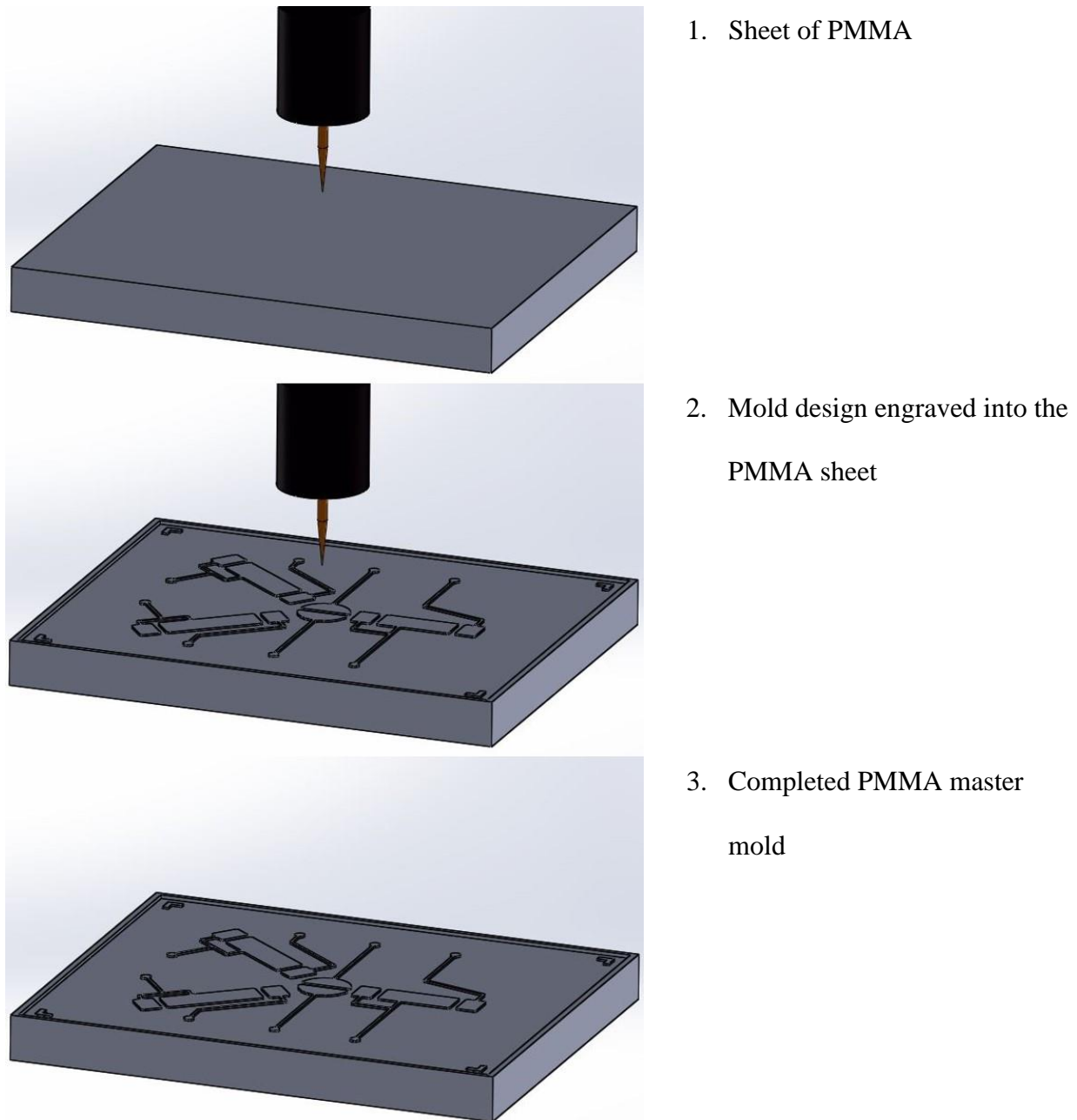


Figure 2.7: Micro-engraving process flow of master mold

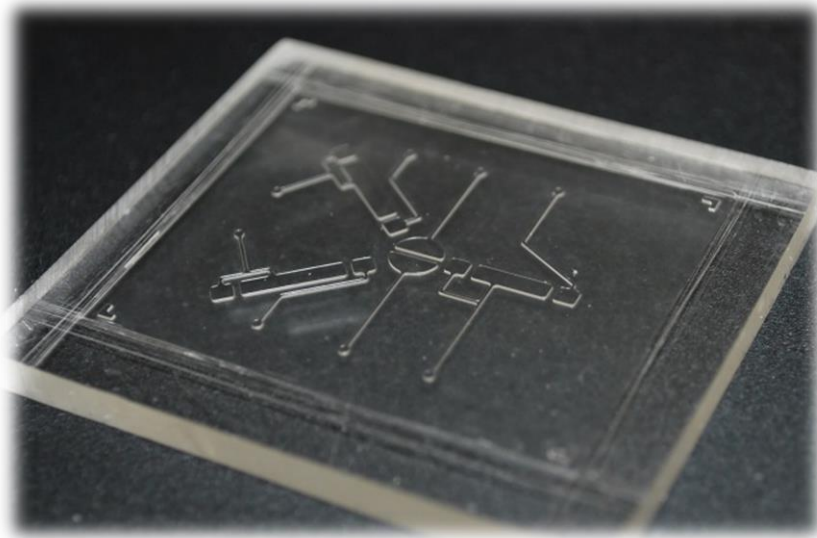


Figure 2.8: Micro-engraved PMMA master mold of control layer

Fluidic Layer PDMS Casting Process - The micro-molding process flow for the fluidic PDMS layer on a PMMA master mold is shown in Figure 2.9.

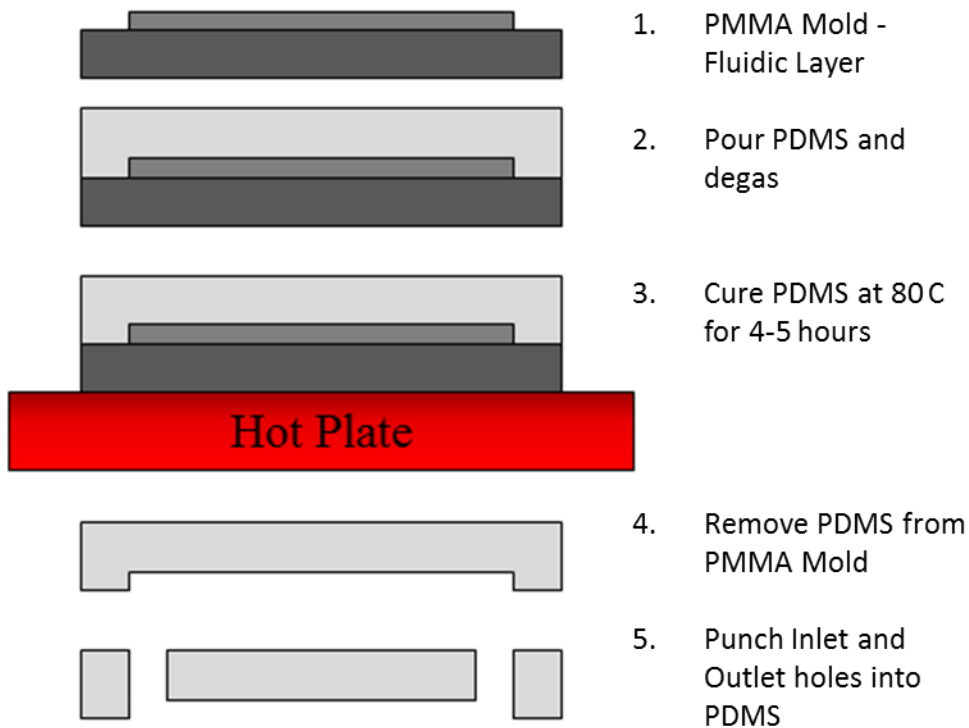


Figure 2.9: Fluidic layer casting process

The detailed fabrication process of the fluidic layer is as follows:

1. The PDMS base and curing agent were mixed in a ratio 10:1 by mass (i.e. 40g base with 4g curing agent) in a petri dish. The open petri dish of the PDMS mixture is placed in a vacuum chamber for 5-10 minutes to remove (degas) the air bubbles. An alternative method is to leave the open petri dish, with PDMS mixture, out for 15-30 minutes.
2. For the fluidic layer, the mold must first have boarders placed around the outer edge of the mold. This is accomplished by applying scotch tape around the entire outer edge of the mold. 15mL of the PDMS mixture is poured uniformly to cover the mold and allowed to spread evenly. Any air bubbles generated while pouring can be removed by placing the mold into a vacuum chamber for 5-10 minutes. Alternative methods for removing the bubble can be achieved by leaving the mold with the PDMS out for 15-30 minutes. Also if there are not a lot of bubbles then they can be removed by piercing the bubbles with a syringe needle.
3. Place the PMMA/3D printed mold on a hot plate at 80°C for 4 hrs.
4. The cured PDMS layer is gently removed from the mold and the edges of access material are cut off with a razor blade.

Figure 2.10 shows the resulted casting of the PDMS fluidic layer from the PMMA mold.

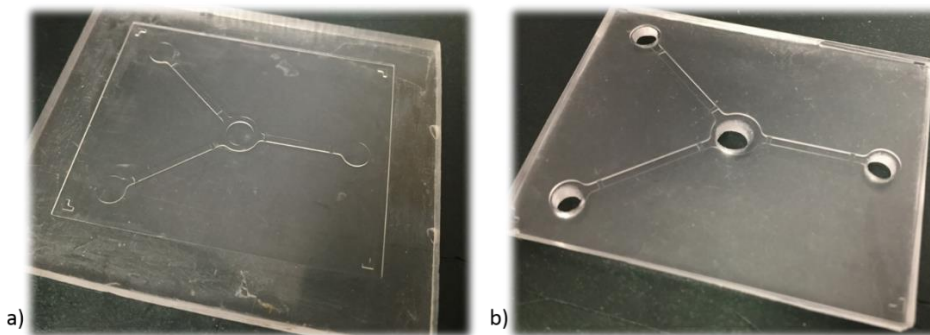


Figure 2.10: Image a: Resulting engraved mold. Image b: Casted PDMS layer with holes cut out for inlets and outlet

Control Layer PDMS Casting Process - The process flow for casting the control PDMS layer on a PMMA master mold is shown in Figure 2.11.

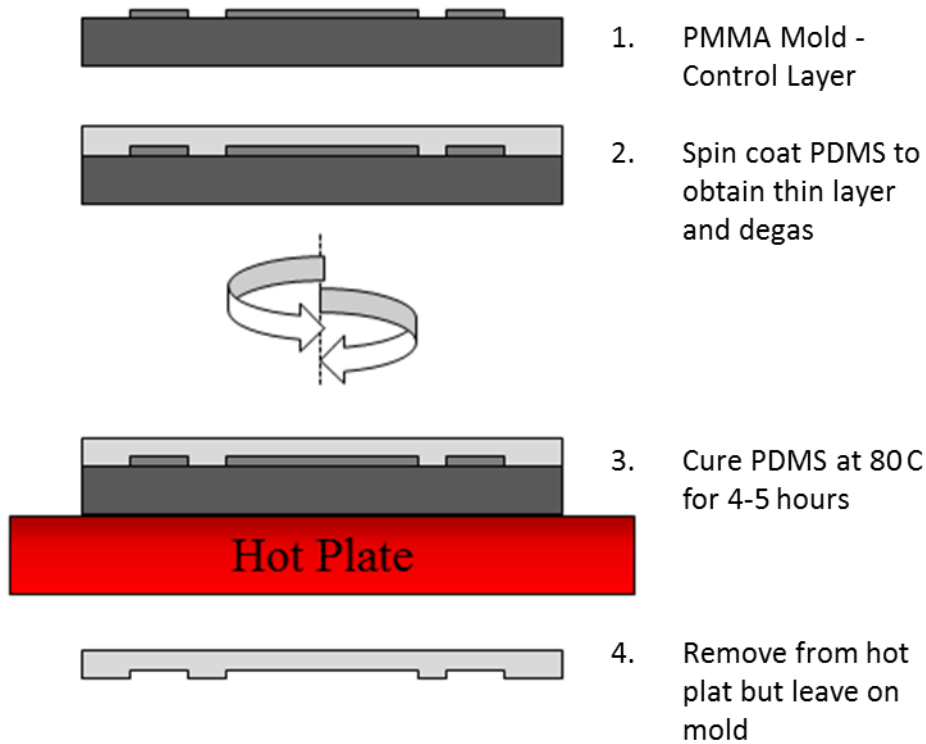


Figure 2.11: Control layer casting process

The detailed fabrication process of the control layer is as follows:

1. PDMS mixture was prepared as described in the fluidic layer section.
2. For the control PDMS layers with diaphragms, it is very crucial to control the layer thickness of the diaphragms. Therefore the PDMS mixture is spin coated on the PMMA at a particular rpm for 1 min to obtain a desired thickness PDMS membrane. The required spin speed was determined from the spin speed vs. thickness plot [23] as shown in Figure 2.12.

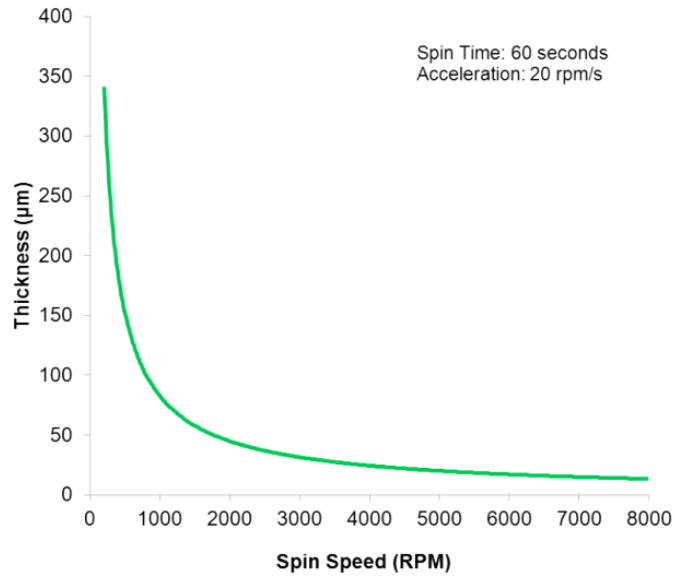


Figure 2.12 PDMS thickness controlled as a function of spin speed [23]

3. The mold is left to sit out to allow for the bubbles to degas.
4. Place the PMMA/3D printed mold on a hot plate at 80°C for 4 hrs.
5. The cured PDMS layer is removed from the hot plate, however it is left on the PMMA/3d printed mold.

Figure 2.13 shows the resulted casting of the PDMS control layer from the PMMA mold.

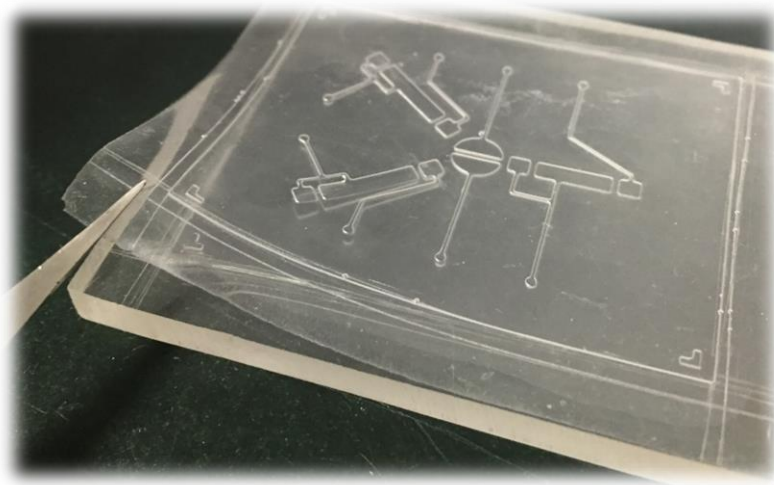


Figure 2.13: Casted PDMS control layer and mold

Oxygen Plasma Bonding - Once the layers of PDMS are cured, they must then be bonded together in order for the microfluidic device to achieve a functionality. This is accomplished with the surface modification bonding technique of oxygen plasma treatment. The exposure to oxygen plasma causes oxidation of the CH₃ groups on the PDMS surface to produce OH groups [24]. The –OH functional groups on the PDMS surface enable bonding to another PDMS surface or glass. In this process, first the surface of the two PDMS layers (thick layer and thin layer) are treated and bonded together. Next the PDMS thin layer is bonded to a glass slide. The bonding of the glass slide provides mechanical support to the device, as well as acts as a capping piece to prevent air/gas leakage. This process is accomplished with the use of an Oxygen plasma chamber (Model PC-150, South Bay Technology, Inc., San Clemente, CA) (fig. 2.14). The process flow for assembling the device is shown in Figure 2.15.



Figure 2.14: Oxygen plasma chamber

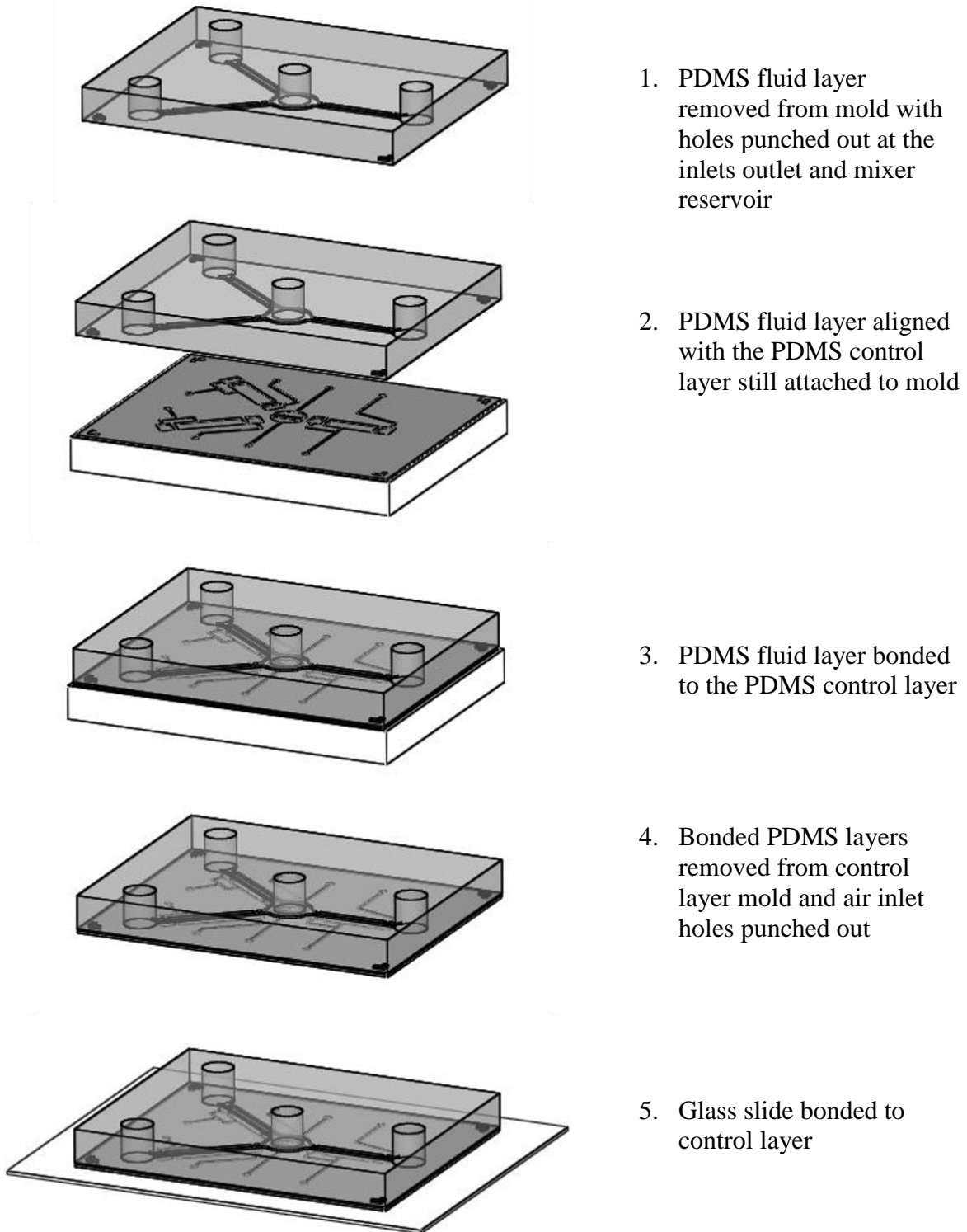


Figure 2.15 Process flow for bonding and assembling PDMS device

The detailed oxygen plasma bonding process is as follows:

1. A soft polymer hole-punch 4mm diameter, was used to punch holes in the areas at the microchannel inlets, outlet, and mixer reservoir. The holes will provide access for fluid to be introduced into the device.
2. The PDMS control layer and fluid layer surfaces must be cleaned before they are bonded together. This is to ensure that there are no particles on the surface which can prevent bonding. This process is detailed below:
 - The surfaces that will be exposed to the oxygen plasma treatment is first rinsed with DI water.
 - Next the surface is rinsed with Isopropyl Alcohol, and then scrubbed gently with a cotton swab.
 - The surface is then rinsed again with DI water.
 - It is critical not to touch the surface of the surface. Therefore it is dried using a nitrogen pressure blast.
3. The PDMS layers were placed inside the Oxygen plasma chamber with their bonding sides facing up. The plasma chamber was operated at 20 W forward power and 0 W reverse power, 100-110 mTorr for 20sec.
4. Bonding of PDMS layer to PDMS layer:
 - After the exposure the bonding process has to be completed within 2 minutes in order to ensure a strong and complete bond. While wearing latex gloves and only touching the edge, the oxygen plasma treated PDMS layers are removed from the chamber. The layers are aligned and the exposed surface of the Fluid layer is brought into contact with the exposed surface of the control layer. The PDMS fluid

layer is gently rolled on top of the control layer to complete this bonding process Figure 2.16. When bonding the PDMS layers together air can become trapped between layers. Therefore the rolling action helps reduce the trapping of air and help induce a greater uniformed bond.

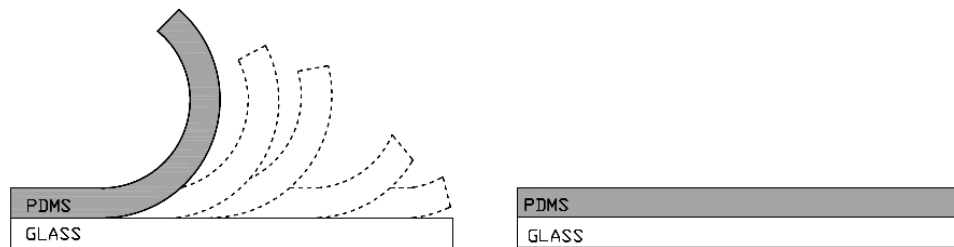


Figure 2.16: Roll technique of PDMS layer to reduce trapped air and induce uniformed bonding

5. A soft polymer hole-punch (Harris uni-core, Ted Pella, Inc. Redding, CA, 1.5mm diameter) was used to punch holes in the areas at the air inlets on the control layer side of the now bonded PDMS layers Figure 2.17.

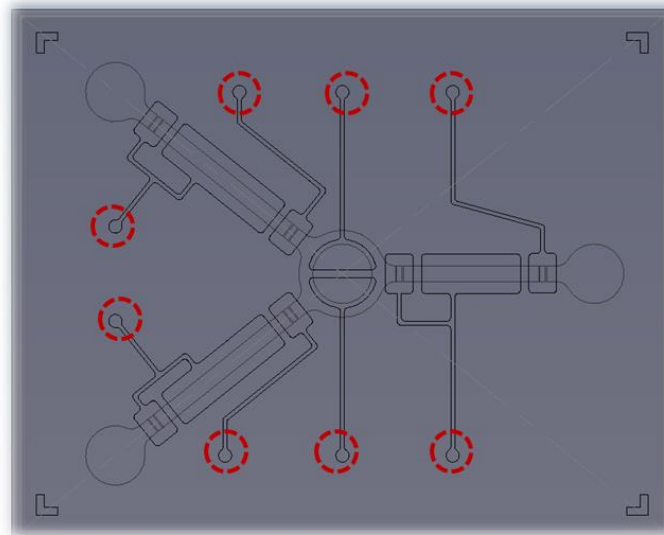


Figure 2.17: 3D CAD design of aligned layers with circles indicating where air inlet holes are punched

6. Bonding of PDMS layer to glass slide:

- The cleaning of the PDMS control layer side and glass slide were cleaned and prepped just as described in step 2.
- The Oxygen plasma chamber was operated with the same parameters as described in step 3.
- The bonding of PDMS to glass required the same steps as described in step 4.

Figure 2.18 shows a resulting PMMA mold PDMS microfluidic device which has been completely assembled and bonded.

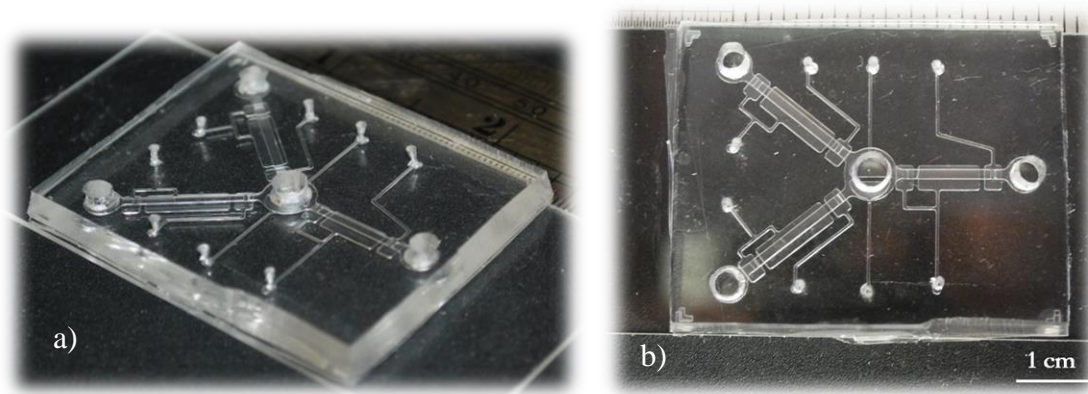


Figure 2.18: Image (a): Completely fabricated microfluidic device. Image (b): Top view of fabricated device

2.2.2 PDMS Device Using 3D Printed Mold

3D printing was utilized to produce a micro-mold for a PDMS microfluidic device. ABS plastic was selected because it is one of the most commonly used thermoplastics for FDM technique, and it is reactive to surface modification with the use of an AVB (acetone Vapor Bath). The design is first modeled with the desired parameters using the 3D CAD software and then the file is saved. The file is then saved again, as a .STL file, this file format is supported by many software packages which are used for rapid prototyping and 3D printing. In order to print the

mold, the previously saved .STL file is first exported into the corresponding software of the 3D printer. The 3D printing process for the micro-mold is illustrated in figure 2.19.

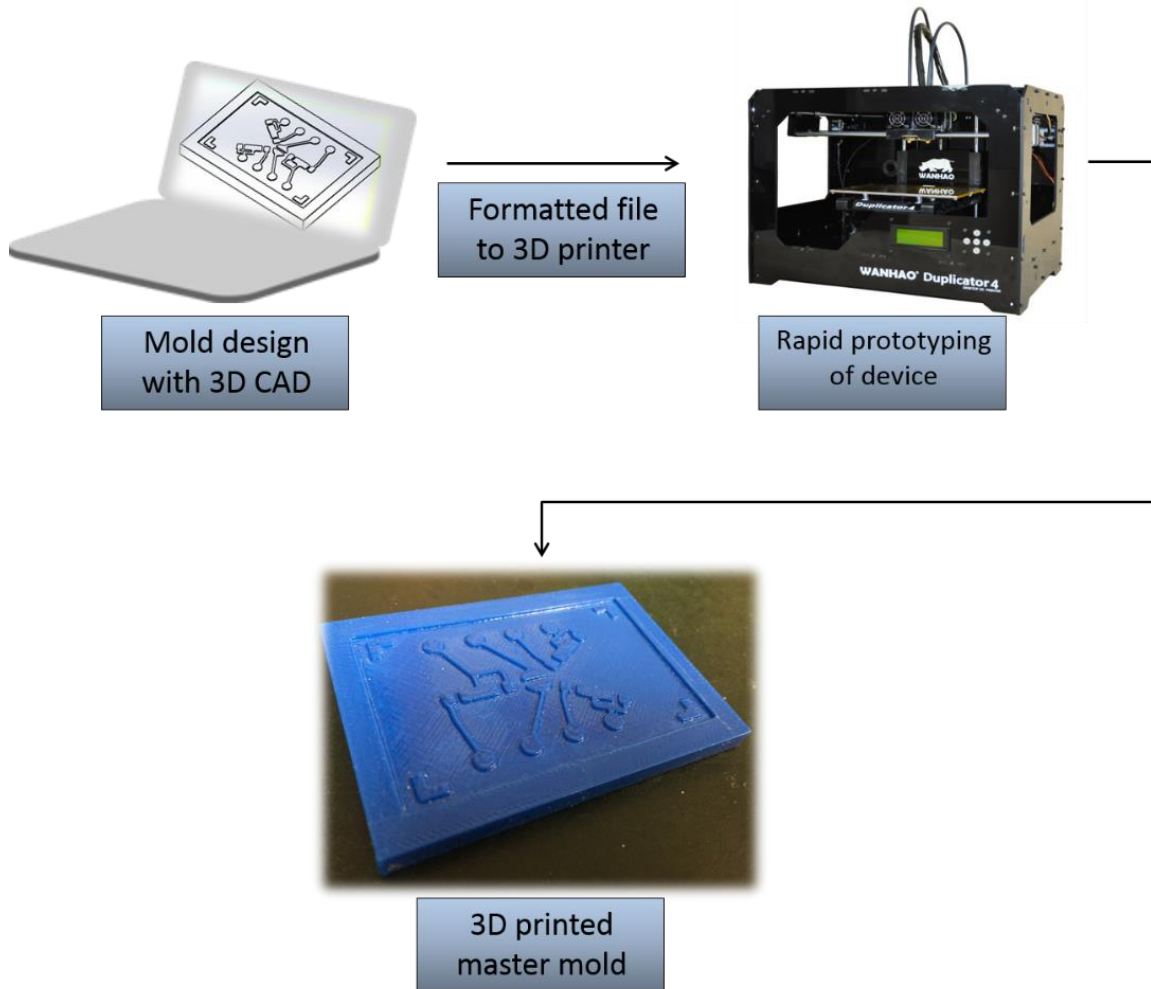
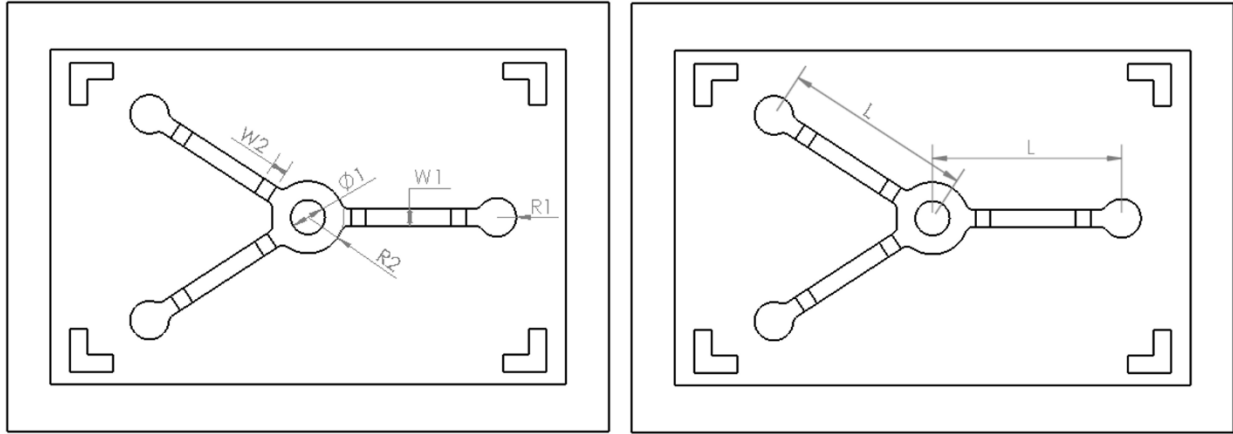


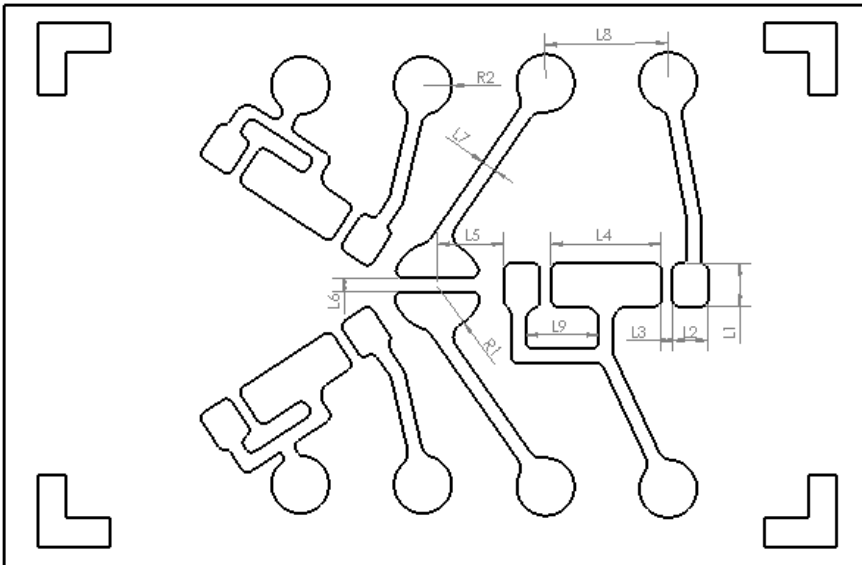
Figure 2.19: Process flow of 3D CAD design, 3D printer, and final master mold

Figure 2.20 shows the design of the fluidic layer which consists of three micro-channels and a reservoir. Two of the micro-channels act as the vessels for the fluid inlets which is directed towards the mixing reservoir that is situated in the center of the device. A third micro-channel, which acts as the vessel for the fluid outlet, is directed from the mixing reservoir towards the fluid outlet. The fluidic layer mold has a channels height of 0.75mm and width of 2mm. It also has a check valve assist with a height of 0.25mm. Figure 2.21 shows the design for the control layer. The features for the control layer mold have a height of 0.35mm.



Label	Dimension (mm)
R1	2.25
R2	4.2
W1	2
W2	1.75
Ø	4
L	22
Channel Height	0.75
Check-Vale Assist Height	0.25

Figure 2.20: 3D print mold design of fluidic layer micro-channel



Label	Dimension (mm)
L1	3
L2	2.5
L3	0.75
L4	7.65
L5	4.63
L6	1
L7	1
L8	8.50
L9	5.08
R1	3.10
R2	2
Feature Height	0.350

Figure 2.21: 3D print mold design of control layer

Acetone Vapor Bath Surface Treatment - The AVB (Acetone Vapor Bath) treatment is a procedure which is used to give the ABS printed model a smooth finish. After the 3D printed mold has been modeled the surface of the mold is very rough. Therefore during the PDMS casting process the PDMS will take-on the mold's surface characteristics (i.e. rough surface). When this occurs the O₂ Plasma bonding of PDMS to PDMS or PDMS to glass cannot be achieved if surface is rough. The AVB treatment will improve the surface smoothness of the mold and therefore O₂ plasma bonding can be achieved. However overexposure to acetone vapor bath can result in diminished or complete loss of mold features. Which means an appropriate apparatus and that the procedure has to be closely monitored. The process flow for the acetone vapor bath surface modification process of the 3D printed master mold is shown in Figure 2.22.

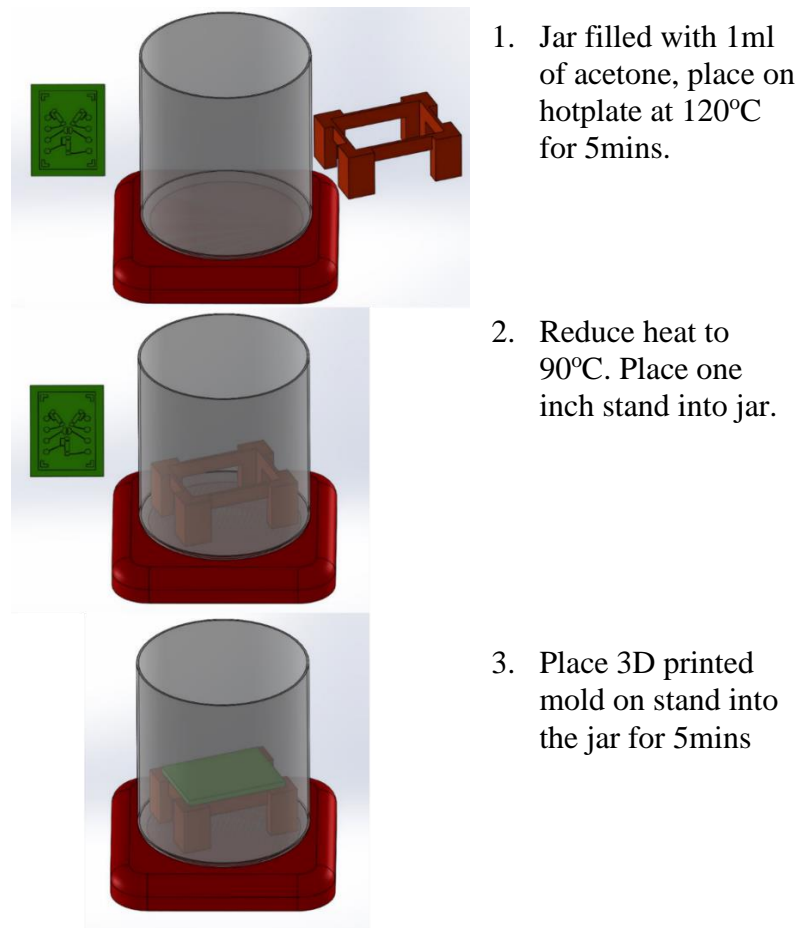


Figure 2.22: Process flow of Acetone vapor bath procedure

The detailed Acetone Vapor Bath process for the surface treatment of 3D printed mold:

1. Place your glass jar on the hot plate and put 1mL of Acetone into the jar (3-4mm deep). Initially the temperature will need to be ramped up to 120°C, for approximately 5 minutes. While the acetone is heating, clean the 3D printed mold with Deionized water and Isopropyl Alcohol to remove dust and fibers. Dry the mold with nitrogen pressure blast. As the jar reaches the desired temp, there will be a slight cloud formation in the jar. Once the vapor reaches the top of the jar, reduce the hot plate temperature to 90°C for the treatment.
2. After the mold is cleaned and dried, place it onto the 1.5in stand. The stand is then placed into the jar, and the jar is covered $\frac{3}{4}$ with aluminum foil.
3. Allow the mold to sit in the jar for approximately 5 minutes.
4. Immediately after 5 minutes, remove the jar from the hot plate and remove the stand with the 3D printed mold from the jar. Allow for the mold to sit out for an additional 5 minutes.
5. Remove the mold from the stand and observe finished results.

Figure 2.23a & b shows the mold before surface treatment and the resulting mold after the surface treatment.

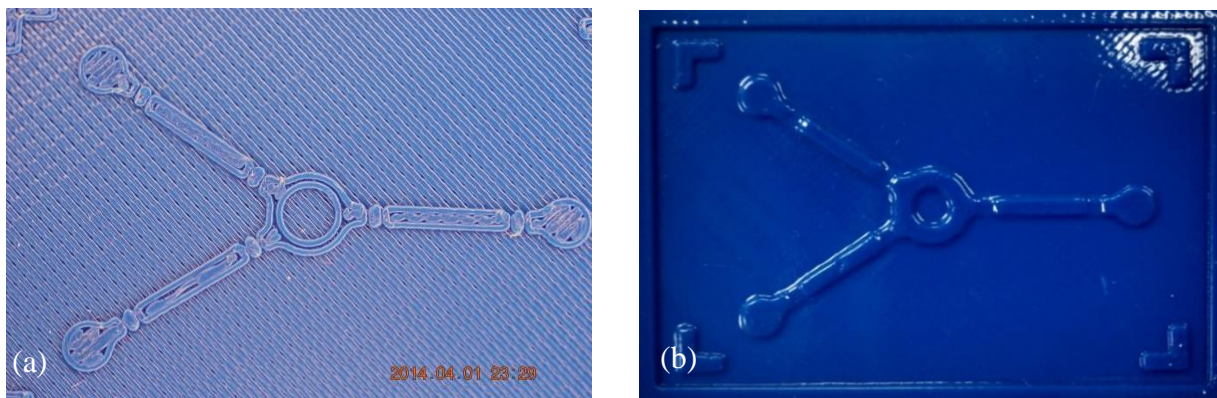


Figure 2.23: Image (a): 3D printed master mold of fluid layer before AVB surface treatment
Image (b): 3D printed master mold of fluid layer after AVB surface treatment

PDMS Casting and Bonding - The PDMS casting and bonding processes, for this device, are prepared as described in the PDMS device fabrication section. Figure 2.24 shows a resulting 3D printed mold PDMS microfluidic device which has been completely assembled and bonded.

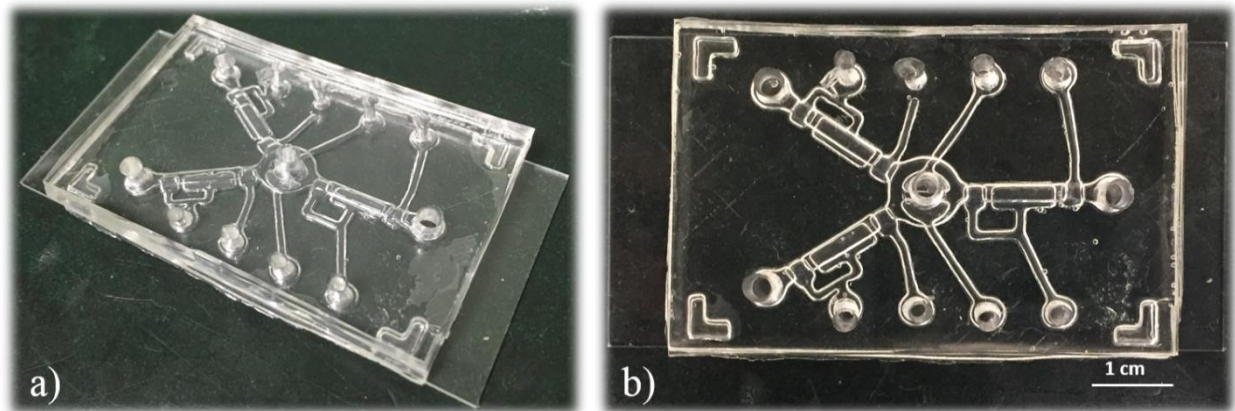


Figure 2.24: Image (a): Completely fabricated microfluidic device. Image (b): Top view of fabricated device

2.2.3 3D Printed Device Fabrication

The technique utilized for this fabrication process is FDM (fused deposition modeling) application. The FDM technique heats a thermoplastic or elastomer material into a quasi-solid form as it comes into contact with a print head nozzle. The material is then extruded through the heated nozzle and deposited onto a build-plate. This extrusion process is repeated thereby creating a layering effect. Unlike the PDMS microfluidic device, which is an assembly of three separate pieces, the 3D printed pump and mixer are modeled entirely with the Fused Deposition Modeling (FDM) technique of 3D printing. In order to utilize 3D printing an appropriate material had to be selected. The materials that are most commonly used for 3D printing are thermoplastics, such as ABS, polycarbonate, engineered thermoplastics elastomers, and etc.

Device Materials - The micro-pump and micro-mixer were printed with a Wanhao duplicator 4 printer (Jinhua Wanhao Ltd., China), which utilize the FDM technique which is an extrusion based

method. This 3D printing technique is used in the experiment to successfully fabricate the micro-pump and micro-mixer. Though the resolution is greater with the SLA method, the FDM printer still has an accuracy of 100 μ m in x, y and z direction which is appropriate for micro-pumps. The selected 3D printer normally prints with Acrylonitrile Butadiene Styrene (ABS) plastic (Young's Modulus = 1.9 – 2.8 GPa) or Polylactic Acid (PLA) plastic (Young's Modulus = 3.5 GPa). Because the Young's Modulus of ABS and PLA are very high and would result in a rigid structure unlike that of PDMS, another material had to be selected. The material selected for the microfluidics devices is Ninja Flex (Fenner Drives Inc, USA), a Thermal Plastic Elastomer (TPE), because of its elastic properties, Young's Modulus = 15.1MPa, similar to that of PDMS. This allows for a flexible printed structure with little rigidity which is much more suitable for moving part. The selected TPE material has an advantage over PDMS by which it has hydrophilic properties. The PDMS material has hydrophobic properties meaning that with no repulsive forces involved, water repels from a mass or surface.

Diaphragm Orientation - The PDMS microfluidic devices are fabricated with the technique of soft-lithography and the layers assembled, with the features aligned, in a stacking method. This assembling process calls for the design of the diaphragm to be horizontally oriented to the surface “x-plane and z-plane”, and positioned either at the roof or the floor of the microfluidic device's micro-channel (fig. 2.25 a1 & a2). When using the FDM 3D printing fabrication technique the material has to be extruded onto a solid surface. If the printer were to print a structure similar to a beam that is supported on both ends (i.e. a bridge) then, depending on the geometry of the modelled structure, the material will begin to droop. This material overhang will cause the modelled structure to fail. If the diaphragm was to be printed in a horizontal orientation, then material overhang and drooping could occur which would cause the diaphragm to fail. To counteract this

dilemma, a small geometry for the diaphragm could be proposed, however this will limit the diaphragms functionality. Therefore the diaphragm was select to be modelled and fabricated in a perpendicular (z-plane) orientation to the build plate in contrast to its PDMS counterpart (fig. 2.25 b1 & b2).

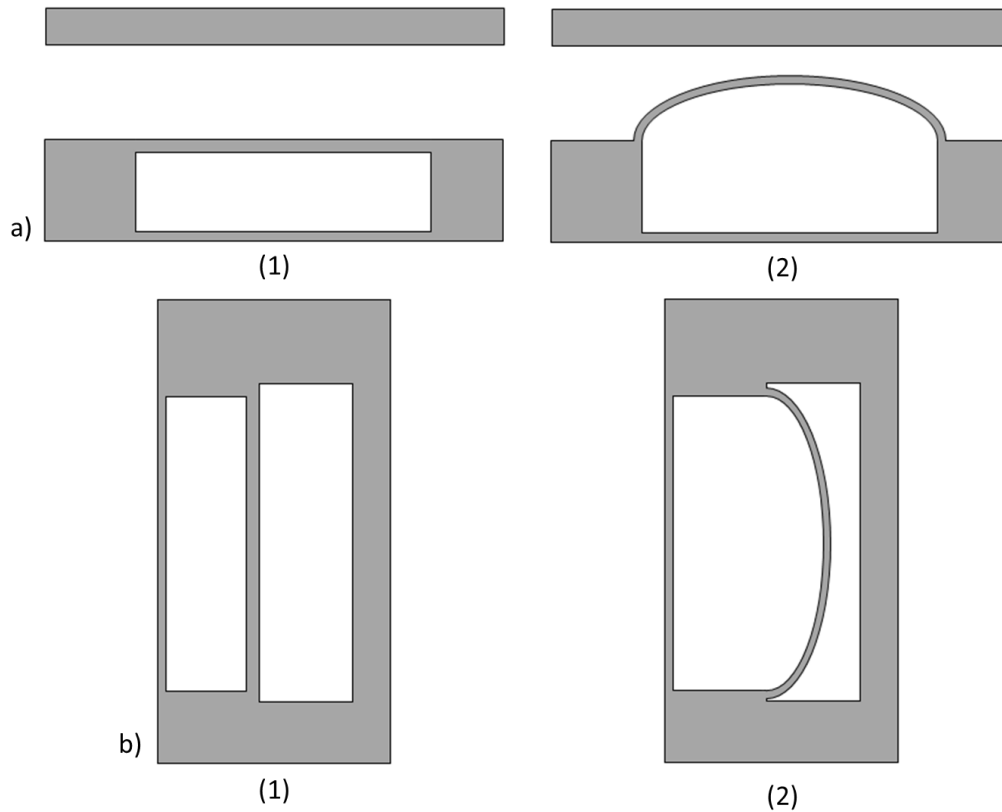


Figure 2.25: Image a: A cross-sectional view of a PDMS diaphragm assembly arranged parallel to the x-plane. (1) Illustrates the diaphragm at rest. (2) Illustrated the diaphragm deflected. Image b: A cross-sectional view of a TPE diaphragm assembly arranged perpendicular to the z-plane along the micro-channel wall. (1) Diaphragm is at rest. (2) Diaphragm is deflected.

Micro-Pump Specifications - The 3D printed microfluidic device is design of two separate components which are the micro-pump and the micro-mixer. The micro-pump consists of a fluid/sample inlet, and an outlet (fig. 2.26a). The inlet and outlet are connected via a fluid micro-channel (0.9mmx5mm) (fig. 2.26a), which is capped off with the TPE material. The critical part of the device is the diaphragm, which is utilized as a pump. This is achieved with an actuation

motion of the diaphragm as it deflects into the micro-channel thereby causing fluid in the channel to displace (fig. 2.26c and fig. 2.26d). In order to achieve the action of pumping, diaphragms are situated parallel to the fluid channel wall. The device consists of two diaphragms side by side one acting as a check valve and the other acting as the driving force pump (fig. 2.26c and fig. 2.26b). The diaphragms are designed with a thickness of 500 μ m and a height of 5mm. The check valve has a length of 6mm, the driving force pump has a length of 12mm, while they have a leading edge spacing between each other of 14mm. The diaphragms are operated pneumatically with air/gas pressure. The diaphragms are operated via a single air inlet, which split into two channels which lead to the respected air chamber. This design leads to a peristaltic actuation of the diaphragms, which causes them to deflect with a slight out of phase offset $\leq 45^\circ$ which squeezes the fluid through the channel.

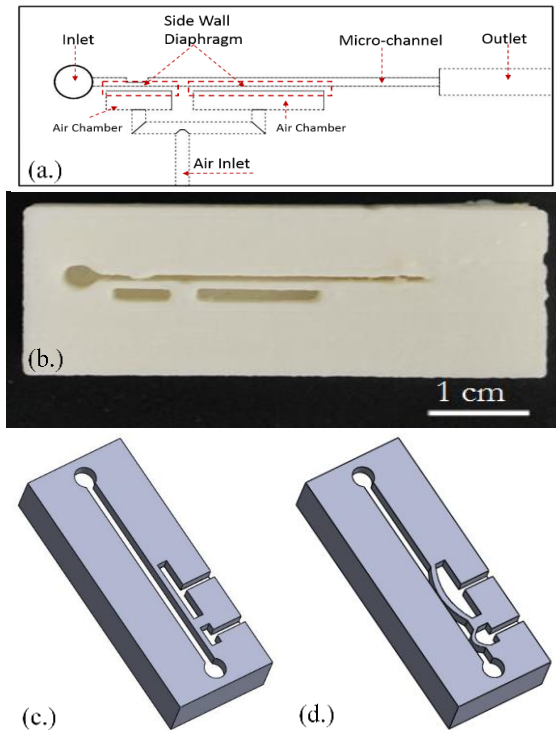


Figure 2.26: Image a: Cross-sectional view of 3D CAD design micro-pump. Image b: Cross-sectional cut out of 3D printed micro-pump showing the sidewall diaphragm and air chamber. Image (c) shows the 3D CAD design of micro-channel with the diaphragms at rest. Image (d) shows the 3D CAD design of micro-channel with the diaphragms deflected.

Figure 2.27 illustrates the 3D CAD design of the micro-pump which consists of the micro-channel and diaphragms. Figure 2.28 shows the micro-pumps design parameters.

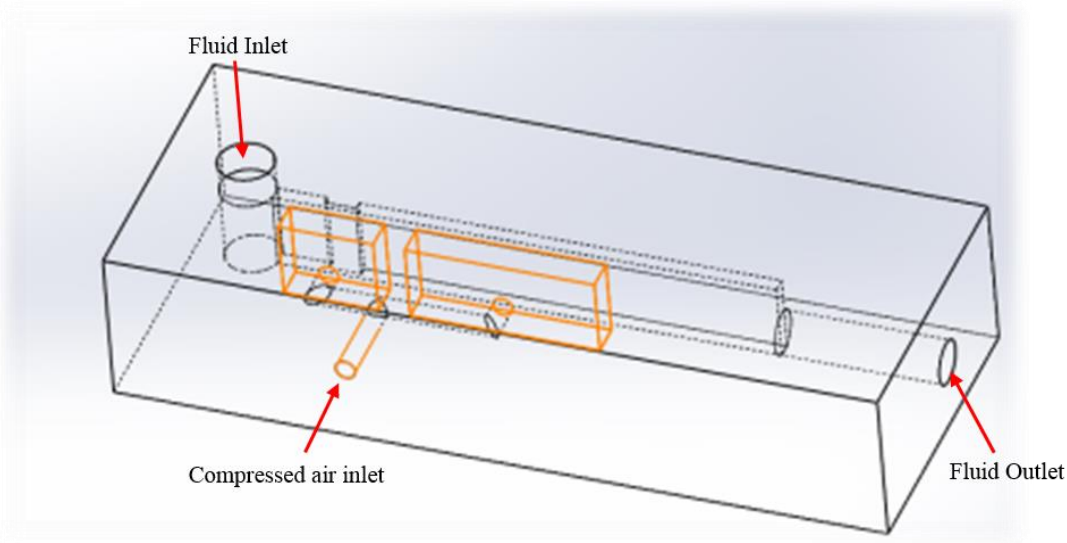


Figure 2.27: 3D model of 3D printed micro-pump. The orange lines indicate the location of the air inlet, and air-chamber aligned to the diaphragms

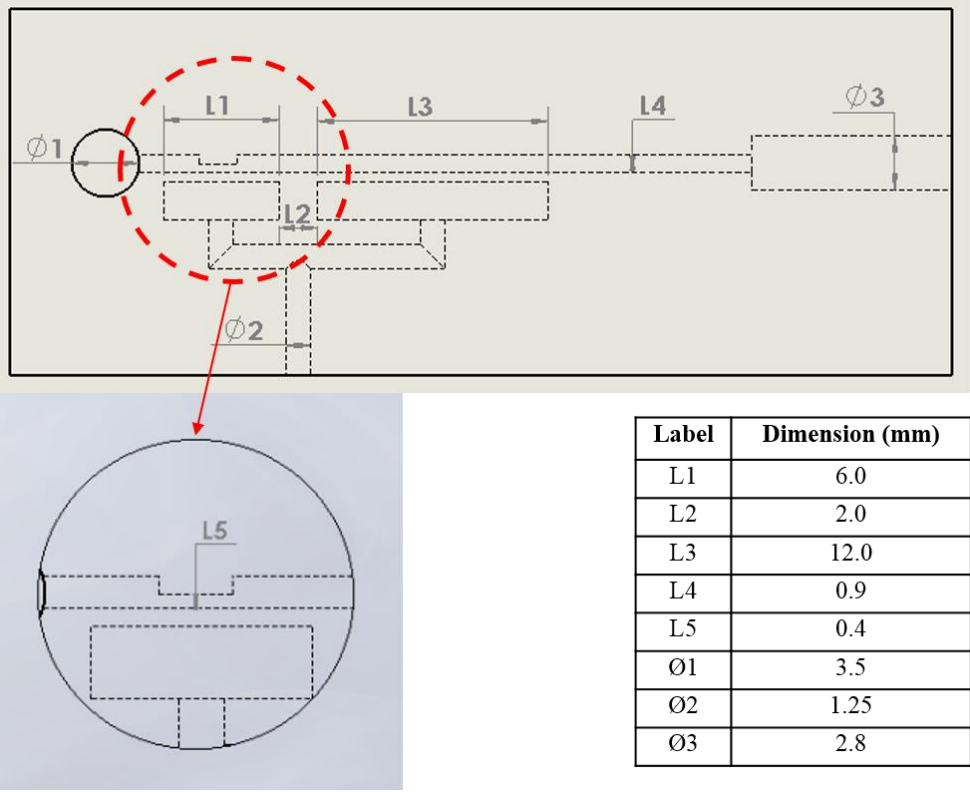


Figure 2.28: Top view of 3D Printed Design of Micro-Pump

Micro-Mixer Specifications - The micro-mixer consists of a fluid/sample reservoir (fig. 2.29a) with a depth of 5mm, which is capped off with a 1mm thick TPE material. The critical part of the device is the diaphragm, which is utilized as an agitator. This is achieved with an actuation motion of the diaphragm as it deflects into the reservoir thereby causing the fluid to be mixed (fig. 2.29 c and d). In order to achieve the action of mixing, the diaphragms are situated parallel to the fluid channel wall. The device consists of two diaphragms on opposite sides of the reservoir (fig. 2.29c and b). The diaphragms are designed with a thickness of 500 μ m and a height of 5mm. Figure 2.30 illustrates the 3D CAD design of the micro-mixer which consists of the fluid reservoir and diaphragms. Figure 2.31 shows the micro-mixers design parameters.

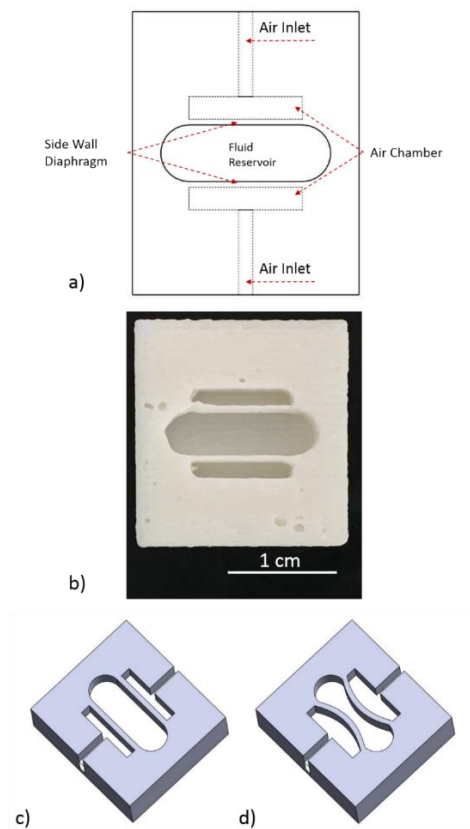


Figure 2.29: Image a: Top down cross-sectional view of 3D CAD design micro-mixer. Image b: Top down cross-sectional cut out of 3D printed micro-pump showing the sidewall diaphragm, reservoir, and air chamber. Image (c) shows the 3D CAD design of micro-mixer with the diaphragms at rest. Image (d) shows the 3D CAD design of micro-mixer with the diaphragms deflected.

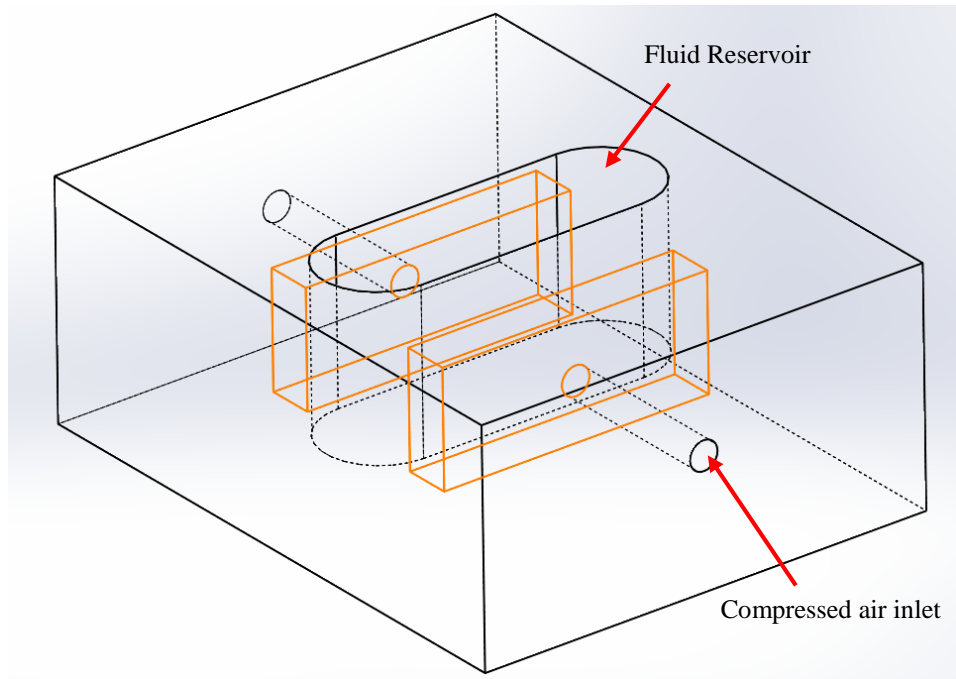
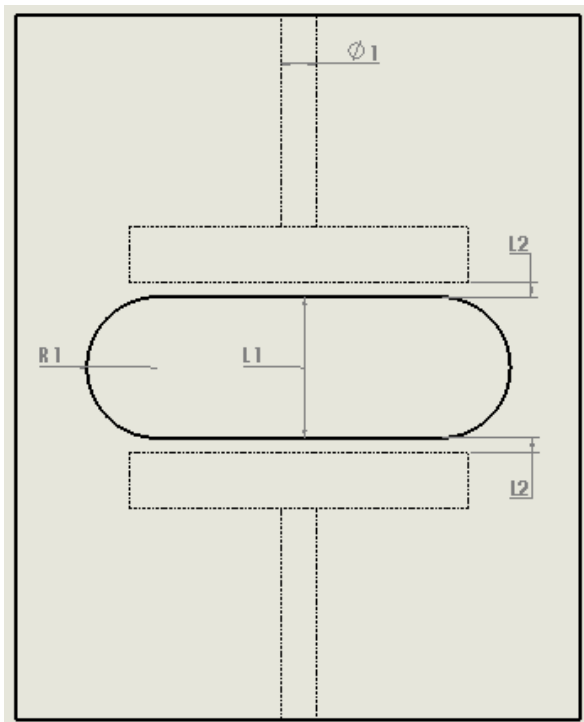


Figure 2.30: 3D model of 3D printed micro-mixer. The orange lines indicate the location of the airchamber aligned to the diaphragms



Label	Dimension (mm)
L1	5.0
L2	0.5
R1	2.5
Ø1	1.25

Figure 2.31: Top view of 3D Printed Device Design of Micro-Mixer

Fabrication Process - The design for the 3D printed micro-pump and micro-mixer are created with any 3D CAD software (i.e. Solid Works). The design is first modeled with the desired parameters using the 3D CAD software and then the file is saved. The file is then saved again, as a .STL file, this file format is supported by many software packages which are used for rapid prototyping and 3D printing. In order to print the device, the previously saved .STL file is first exported into the corresponding software of the 3D printer. The printer has been modified to enhance printing of the TPE material. For best results the printer's heated base plate will operate at a temperature of 110°C and the TPE material will be extruded at a temperature of 235°C. The speed, height and infill, also being a significant parameter, operates at a print speed of 20mm/s, a travel speed of 20mm, a layer height of 0.1mm, with 100% infill. The process flow for the fabrication process is shown in Figure 2.32. The detailed design and model process is as follows:

1. The design for the micro-pump and micro-mixer were first created in modeled using 3D AutoCAD (i.e. SolidWorks)
2. The part is then exported via the stereolithography (.STL) format from the CAD software.
3. The .STL file was then transferred to the 3D printing software where the respective print parameters are input.
4. Print parameters:
 - Infill: 100%
 - Number of Shells: 1
 - Layer Height: 100µm - 200µm
 - Feed Rate (Print speed): 20mm/s
 - Travel Rate: 20mm
 - Print Temperature: 235°C

- Heated Build Plate Temp: 110°C

5. The G-Code is then generated from the printing parameters.

6. The G-Code was then used to print the part.

The printing parameters acquired for this experiment were based on multiple trial tests which ultimately yielded the most optimal printing results for the devices. Without the proper parameters errors can occur, such as the material not extruding from the 3D printer correctly. The material may not have proper contact and adhere to the heated build plate. The material may not fill in correctly which will cause holes.

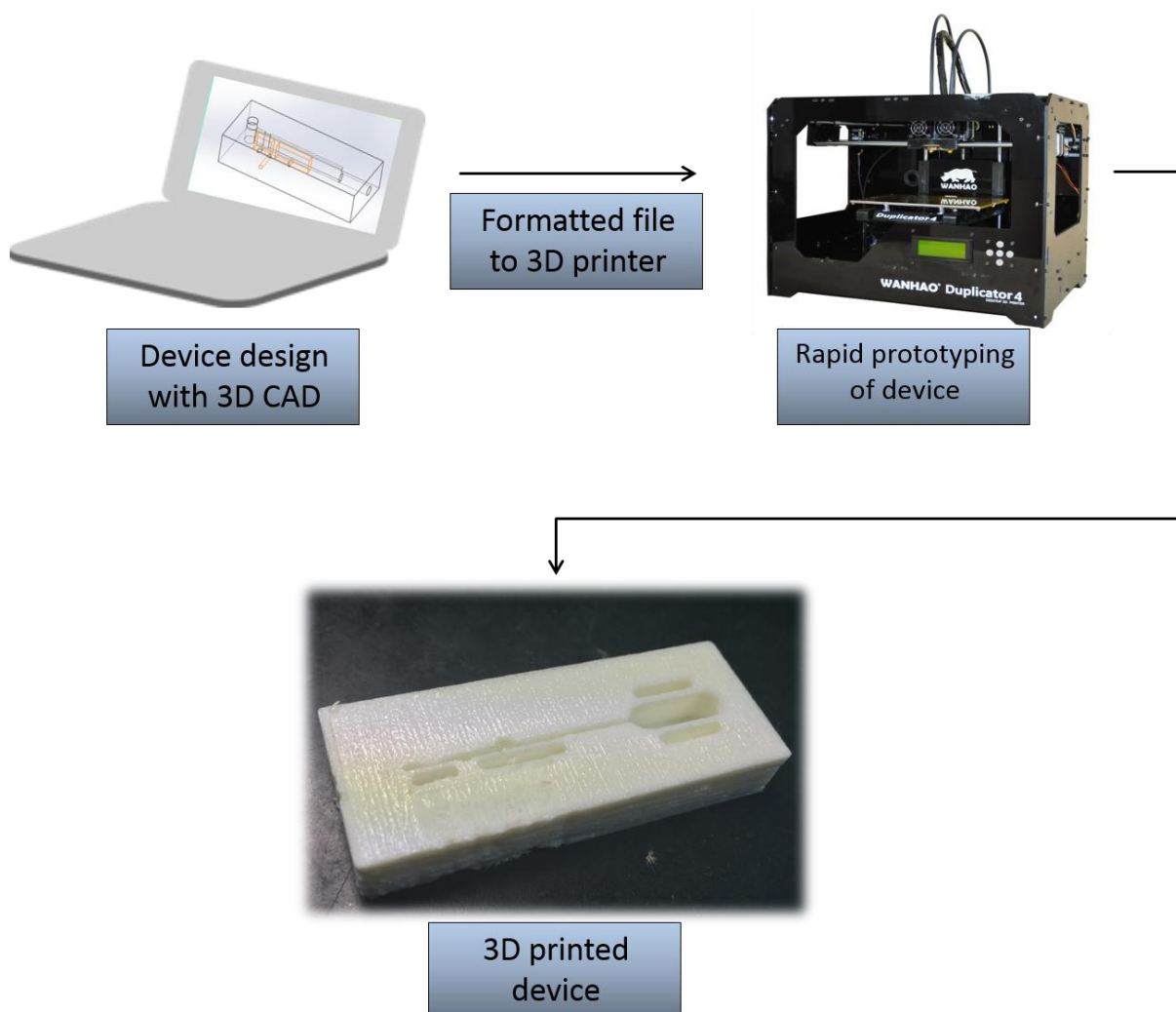


Figure 2.32: Process flow of 3D CAD design, 3D printer, and final device

2.3 Control System

The fabricated device in the previous section utilizes multiple pumps and valves during its operation sequences; the device requires timed sequences when utilizing its micro-channels, and micro-mixer. One channel will be actively pumping for a period of time while the other channels are closed. The same goes for the micro-mixer, which requires the channels to be closed and the mixing diaphragms to be active for a period of time. Therefore, this control system implements multiple diaphragm usage with timed sequences. Figure 2.33 illustrates a process flow of the active valves pump under timed sequences.

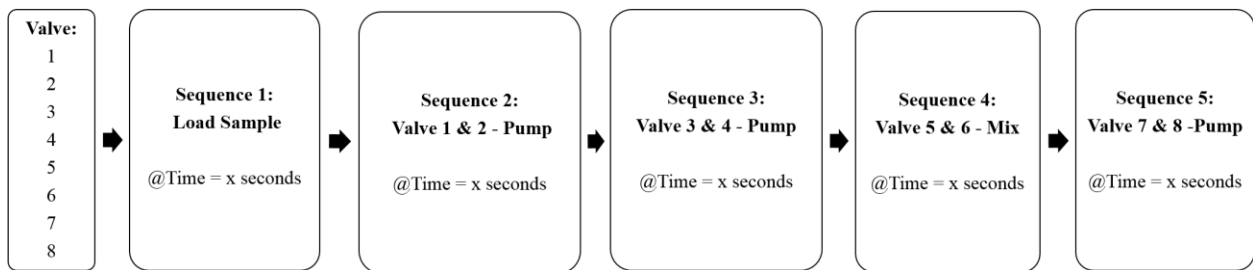


Figure 2.33: Control System Process Flow

2.3.1 Control System Components

The key components for operating the microfluidic devices include a compressed air/gas source, electromagnetic valves, an analog signal converter, and a control system. When the compressed air/gas is supplied to the air chamber the diaphragm is pushed into the micro-channel. When the compressed air/gas is cut off the diaphragm will return back to its “at rest” position. In order to regulate the air flow, the compressed air/gas source is connected to a solenoid valve (S070C-5BG-32, SMC Pneumatics, Noblesville, IN) that is connected to the micro-pump. Figure 2.34a shows the solenoid valve along with the tubing that leads to the 3-ports of the valve and the

compressed air/gas source. The 3-ports have specific duties with one leading to the pressure source, one leading to the micro-pump/mixer, and one leading to the atmosphere. The opening and closing of the solenoid valve allow and restrict the flow of the compressed air/gas. This opening and closing is governed via a wave function which is created in and generated from LabVIEW (Laboratory Virtual Instrumental Engineering Workbench) software. Then frequency of the wave is also controlled from LabVIEW. Once the wave is produced from LabVIEW it is converted to an AC signal by an Analog signal converter (USB-1608G High Speed Multifunction DAQ), which the solenoid valve is wired to (figure 2.34b).

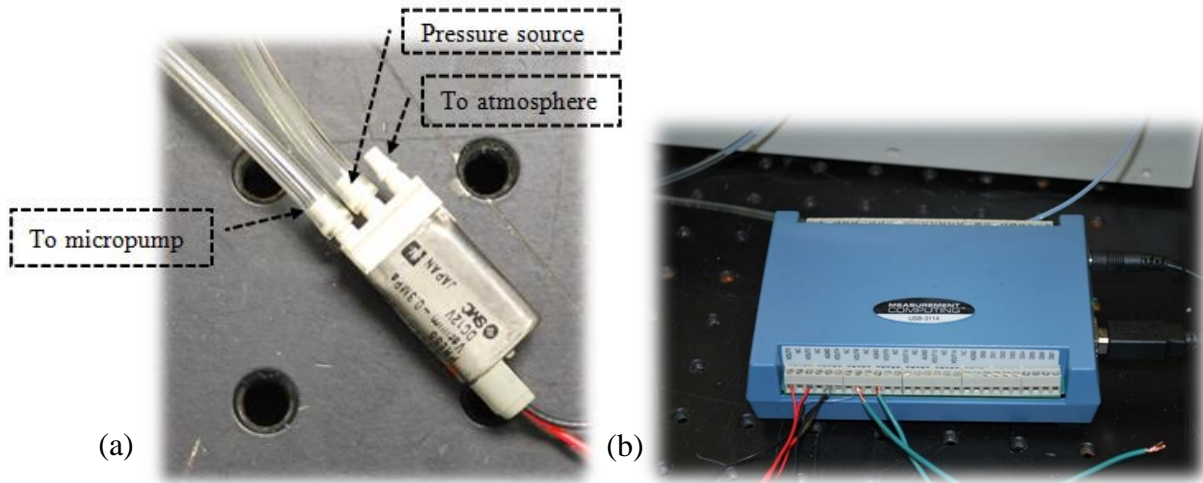


Figure 2.34: Image (a): The 3-port solenoid valve with the connections to the micro-pump and the to the pressure source. Image (b): The analog signal converter that is connected to laptop with LabVIEW software, and solenoid valve connected to converter.

2.3.2 LabVIEW Control System

In previous work, to operate the solenoid valve, a wave signal was generated with a function generator. However for this experiment, LabVIEW software is used to generate the wave signal. LabVIEW short for (Laboratory Virtual Instrument Engineering Workbench) is a system design platform and development environment that uses visual basics to structure programmable

graphical block diagrams for which the user can connect different function nodes by using graphic user interface wire connection. This allows for the user to custom design a multi-purpose control system. The previous PDMS microfluidic devices consist of multiple micro-channels which must be time independently operated. The LabVIEW software is utilized to setup a control system in order to regulate the functions of the solenoid valves. LabVIEW was used to generate a custom wave function for an AC signal of 10V peak to peak with a 5V DC offset, which was then used to power the solenoid valve. Figure 2.35 shows a screen shot of a block diagram setup of two physical channel parallel wave functions which operate within the same time loop along with additional physical channels with DC functions. The DC functions are in separate loops from the parallel wave functions however they operate under the same time function.

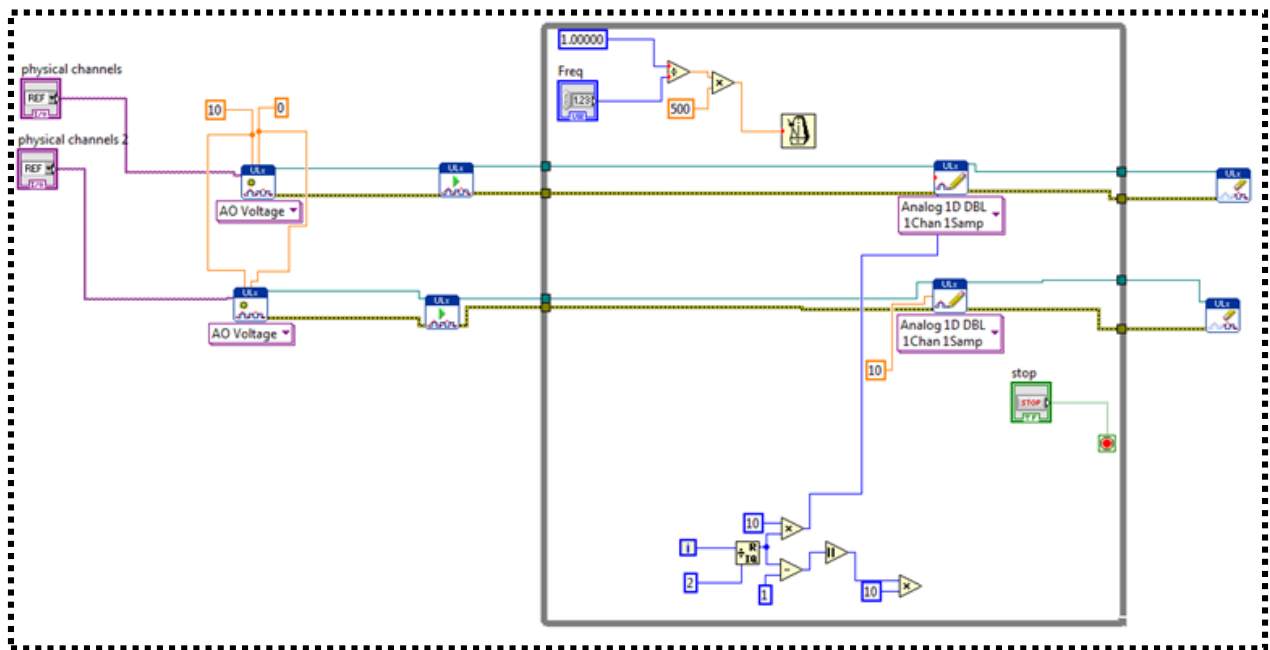


Figure 2.35: Screen shot of a block diagram setup of LabVIEW

2.3.3 Control System Integration

Multiple solenoid valves were used to operate the PDMS microfluidic device. This could lead to the equipment becoming unorganized and cause confusion of which switch operates which solenoid valve. Therefore the control system equipment was consolidated into a project enclosure (Radio Shack, 8x6x3in). Figure 2.36 shows the solenoid valves along with the analog signal converter combined into the enclosure, it also shows a fully enclosed box with the each valve port labeled. The analog signal converter is placed at the base of the enclosure.

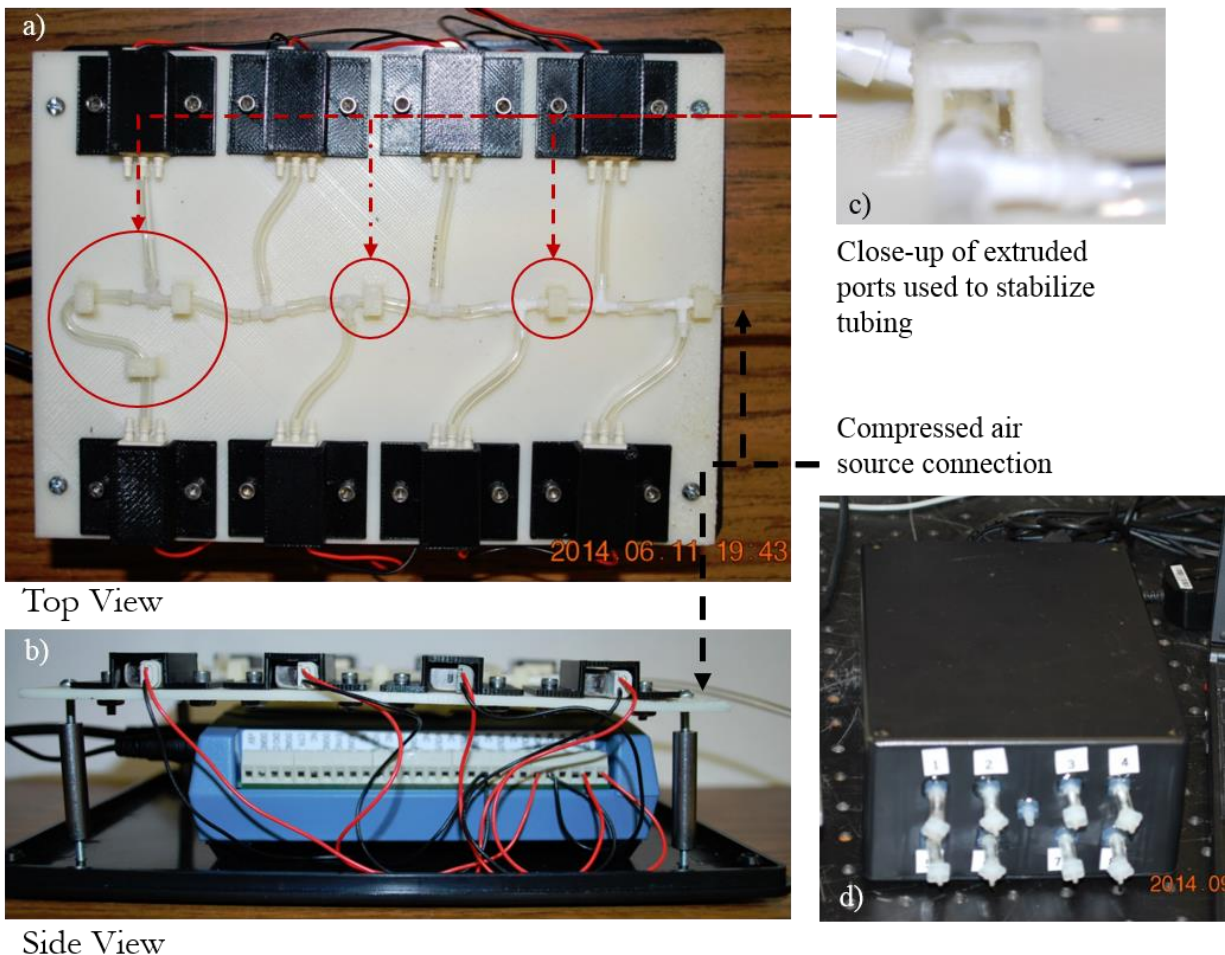


Figure 2.36: Image (a): Top view of enclosure with valves positioned on plate secured with clams and tubing connection. Image (b) Side view of enclosure showing valves wired to signal converter. Image (c): Extruded ports used to stabilize air tubing. Image (d): Fully enclosed box with labeled valve ports.

3D printing was used to create a flat plat (ABS plastic, 6x4x0.2in), which the solenoid valves were positioned. The valves are secured to the plate with 3D printed clamps (fig 2.37). Figure 2.38 shows a schematic of the experimental setup layout for testing the 3D printed micro-pump.

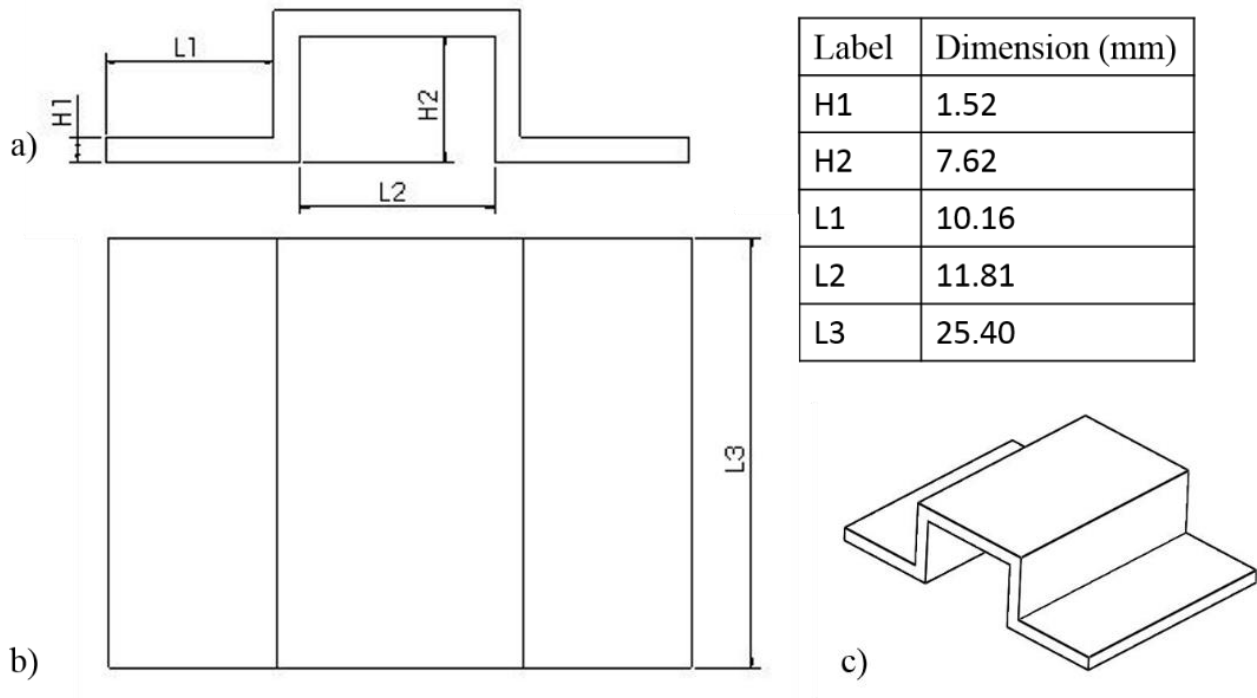


Figure 2.37: Image (a): Cross-section view of clamp with corresponding dimensions. Image (b) Top view of clamp with corresponding dimensions. Image (c): 3D CAD design of clamp

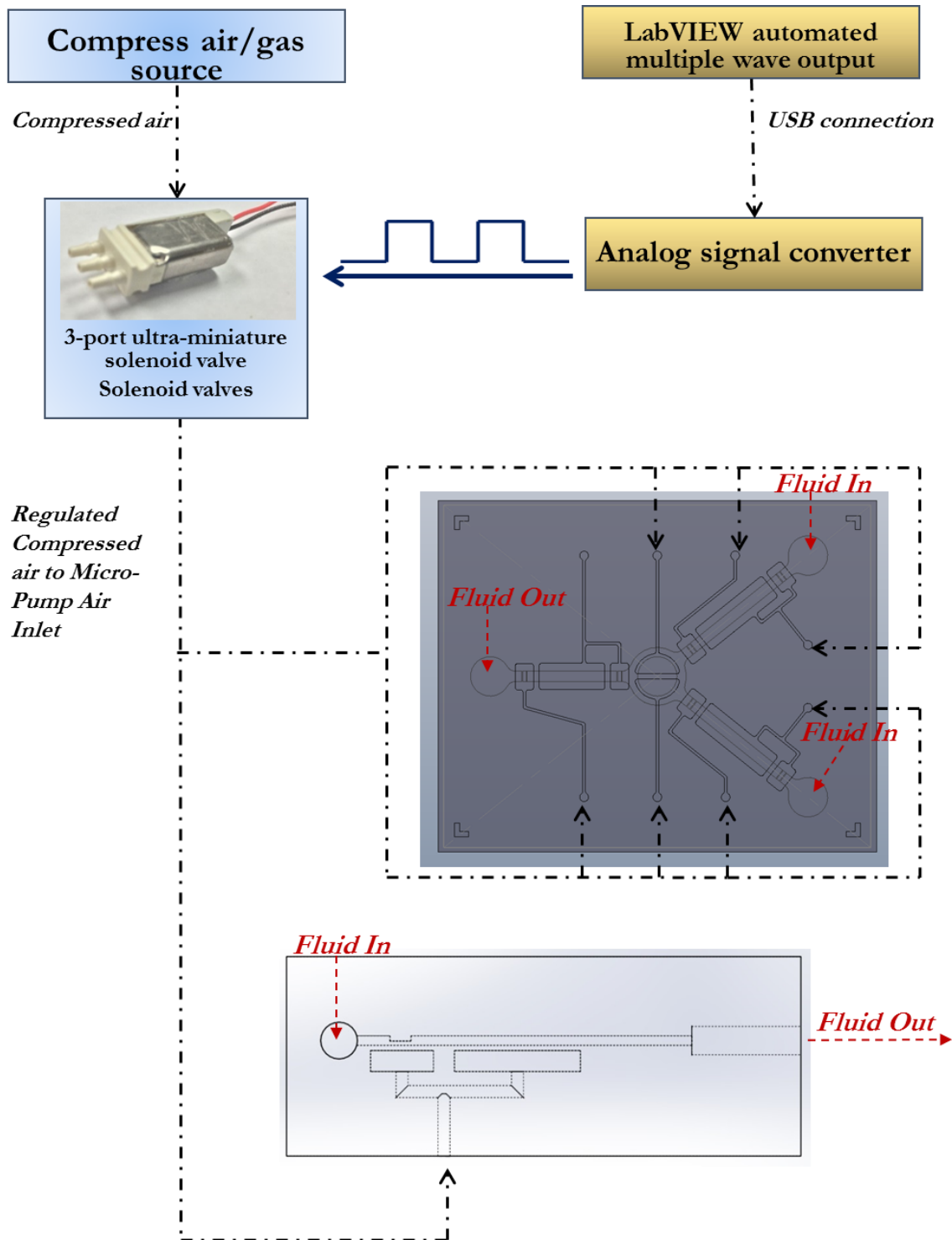


Figure 2.38: Schematic of the experimental setup layout describing the integrated connectivity for operating the PDMS and the 3D printed device

2.4 Hydrophobic and Hydrophilic Testing

PDMS is naturally hydrophobic [25], and a number of techniques have been utilized to modify the surface of PDMS micro channels [26-28]. NinjaFlex has an advantage over PDMS because it has a naturally hydrophilic surface therefore not requiring any surface treatment. A water contact angle (WCA) measurement was utilized to get a better understanding of the PDMS's hydrophobic surface and to characterize the hydrophilic stability of NinjaFlex. A pipette was used to deposit a small droplet of deionized water, mixed with blue dye, onto the PDMS surface and the NinjaFlex surface. The WCA was observed by a Nikon camera (Nikon D5300) using a Macro Lens (Sigma, 50mm, 1:2.8, DG Macro) and measured by Microsoft Power Point. Figure. 2.39 shows the contact angle of the PDMS is about $115^\circ > 90^\circ$ meaning that the water will repel from the surface. The contact angle of NinjaFlex is about $44^\circ < 90^\circ$ meaning that water has an attraction to the material surface.

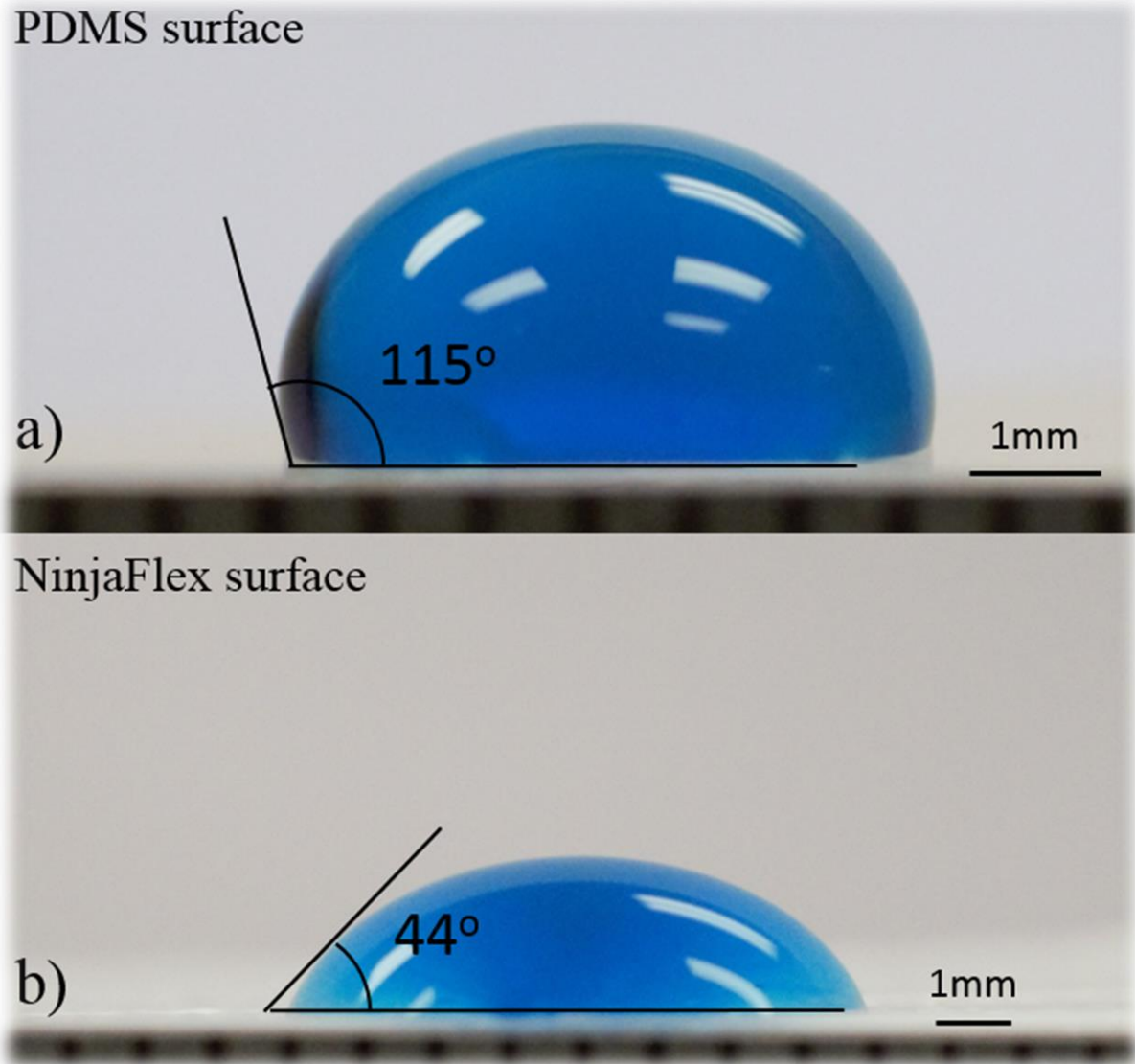


Figure 2.39: Image (a): Hydrophobic test of PDMS with contact angle of about 115°
Image (b): Hydrophilic test of NinjaFlex with contact angle of about 44°

2.5 PDMS surface modification

As stated in the previous section PDMS is a hydrophobic material, which can lead to the formation of air bubbles within a PDMS micro-channel. Bubble would not normally be an issue dealing with fluid flow, however on a micro scale it can be a problem. This can result in blockage in the micro-

channel, as well as interference with biological applications [29]. As previously stated there are many techniques used to treat the hydrophobicity of a material. For this experiment the PDMS surface was treated with Pluronic F108 surfactant (#F018, BASF, Florham Park, New Jersey) to make it hydrophilic. Pluronic has an extremely low toxicity response and therefore will not affect any biological applications of the device [30]. The Pluronic solution was prepared using a 100:1 ratio by which 1g of Pluronic was mixed with 100mL of DI water. Using a syringe the PDMS micro-channel was primed with the Pluronic solution and allowed to sit for at least 1 hour. The surface modification can last up to 1 day, however it was observed that if the solution was allowed to sit longer (i.e. 4 hours) the modification can last a several days.

2.6 Bonding TPE to Glass/TPE to ABS

Typically with microfluidics bonding takes place with PDMS to PDMS or PDMS to glass. However NinjaFlex is very responsive to bonding with oxygen plasma surface treatment, and therefore the bonding capability was observed. The detailed oxygen plasma bonding process is as follows:

The detailed oxygen plasma bonding process:

1. The NinjaFlex, glass, and ABS surface must be cleaned before they are bonded together.

This is to ensure that there are no particles on the surface which can prevent bonding. This process is detailed below:

- The surfaces that will be exposed to the oxygen plasma treatment is first rinsed with DI water.
- Next the surface is rinsed with Isopropyl Alcohol, and then scrubbed gently with a cotton swab.

- The surface is then rinsed again with DI water.
 - It is critical not to touch the surface of the surface. Therefore it is dried using a nitrogen pressure blast.
2. The NinjaFlex layer, glass, and/or ABS are placed inside the Oxygen plasma chamber (Model PC-150, South Bay Technology, Inc., San Clemente, CA) with their bonding sides facing up. The plasma chamber was operated at 20 W forward power and 0 W reverse power, 100-110 mTorr for 20sec.
 3. The bonding technique is similar to the one mention in the oxygen plasma bonding section 2.2.6. Therefore rolling technique should be considered to help reduce the trapping of air and help induce a greater uniformed bond.

Chapter 3. Results and Discussion

Once the devices have been successfully designed and fabricated, performance testing should be implemented to determine its efficiency. This following section will detail the experimental methods utilized in the testing procedures as well as results. A detailed characterization was conducted to get a better understanding of the micro-pump diaphragms in relation to the fluid flow. A mixing assessment was performed utilizing a biological protocol in order to determine the micro-mixers efficiency.

3.1 PDMS Device Testing

In order to evaluate the pumping efficiency of the fabricated devices, a fluid flow performance characterization test was conducted. There are two main control parameters that affect the performance of the micro-pumps, which are the compressed air/gas pressure and the actuation frequency of the diaphragm. In this fluid flow investigation, the flowrate was observed with respect to the diaphragms driving pressure and the diaphragms actuation frequency. To achieve pneumatic actuation, a PTFE tubing (O.D = 1/16", I.D. = 0.04") is connected to the micro-pump's air inlet, while the opposite end was connected into a tygothane tubing (O.D = 1/8", I.D = 1/16") leading from the solenoid valve.

3.1.1 Micro-Pump: Test Setup and Results

The PDMS device fabricated from the PMMA mold and the 3D printed mold were both tested on their pumping efficiency. For simplicity reasons the devices will be referred to as Device 1 (PMMA mold) and Device 2 (3D printed mold). Device 1 and Device 2 performance testing was carried out with a pressure range of 10Psi, 15Psi, and 20Psi with a diaphragm deflection frequency step of 5Hz, 7Hz, 10Hz, 12Hz, and 15Hz. Figure 3.1 shows the test fixture on an optical

table that is used in the flowrate testing. A pipette tip (1-100 μ L) is outfitted at the inlets and outlet of the microfluidic device, to be used as reservoirs to deposit and collect the fluid sample. The micro-channels were first primed with DI water. The diaphragms were then used to close off the micro-channels. At this point, using a pipette, fluid is deposited into the inlet reservoir. The diaphragms are then activated with the respected oscillation frequency. The fluid level will begin to rise in the outlet reservoir with respect time. At this point, after time has passed, the fluid is collected in the reservoir and transferred into a microcentrifuge tube (VWR Int., 1.5mL). The mass of the microcentrifuge taken before and after the addition of the fluid sample to calculate the change in mass. The measurement of the water is in milligrams and then converted microliters which is a 1:1 ratio. The calculated change in volume is taken with respect to the change in time, which results in the volumetric flowrate. The volumetric flowrate was calculated by the following equation:

$$\text{Mass to Volume Ratio } (\Delta m) = (\Delta V) \quad (\text{eq. 3.1})$$

$$\text{Volumetric Flowrate } (Q) = \frac{\Delta V}{\Delta t} \quad (\text{eq. 3.2})$$

where Q is the volumetric flowrate, Δm is the change in mass, ΔV is the change in volume, and Δt is the change in time.

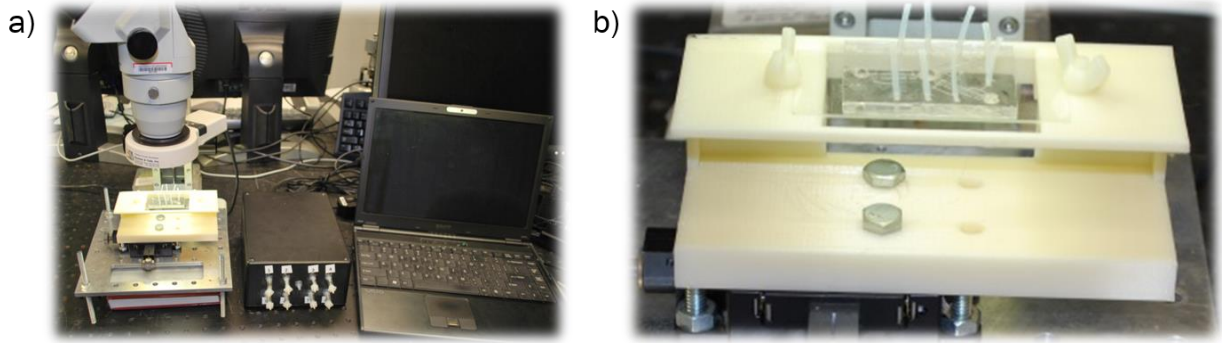


Figure 3.1: Image (a): Test fixture for the PDMS device with project enclosure and computer control system. Image (b): Close up of PDMS test fixture mounted on x-y stage with PTFE tubing connected to air inlets of device.

The life span ratio of the PDMS device for this experiment were low, which means that after multiple used the device would fail due to channel blockage, diaphragm failure, or leakage. This was an occurrence on multiple occasions. Because of this, only limited results for the PDSM devices were achieve. Both device were tested at a driving pressure of 10psi. Device 1 was tested at an actuation frequency of 5Hz-7Hz. Device 2 was tested at an actuation frequency of 5Hz, 7Hz, 10Hz, 12Hz, and 15Hz. Based on the results it is observed that Device 2 has a greater slope than Device 1. This is confirmed in figure 3.2 that shows at 5Hz and 7Hz, which shows that Device 1 has a flow rate of 60 μ L/min and 75 μ L/min and Device 2 has a flowrate of 124.8 μ L/min and 168 μ L/min. The greater flow rate for device 2 is due to the larger area in the micro-channel. Device 1 micro-channel cross-sectional area: 1.2mm x 0.3mm = 0.36mm², Device 2 micro-channel cross-sectional area: 0.9mm x 5mm = 4.5mm². Therefore, the volume of fluid that is displaced in the micro-channel of device 2 is much greater than that of device 1. This is demonstrated in the following equation:

$$\text{Volumetric Flowrate } (Q) = V \cdot f \quad (\text{eq. 3.3})$$

where Q is the volumetric flowrate, V is the volume of fluid in the micro-channel, and f (Hz) is the diaphragm's actuation frequency (Hz).

This equation shows that the fluid volume has a direct relationship with the flowrate, which means if there is an increase or decrease in one variable this causes the same change to occur in the second variable.

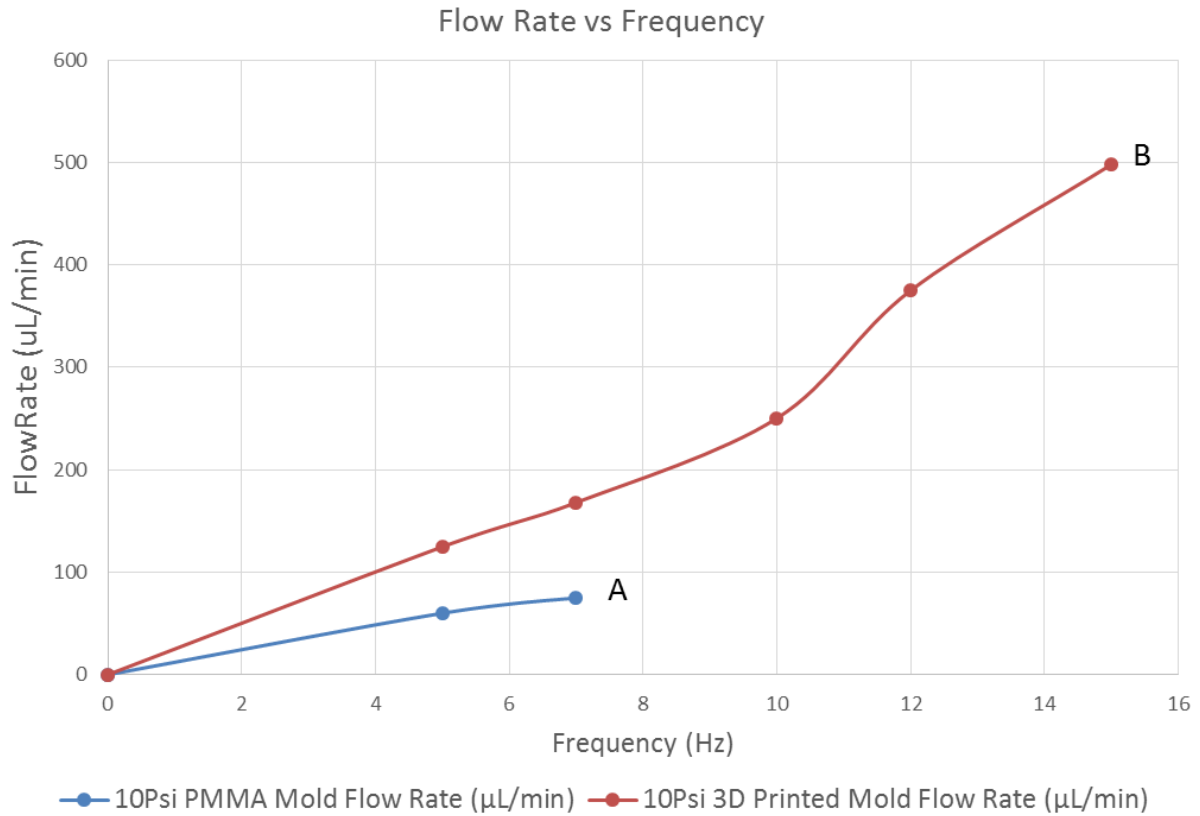


Figure 3.2: Flowrate of micro-pump’s with respect to the diaphragm actuation frequency and driving pressure; Curve (a) (Device 1): 5Hz-7Hz; Curve (b) (Device 2): 5Hz-10Hz

3.2 3D Printed Micro-Pump Testing

3.2.1 Test Setup and Results

The 3D printed micro-pump performance testing was carried out with a pressure range of 20psi, 30psi, and 40psi each with the diaphragm deflection frequency ranging from 10Hz-70Hz.

Figure 3.3 shows the test fixture on an optical table that is used in the flowrate testing. A pipette tip (1-100 μ L) is outfitted at the inlet of the micro-pump. This is used as the reservoir to deposit the fluid sample. Tygonthane tubing is connected to the outlet of the micro-pump. The tubing is elevated at the outlet to match the fluid inlet elevation in order to counteract the effects of gravity driven pressure. The micro-pump was then primed with DI water which is dyed for visibility. The initial position and final position of the fluid front in the outlet tubing was observed and measured with a ruler that was placed next to the tubing (fig. 3.4a & b). The change in the fluid position with respect to the pumping time is used to calculate the velocity of the fluid displacement. The following equations were used to obtain the volumetric flowrate:

$$(\text{velocity}) v = \frac{\Delta x}{\Delta t} \quad (\text{eq. 3.4})$$

$$(\text{volumetric flowrate}) Q = v \cdot A \quad (\text{eq. 3.5})$$

where Q is the volumetric flowrate, v is the velocity, Δx is the fluids change in length, Δt is the time frame of the fluids change in length, and A is the cross-sectional area of the outlet tubing.

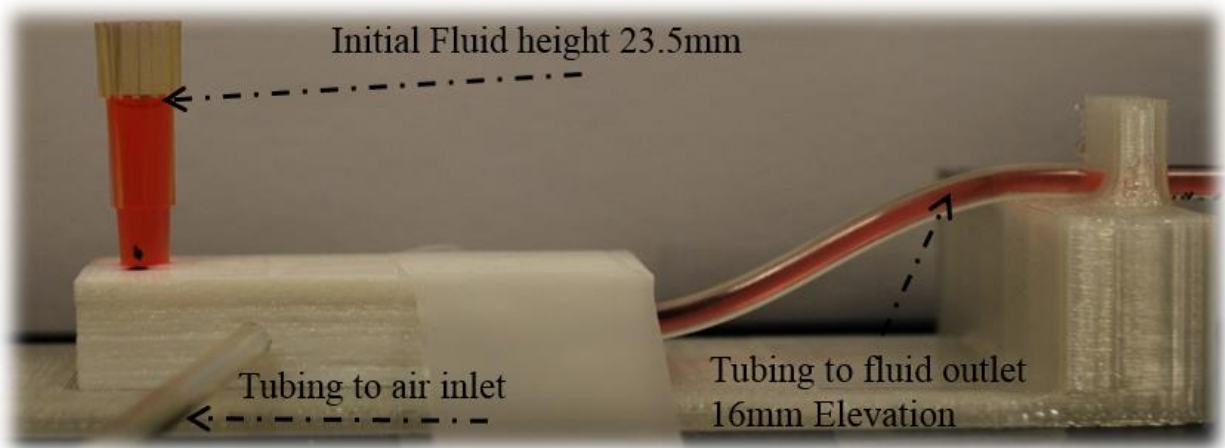


Figure 3.3: Test fixture for the micro-pump testing with the connected components

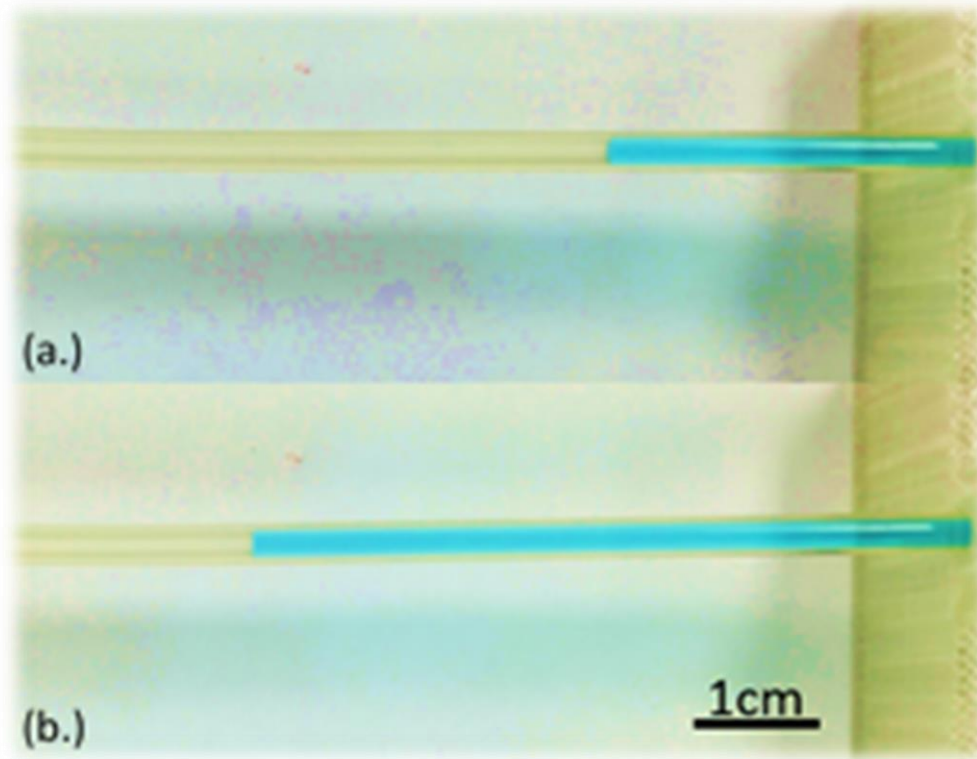


Figure 3.4: Image (a): The initial position of the fluid at $t=0$. Image (b): The final position of the fluid at $t=5s$.

After testing it was noted that a maximum flowrate of $1120\mu\text{L}/\text{min}$ was achieved at an actuation frequency of 10Hz with an applied driving pressure of 40psi (fig 3.5). Prior to flowrate testing, it would be appropriate to assume that if the diaphragms actuation frequency were to continue to increase then so shall the micro-pumps flowrate. However figure 3.5 illustrates that as the flowrate starts to reach its optimal height with respect to the frequency, then the flowrate will begin to taper off and decrease as the frequency continues to increase. This flowrate drop is shown to happen much quickly as the diaphragms driving pressure is increased. As it is also shown in figure 3.5, the 40psi has the highest and most rapidly increase in flowrate, however it has the most rapid decrease in flowrate. This is due to the diaphragms stroke-volume.

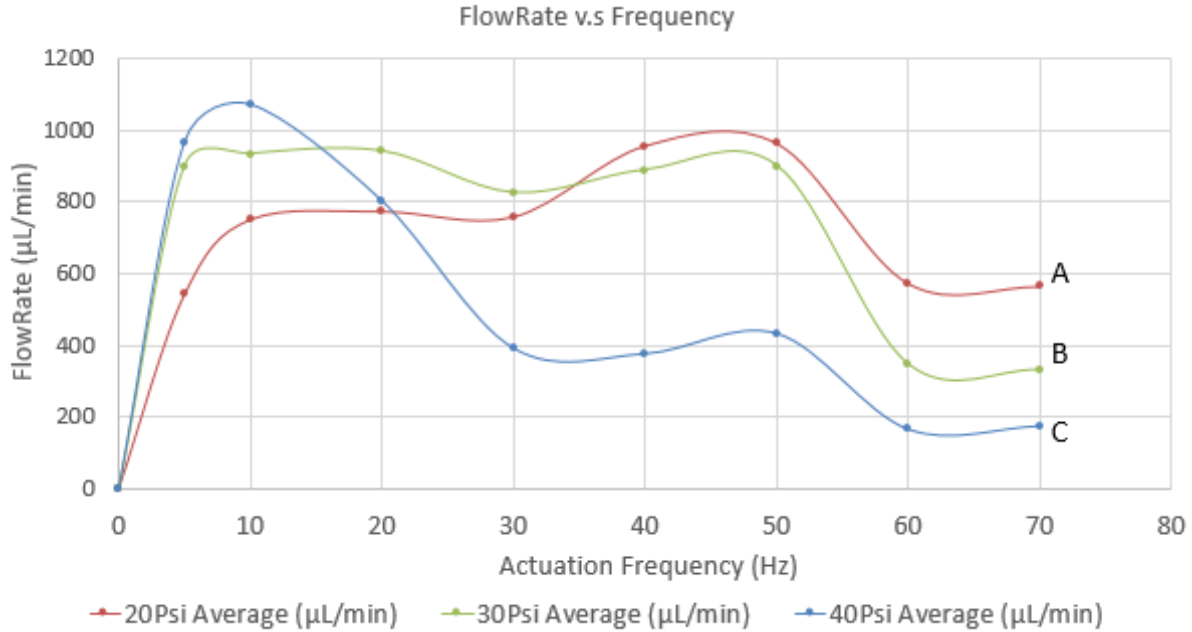


Figure 3.5: Flowrate of micro-pump with respect to the diaphragm's actuation frequency ranging from 10Hz-70Hz; Driving Pressures: Curve (a): 20psi; Curve (b): 30psi; Curve (c): 40psi

3.2.2 Diaphragm Deflection Testing

As stated in the previous section it is observed that the micro-pump reaches an optimal flowrate with respect to the diaphragms actuation frequency. However as the frequency continues to increase it is observed that the flowrate will taper off and decrease. This occurrence is speculated to be from a decrease in the diaphragms stroke-volume. During the actuation of the diaphragm, it expands a maximum volume while also retracting a minimum volume, the difference of the maximum and minimum deflection is the stroke-volume. To study this speculated occurrence a visual study, a surface height study, and a numerical simulation were conducted on the diaphragm of the micro-pump.

Optical Measurement and Results - The visual study was performed with a stroboscope. This device emits a flashing light which if matched correctly with the oscillating frequency of the

diaphragm, then one is able to observe the behavior of the diaphragm. The experiment was carried out at an optimal pressure of 30psi with a frequency range of 10Hz-70Hz. While observed and images captured under a microscope, figure 3.6 illustrates a micro-channel with a (a) diaphragm at rest, and (b) and (c) showing a diaphragm at its maximum and minimum deflection as it actuates at a frequency of 10Hz with a pressure of 30psi.

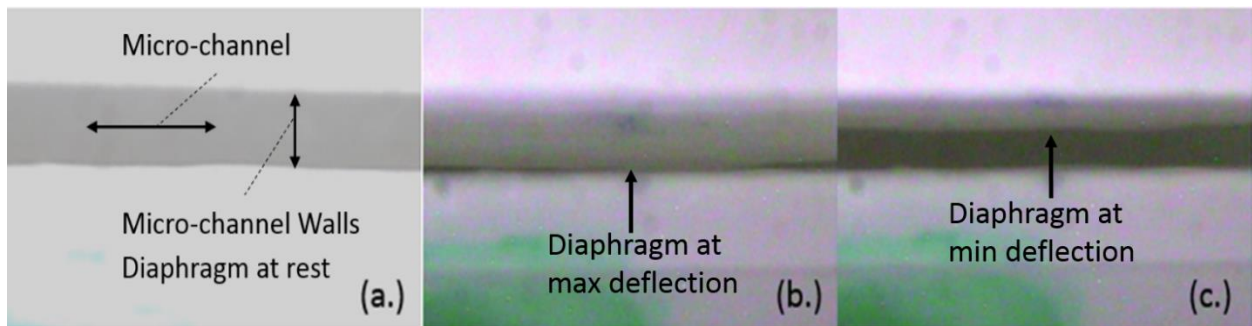


Figure 3.6: Diaphragm at 10Hz deflection frequency with 30psi pressure. Image (a) shows the diaphragm at rest “no deflection”. Image (b) shows the diaphragm at maximum deflection with respect to the open valve. Image (c) shows the diaphragm at minimum deflection with respect to the closed valve.

Figure 3.7 illustrates the diaphragms minimum deflection behavior at a driving pressure of 30Psi with a frequency ranging from 10Hz-70Hz. These images shows that the distance between the diaphragm’s minimum deflection and the micro-channel wall will decrease as the diaphragms actuation frequency increases. This distance between the maximum deflection and the minimum deflection is referred to as the stroke length.

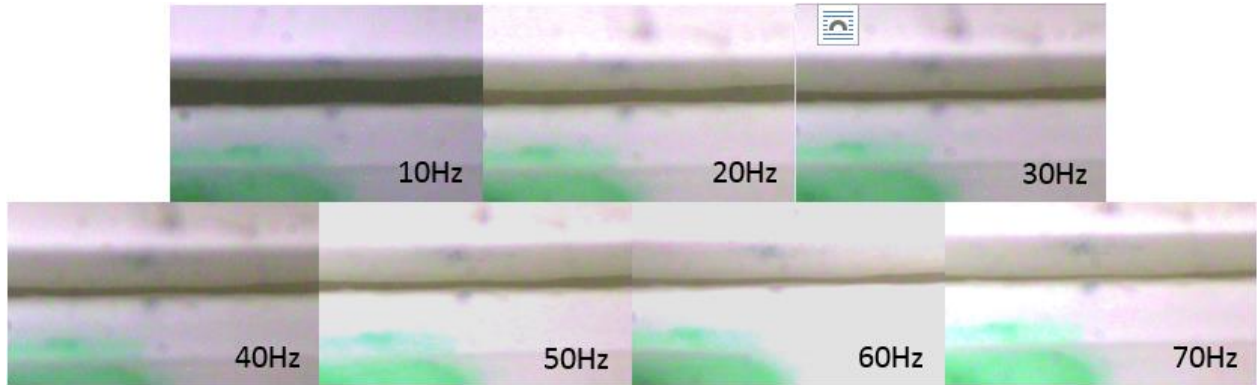


Figure 3.7: This figure shows a sequence of tests with the diaphragm operating at a driving pressure of 30psi, with each image corresponding to its respective frequency. Each image represents the minimum deflection “at rest position” of the diaphragm’s behavior at 10Hz-70Hz.

Quantitative Measurement and Results - The study was performed with a semiconductor laser proximity probe (Keyence, Chicago, IL, LK-2001 laser displacement sensor, with LK-031 Laser) which records the diaphragm’s surface change in distance. An oscilloscope (Agilent, Santa Clara, CA, 54622A Oscilloscope) was used to display the numerical value.

To perform this study, a portion of the micro-pump is secured on a xy-stage directly under the laser with the diaphragm facing up. Compressed air/gas is pumped into the diaphragm chamber causing the diaphragm to deflect. The diaphragm doesn’t deflect uniformly, therefore the xy-stage is used to position the maximum deflected point of the diaphragm under the laser. The point was then noted. The diaphragm was operated at a frequency at which the diaphragm’s maximum and minimum deflection were recorded. The tests were performed with a pressure ranging from 20psi-40psi with a frequency ranging from 10Hz-50Hz. Just like the visual observation in the previous section, these tests confirm that the diaphragm’s minimal deflection will increase as the actuation frequency increases, which results in a decreasing stroke length. The stroke length values were achieved from the following equation:

$$(\text{Stroke length}) \Delta x = x_{max} - x_{min} \quad (\text{eq. 3.6})$$

where Δx is the stroke length, x_{\max} is the diaphragms maximum deflection point, and x_{\min} is the diaphragms minimum deflection point.

At 20Psi at 50Hz has a $x_{\max} = 364.3\mu\text{m}$ and a $x_{\min} = 296.6\mu\text{m}$, resulting in a stroke-length of $67.7\mu\text{m}$. 30Psi at 50Hz has a $x_{\max} = 565.7\mu\text{m}$ and a $x_{\min} = 491.2\mu\text{m}$, resulting in a stroke-length of $74.5\mu\text{m}$. 40Psi at 50Hz has a $x_{\max} = 728.8\mu\text{m}$ and a $x_{\min} = 673.2\mu\text{m}$. These results show that a higher driving pressure will result in a smaller stroke-length. Figure 3.8-3.10 shows the diaphragms maximum deflection behavior with respect to the actuation frequency; it shows the increase of the diaphragm's minimum deflection as the frequency increases; it shows diaphragms resulting stroke-length with respect to the actuation frequency. Figure 3.11 shows a comparative of the diaphragm's 20psi-40psi stroke-length.

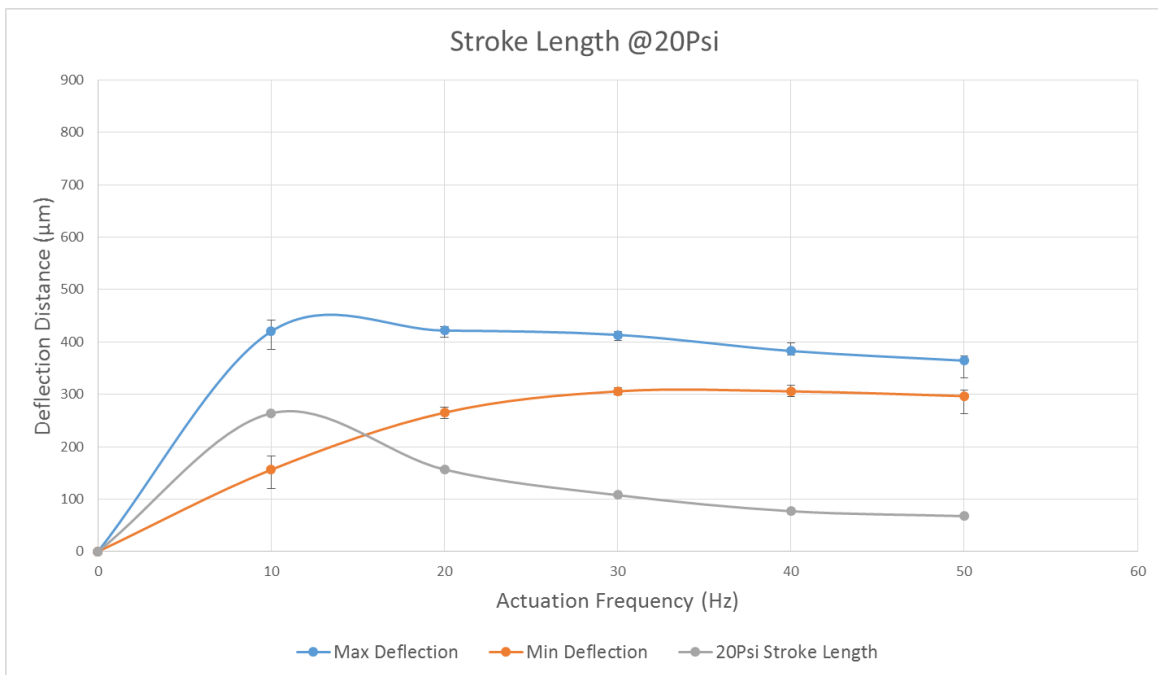


Figure 3.8: 20Psi driving maximum and minimum deflection behavior and resulting stroke-length with respect to actuation frequency

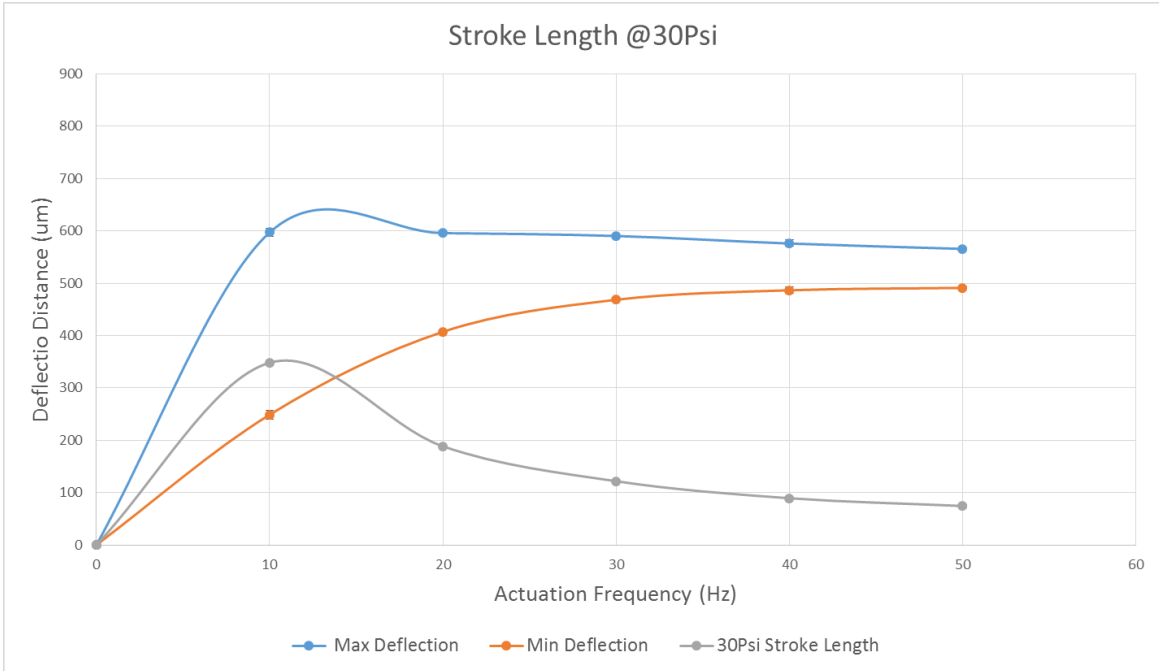


Figure 3.9: 30Psi driving maximum and minimum deflection behavior and resulting stroke-length with respect to actuation frequency

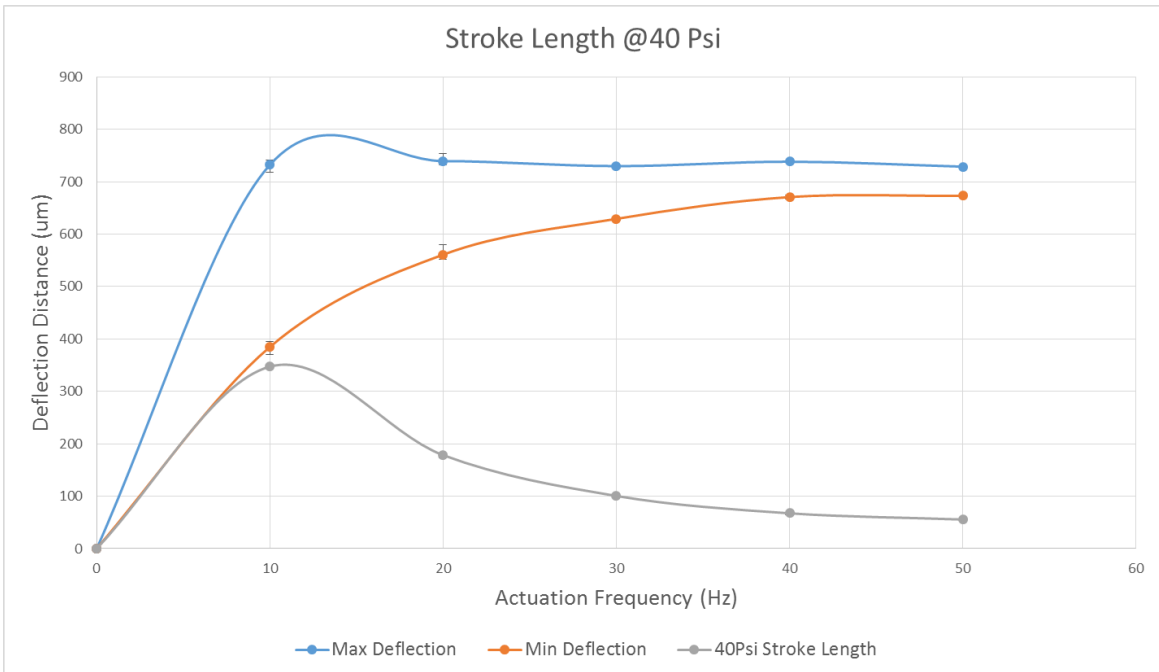


Figure 3.10: 40Psi driving maximum and minimum deflection behavior and resulting stroke-length with respect to actuation frequency

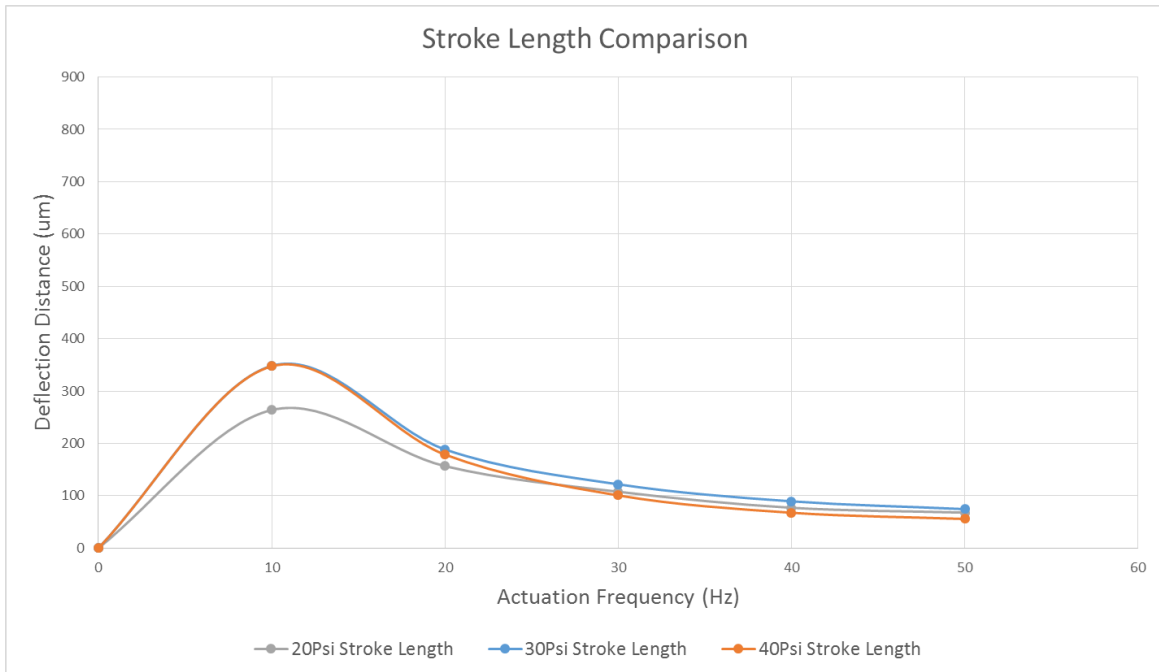


Figure 3.11: Stroke-length comparison for 20Psi-40Psi driving pressures per actuation frequency

Numerical Simulation and Theoretical Flowrate Results - A theoretical volumetric flowrate was calculated to compare to the experimental flowrate results. The theoretical volumetric flowrate is obtained by multiplying the stroke-volume with the respective actuation frequency. SolidWorks' simulation package was utilized to obtain the diaphragm's stroke-volume. A modeled diaphragm was simulated to deflect the maximum and minimum stroke-lengths from the values obtained in the previous section (figure 3.12). The simulation was modeled under the conditions of a plat rectangular plate with clamped edges that has a distributed uniform load applied (figure 3.13).

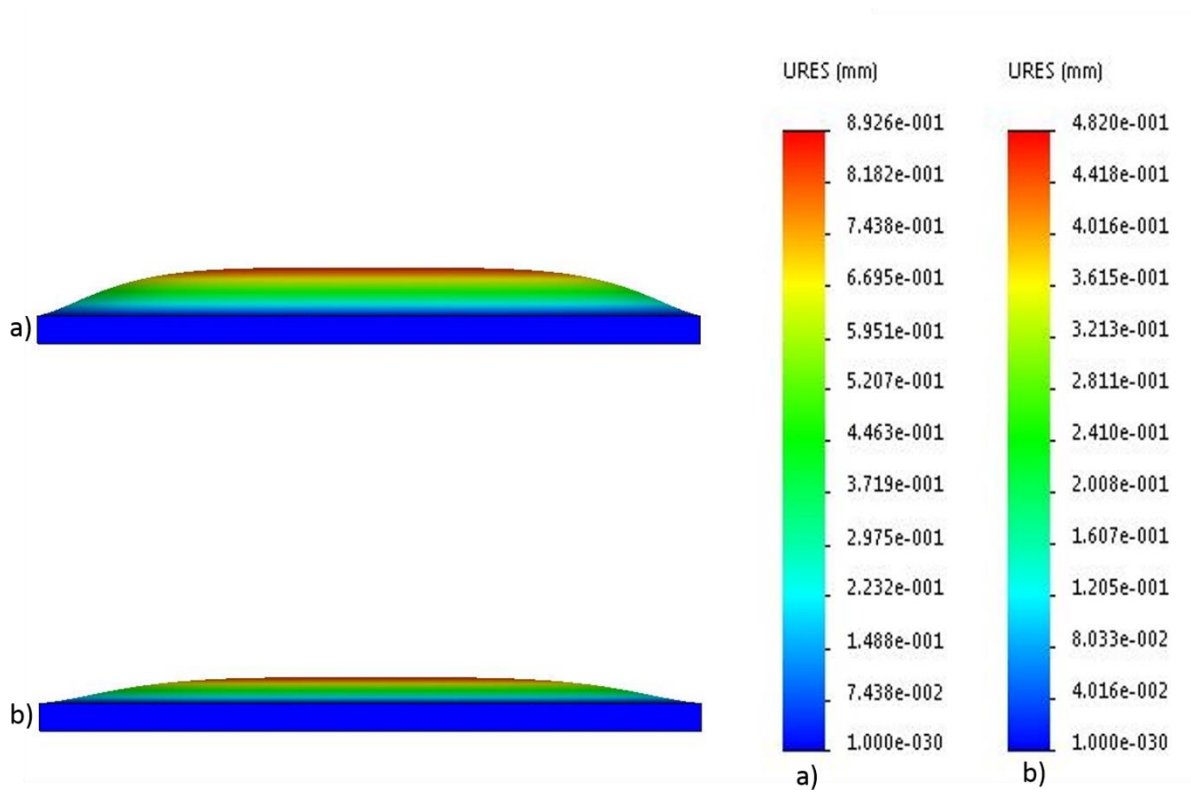


Figure 3.12: SolidWorks Diaphragm Deflection Simulation. Image (a): Maximum Deflection
Image (b): Minimum Deflection

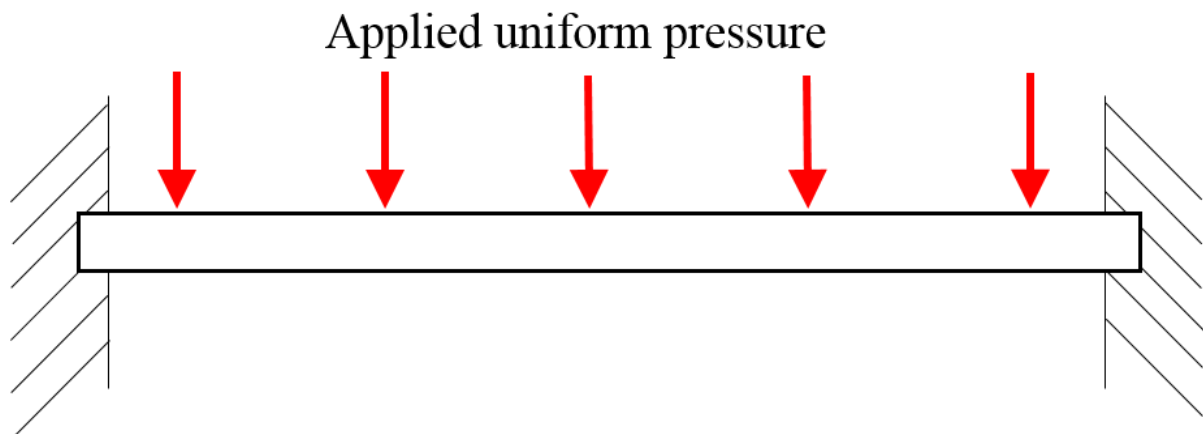


Figure 3.13: Flat plate with clamped edges and applied uniform pressure

Based on the simulated deflections, the maximum and minimum diaphragm volume was calculated, and the difference of the two result in the stroke-volume. Table 1 shows the obtained stroke-volumes with the corresponding driving pressure and actuation frequency. The stroke volume and theoretical flowrate were obtained using the following equations:

$$\text{Stroke Volume } (\Delta V) = V_{max} - V_{min} \quad (\text{eq. 3.7})$$

$$\text{Actuation Frequency } (f) = \frac{1}{s} \quad (\text{ep. 3.8})$$

$$\text{Theoretical Flowrate } (\dot{V}) = \Delta V \cdot f \quad (\text{eq. 3.9})$$

where ΔV is the diaphragms stroke volume, V_{max} and V_{min} are the diaphragms maximum and minimum volume displaced, \dot{V} is the theoretical flowrate, and f is the diaphragms actuation frequency.

Table 1: Minimum and Maximum Volume Displacement and resulting Stroke-Volumes

20psi				30psi				40psi			
Hz	Minimum Deflection Volume (μL)	Maximum Deflection Volume (μL)	Stroke-Volume (μL)	Hz	Minimum Deflection Volume (μL)	Maximum Deflection Volume (μL)	Stroke-Volume (μL)	Hz	Minimum Deflection Volume (μL)	Maximum Deflection Volume (μL)	Stroke-Volume (μL)
0	0	0	0	0	0	0	0	0	0	0	0
10	3.7	10.3	6.6	10	5.87	15.2	9.33	10	9.36	19	9.64
20	6.11	10.3	4.19	20	9.89	15.1	5.21	20	14.1	19.2	5.1
30	7.24	10.1	2.86	30	11.5	14.9	3.4	30	16	18.9	2.9
40	7.24	9.31	2.07	40	12.1	14.5	2.4	40	17.3	19.2	1.9
50	7.08	8.82	1.74	50	12.3	14.2	1.9	50	17.3	18.9	1.6

a)

b)

c)

Figure 3.14 shows the resulting theoretical flowrate obtained from the stroke-volume calculation. Figure 3.15-17 shows a normalized theoretical flowrate compared to its experimental counterpart. The graphs indicate that even though the values are slightly skewed from the experimental values, they still follow the same trend of reaching an optimum flowrate height, tapering off to a decline in flowrate. This displacement of the theoretical values and the experimental values is possibly be due to a number of reasons. One could be that the diaphragm in the numerical simulation has an exact thickness of 500 μm , but the actual diaphragm thickness could range from 400 μm - 600 μm . Another could be that the values achieved from the “Diaphragm Surface Displacement Measurement” section may slightly be off due to the additional noise that was picked up from the instruments used during the measurement.

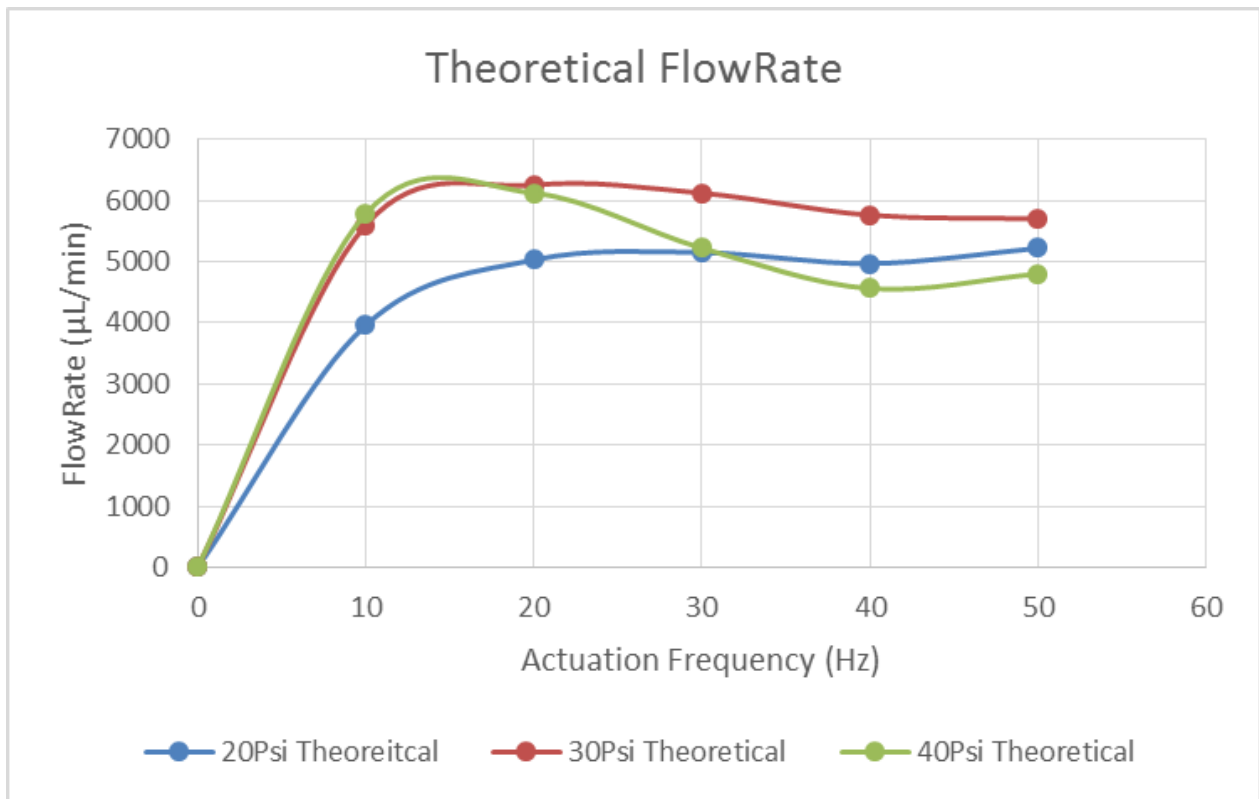


Figure 3.14: Theoretical Flowrate results

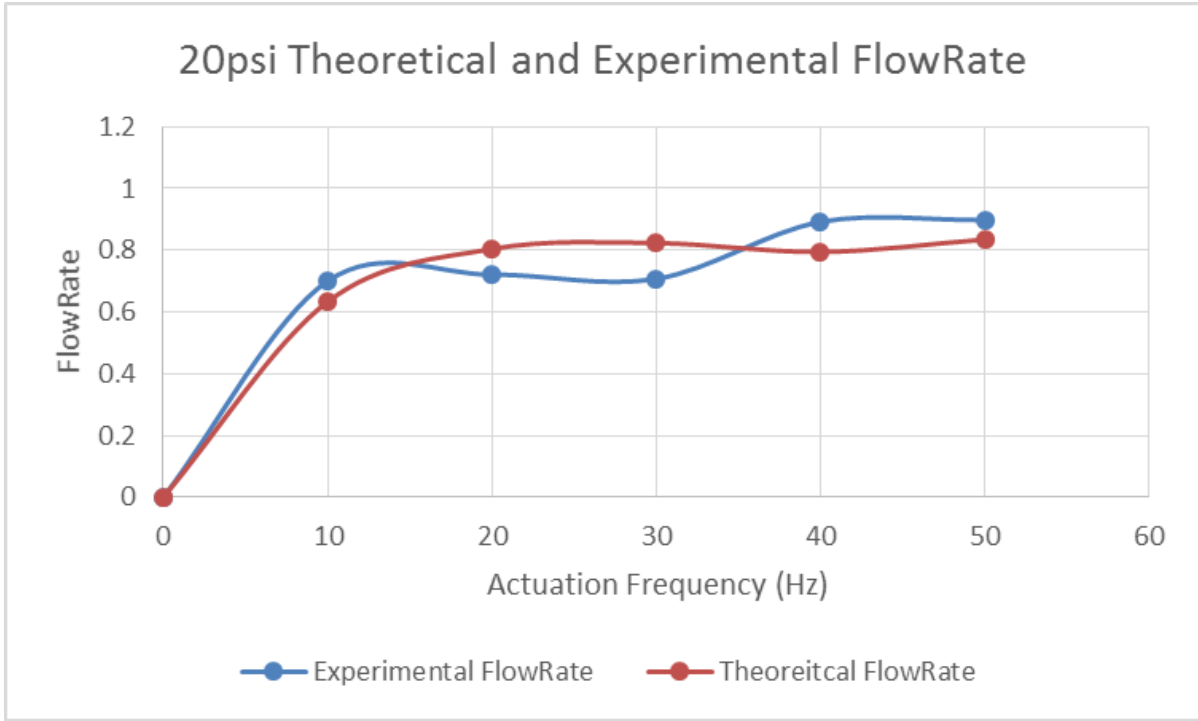


Figure 3.15: Normalized Theoretical and Experimental Flowrate comparative at 20psi

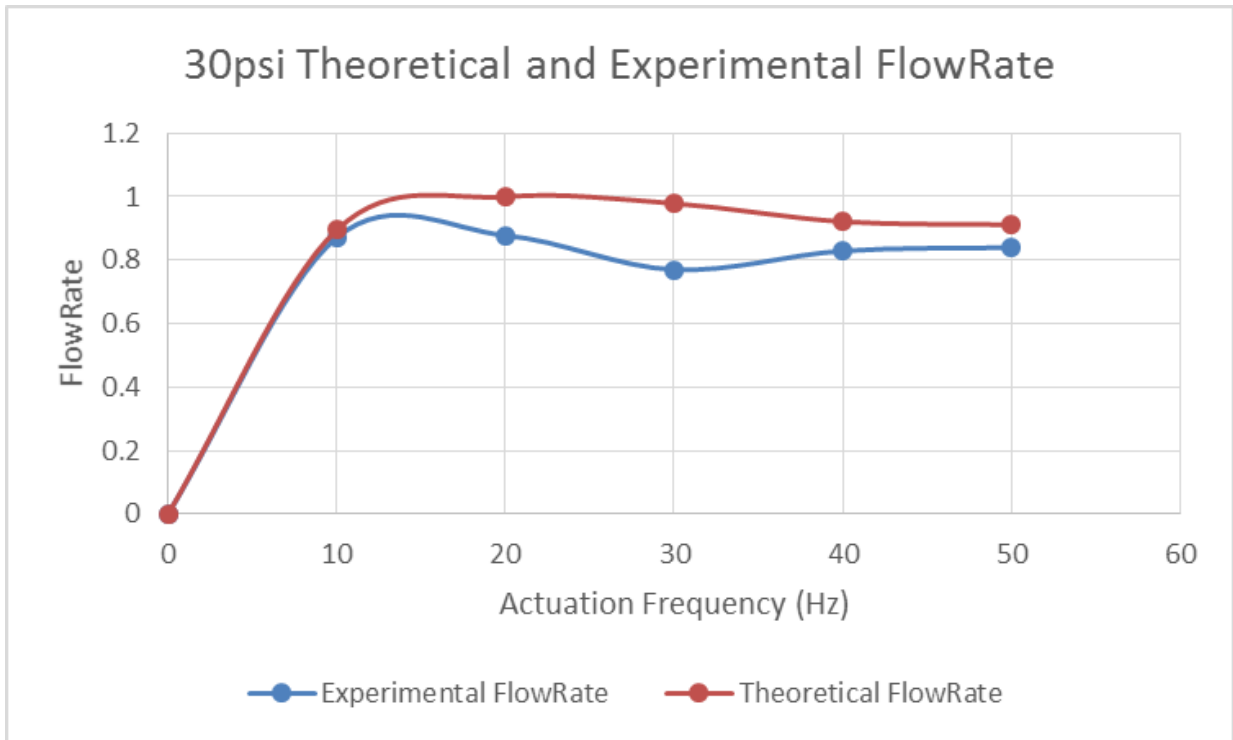


Figure 3.16: Normalized Theoretical and Experimental Flowrate comparative at 30psi

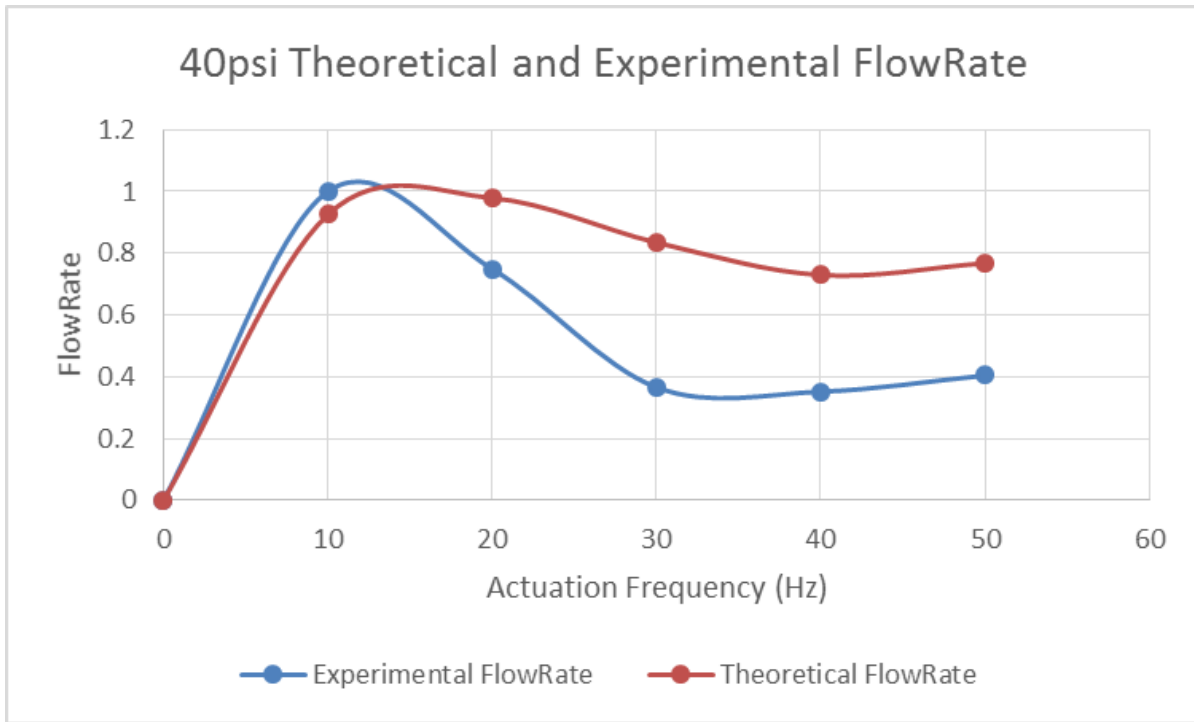


Figure 3.17: Normalized Theoretical and Experimental Flowrate comparative at 40psi

Correlation between Stroke Volume and Flowrate - The valve, which controls the air/gas flow, opens and closes according to the governed frequency. The diaphragms responds by expanding and retracting as air/gas is introduced into the air chamber and is expelled from the diaphragms air chamber due to the elastic properties of the Ninja Flex material. However the mechanical structure of the diaphragm cannot keep pace with the air/gas i.e. the diaphragm will expand and retract as much as possible with respect to the air/gas flow frequency but will not always reach its maximum expansion point or its minimum retraction “at rest” point. The stroke volume has a direct relation to the flowrate which is indicated form equation 3.8. This indicates that if there is increase or decrease in the stroke volume this will cause the flowrate to increase or decrease.

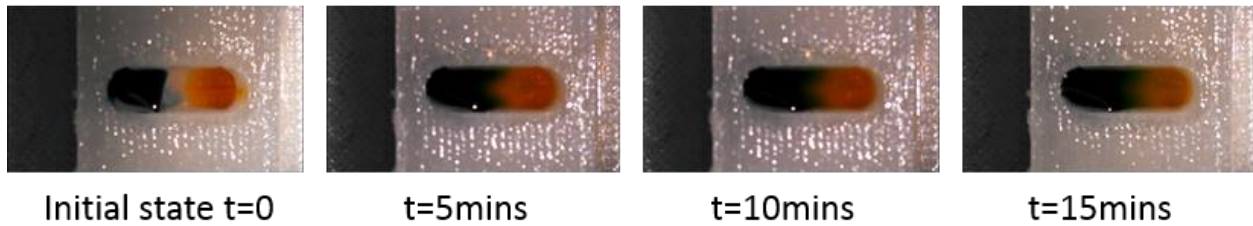
3.3 3D Printed Micro-Mixer Testing

3.3.1 Test Setup and Results

In order to evaluate the efficiency of the fabricated micro-mixer, a qualitative mixing performance assessment was conducted. Just like the micro-pump, the two main control parameters that affect the performance of the micro-mixer, are the compressed air/gas pressure and the actuation frequency of the diaphragm. In this mixing investigation, the fluid was observed with respect to the diaphragms “at rest” and the diaphragms “active”. To achieve pneumatic actuation, the same type of PTFE tubing used in the pumping test is also connected to the micro-mixer’s air inlet, while the opposite end was connected into a tygothane tubing leading from the solenoid valve.

The micro-mixer performance testing was carried out with a pressure of 30psi with the diaphragm deflection frequency at 10Hz. This is because it is noted that during the micro-pump test the optimal fluid flow for all pressures was reached at 10Hz. The micro-mixer reservoir was first primed with 300 μ L of DI water. Next, 0.3 μ L of a blue dye and 0.3 μ L of yellow dye are deposited into separate ends of the micro-mixer reservoir. A stationary test is performed first with the diaphragms at rest or “off”. During the stationary test it is observed that through molecular diffusion the blue dye and yellow dye partially mix over a course of 30mins. Next an active test is performed with the diaphragms actuated at a frequency of 10Hz with an air/gas pressure of 30psi. During the active test it is observed that the molecular diffusion is accelerated via chaotic convection, therefore the blue dye and yellow dye completely mix over a course of 15mins (fig. 3.18).

a) Inactive Diaphragms “at rest”



b) Active Diaphragms actuate at 10Hz 30Psi

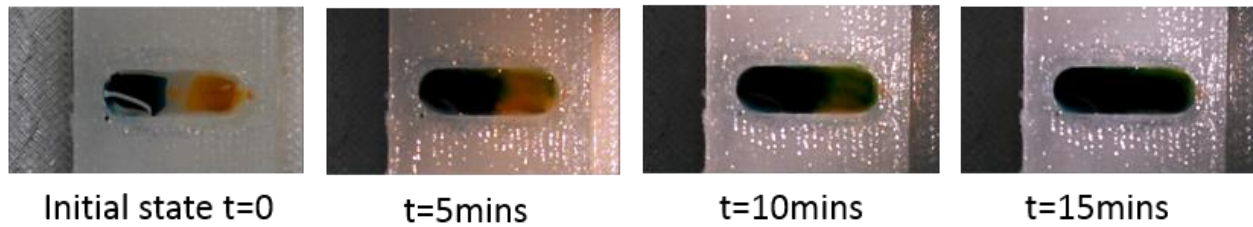


Figure 3.18: Image (a): Inactive diaphragms, unassisted diffusion process with at varying times. Image (b): Active diaphragms assisted diffusion at varying times.

3.3.2 Biological Testing

An *E. coli* capturing efficiency test was performed with the micro-mixer compared with that of a macro-scale rotator-mixer (Grant-bio, PTR-30, Shepreth, Cambridgeshire, England). A micro-mixer and a rotator-mixer were used to mix *E. coli* with anti-*E. coli* antibodies coupled with magnetic microbeads. After this the cell culture was plated, and allowed to incubate overnight. The plated cell culture is then removed from incubation where newly formed cell cultures are observed.

Materials - The materials used in the biological testing are described as in the following. *Escherichia coli* O157:H7 was purchased from American Type Culture Collection (ATCC 43888) and stored in brain heart infusion broth (BHI, Remel Inc., Lenexa, KS) at -80 °C. The culture was grown in brain heart infusion broth BHI at 37 °C for 18 h. For enumeration the culture was serially diluted in phosphate buffered saline (PBS; 0.01 M; pH 7.4; Sigma-Aldrich, St. Louis, MO) and

plated on tryptic soy agar (TSA, Becton-Dickinson, Spark, MD) incubated at 37 °C for 22-24 h. Due to biosafety concerns, the bacteria testing was performed in a BSL II laboratory. Magnetic microbeads (Fe₃O₄; ~1 μm diameter, 10 mg/mL) coated with streptavidin suspended in 10 mM PBS were purchased from Ocean NanoTech (San Diego, CA) and diluted to 1 mg/ml before testing. Phosphate buffered saline (PBS; 0.01 M; pH 7.4) was purchased from Sigma Aldrich (St. Louis, MO). Bovine Serum Albumin (BSA, 3% in 0.01 M PBS) was purchased from Sigma-Aldrich, St. Louis, MO. Biotin-labeled anti-*E. coli* antibody was purchased from Meridian Life Science (Memphis, TN) and diluted to 0.4-0.5 mg mL⁻¹ with PBS for use in tests. All solutions were prepared with deionized water from Millipore (Milli-Q, 18.2 MΩ cm, Bedford, MA).

NinjaFlex Toxicity Testing - The NinjaFlex material was first tested to determine if it had any toxic characteristics that would be detrimental to *E. coli* cell growth. To begin, 1 ml 3% BSA was added to a number micro-centrifuge tubes and mix in the rotator- mixer for 1 hour. The BSA was discarded, then the tubes were centrifuged for several seconds to push the rest of the BSA to the bottom of the tubes. The rest of the BSA is discarded, making sure none remains in the tubes. Next 1 ml 10³ cfu/ml *E. coli* and the NinjaFlex material were added to each of the tubes. One of the tubes only *E. coli* was added, this was the control for the experiment. The mix is allowed to incubate for 45 min. Each tube is diluted 10 fold, and is plated at x10³ and x10² concentration. After incubation, the tubes with *E. coli* and NinjaFlex were compared to the tube with just *E. coli* to see how much bacteria, if any, was killed or lost due to the material. It was concluded that the bacteria plate counts for both the tube with NinjaFlex and the tube without NinjaFlex were the same. Which indicates that the NinjaFlex isn't toxic to *E. coli* cell growth.

Biological Sample Preparation - To begin with, each tube was coated with 800 μL of 3% BSA and rotated at 15 rpm for 1 hr to block the tube sides so no microbeads would stick to the tube.

Tubes with antibody-coated microbeads were prepared by mixing 10 μL of magnetic microbeads with 10 μL of anti-E. coli O157:H7 antibody in 200 μL of PBS for 45 min in a rotating mixer at 15 rpm. A magnetic field (~ 1.3 T) was applied using a magnetic separator consisting of six permanent magnets (Aibit LLC, Jiangyin, China) for 3 min and the bead/antibody complexes were washed once with 200 μL of PBS. A 200 μL sample of 103 cfu/mL E. coli O157:H7 was added to two different tubes containing antibody-coated microbeads and diluted with 100 μL of PBS for a total of 300 μL for each tube. Another antibody-coated microbead tube was filled with 300 μL PBS as a negative control. One last tube without antibody-coated microbeads was filled with a 200 μL sample of 103 cfu/mL E. coli O157:H7 and 100 μL PBS to form a positive control.

E. Coli Capturing Efficiency Test and Results - The first test was conducted with the rotator-mixer, where all of the tubes were mixed for 15 min except one of the antibody-coated microbead tubes prepared with a sample of 103 cfu/mL E. coli O157:H7 and 100 μL PBS, which was allowed to remain still for 15 min (no mixing). The next set of tubes samples were mixed using the micro-mixer. The tube samples were mixed using a driving pressure of 30Psi with an actuation frequency of 0Hz (no mixing), and 10Hz-40Hz (active mixing) for a time of 15 min. After the mixing period, all tubes were magnetically separated for 3 min, and re-suspended in 300 μL PBS. Both the waste and the captured cell solutions were plated (100 μL per plate) for capture efficiency results. The mixer was washed with 1:700 quaternary ammonium sanitizer at first, and then thoroughly with water to return the mixer to a clean state. This wash process was repeated for every mixing test, to recreate the same mixing conditions per test. The capture efficiency was calculated by the following equation:

$$CE(\%) = \frac{N_c}{N_o} \times 100 \quad (\text{eq. 3.9})$$

where CE is capture efficiency (%), N_c is the number of captured cells, and N_o is the number of original cells. . Figure 3.19 illustrates the process flow for the E. coli mixing and cell capturing procedure.

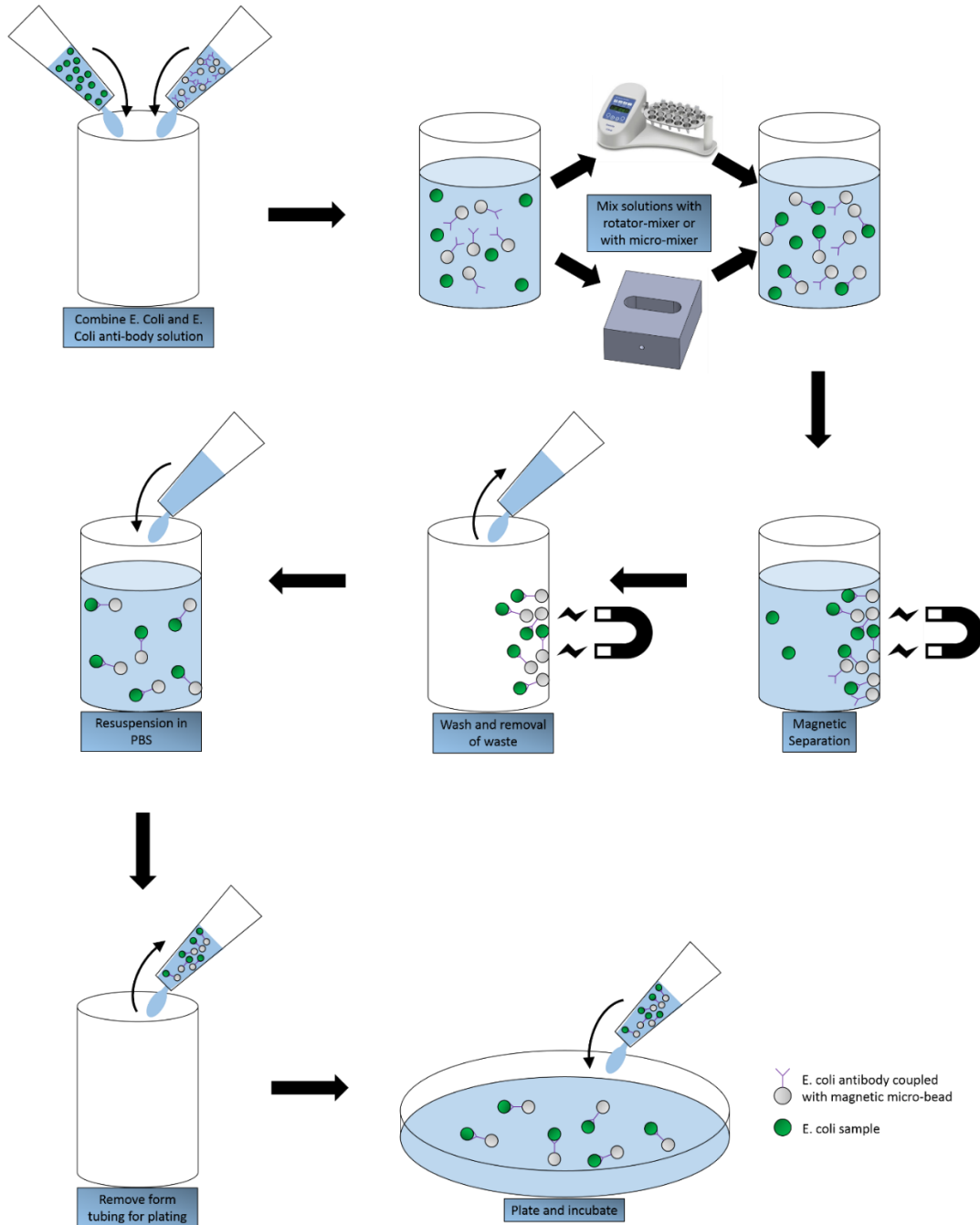


Figure 3.19: Process flow of mixing and E. coli cell capturing process

Testing indicated that the rotator-mixer was able to produce a capturing efficiency (CE) of 80% while the micro-mixer produced a maximum CE of 51%. This is mainly because the rotator-mixer is used commercially and therefore has been optimized over the years. The results showed that the capturing efficiency would be roughly the same despite the change in the actuation frequency. The micro-mixer is a relatively new concept and has yet to be optimized, therefore the proof of concept is what was being tested in the experiment. The concept of mixing is proven by comparing the micro-mixer's "no mixing" test with the "active mixing" test. These results show that the "no mixing" test has a CE of 30%, comparing that to the "active mixing" CE of 51%. This indicates that some E. coli cell capturing takes place however more capturing can be produced from the diaphragm mixing. Figures 3.20 show the increases in E. coli cell capturing efficiency for all the frequency cases for the micro-mixer; it shows the capturing efficiency of the rotator mixer.

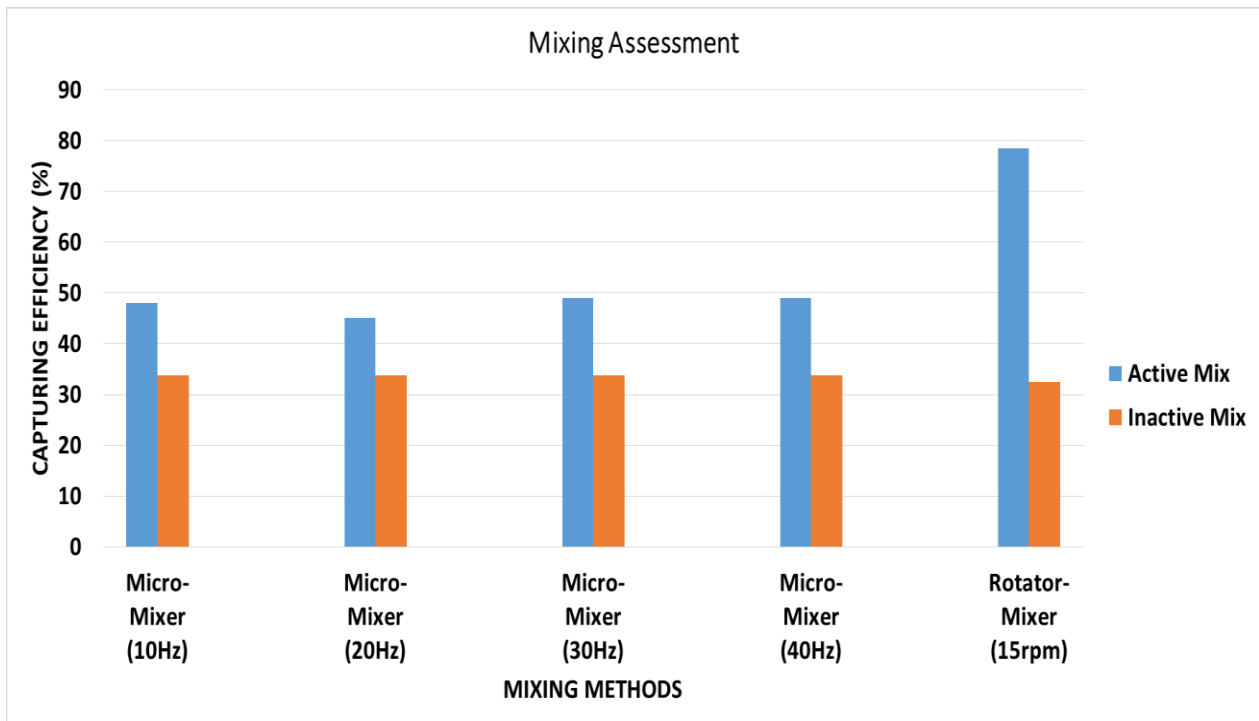


Figure 3.20: Active and Inactive capturing efficiency for micro-mixer at varying operating frequencies and rotator-mixer

Chapter 4. Conclusion

An established protocol was used to successfully fabricate a PDMS microfluidic device. In addition, rapid prototyping was utilized to 3D print a micro-mold to fabricate a PDMS microfluidic device. Performance testing indicated that Device 2 has larger flowrate of $124.7\mu\text{L}/\text{min}$ which was taken at 5Hz. Device 2 also has a greater rate of change of 21.5 which was taken at a frequency range of 5Hz-7Hz.

This study demonstrated a new methodology for fabricating a micro-pump and micro-mixer with the use of the fused deposition modelling technique of 3D printing. This study also demonstrates that Ninja Flex, a Thermal Plastic Elastomer, can be an alternative material for PDMS. The fluid flow capability of the micro-pump was established through flowrate characterization tests. These tests show that the micro-pumps optimal fluid flow output in relation to the driving pressure at 40Psi and the diaphragms actuation frequency at 10Hz was $1120\mu\text{L}/\text{min}$. These tests also demonstrate that after the optimal flowrate is reached then it will decrease as the actuation frequency increases. A stroboscope test visually confirmed that the diaphragms stroke-length will start to decrease as the actuation frequency increases. A semiconductor laser proximity probe was used to determine numerical values of the decreasing stroke-length in relation to the actuation frequency. It was determined that as the frequency of the compressed air/gas flow increases there is a decrease in the stroke volume. This is a result from the diaphragms deflection and retraction response time.

A micro-mixer performance test was successfully accomplished for comparing both inactive and active conditions. The results showed that with fluid agitation the two dye samples completely mixed at a rate of 15min as opposed to the inactive condition in which the two dye

samples did not completely mix. The E. coli cell capturing test also showed that the active mixer resulted in a higher cell capturing efficiency in comparison to the inactive mixer condition.

Through the practice of rapid prototyping, a new method of microfabrication with the use of thermoplastic-elastomer and the 3D printing technique of fused deposition modelling has been demonstrated to be an effective method as well as an alternative method of micro-fabrication.

Chapter 5. Future Work

5.1 Incorporation of Shut off Valve

In the present study, the micro-pump is a continuous flow and there is no way to stop the fluid flow. Therefore the inclusion of a shut off valve would help expand the current design and allow for a performance of multiple process. The incorporation of a shut off valve would allow the integration of a micro-mixer

5.2 Integrated Micro-pump with Micro-Mixer

The present study designed the micro-pump and the micro-mixer as two separate components. The integration of both components would optimize the design into an all in one device, which are the current bar that is set from the PDMS devices that are generally used.

5.3 3D Printing Resolution

Optimizing the print resolution would allow for a higher quality print. A higher quality print would mean that the printer would less likely produce any holes in the device pump or mixer. This would also assist in creating features that would be beneficial to the optimizing the design of the devices.

References

- [1] Ashraf, M., Tayyaba, S., & Afzulpurkar, N. (2011). Micro Electromechanical Systems (MEMS) Based Microfluidic Devices for Biomedical Applications. *IJMS International Journal of Molecular Sciences*, 3648-3704.
- [2] D. J. Beebe, G. A. Mensing and G. M. Walker, *Annu. Rev. Biomed. Eng.*, 2002, 4, 261–286.
- [3] Maluf, N. and K. Williams, *Introduction to microelectromechanical systems engineering2004*: Artech House.
- [4] Hsu, T. *MEMS & Microsystem Design and Manufacturing*, 1st ed.; McGraw-Hill: New York, NY, USA, 2002.
- [5] Ho, C., Ng, S., Li, K., & Yoon, Y. (n.d.). 3D printed microfluidics for biological applications. *Lab Chip*, 3627-3637.
- [6] P. N. Nge, C. I. Rogers and A. T. Woolley, *Chem. Rev.*, 2013, 113, 2550–2583.
- [7] Grayson, A.R.; Shawgo, R.S.; Johnson, A.M.; Flynn, N.T.; Yawen, L.; Cima, M.J.; Langer, R. A BioMEMS review: MEMS technology for physiologically integrated devices. *Proc. IEEE* 2004, 92, 6–21.
- [8] Karman, S.; Ibrahim, F.; Soin, N. A review of MEMS drug delivery in medical application, *Biomed 06. Proc. IFMBE* 2007, 15, 312–315.
- [9] Edel, J.B. and A. De Mello, *Nanofluidics: nanoscience and nanotechnology2009*: Royal Society of Chemistry.
- [10] Chin, C.D., V. Linder, and S.K. Sia, *Lab Chip. 2007*: p. 7, 41–57.
- [11] Ghallab, Y.H. and W. Badawy, *Lab-on-a-chip: techniques, circuits, and biomedical applications2010*: Artech House.
- [12] Au, A., Bhattacharjee, N., Horowitz, L., Chang, T., & Folch, A. (n.d.). 3D-printed microfluidic automation. *Lab Chip*, 1934-1941.
- [13] Xing, W. and J. Cheng, *Frontiers in Biochip Technology*. Boston, MA: Springer Science+Business Media, Inc., 2006.
- [14] Au, A. K. 2014. 3D-printed microvalves and micropumps, *International Conference on Miniaturized Systems for Chemistry and Life Sciences*, San Antonio, Texas, 2014. San Antonio, TX: Royal Society of Chemistry
- [15] E. C. Spivey, B. Xhemalce, J. B. Shear and I. J. Finkelstein, *Anal. Chem.*, 2014, 86, 7406–7412.
- [16] A. Bonyár, H. Sántha, B. Ring, M. Varga, J. Gábor Kovács and G. Harsányi, *Procedia Eng.*, 2010, 5, 291–294.

- [17] A. K. Au, W. Lee and A. Folch, *Lab Chip*, 2014, 14, 1294–1301.
- [18] P.K. Yuen, “SmartBuild – A Truly Plug-n-Play Modular Microfluidic System,” *Lab Chip*, 8, 1374-1378, 2008.
- [19] C. W. Hull, *Journal*, 1986.
- [20] Wong, K. V., & Hernandez, A. (2012). A review of additive manufacturing. *ISRN Mechanical Engineering*, 2012.
- [21] C. K. Chua, K. F. Leong and C. S. Lim, *Rapid prototyping: principles and applications*, World Scientific, 2010.
- [22] Lai, H., & Folch, A. (2010). Design and dynamic characterization of “single-stroke” peristaltic PDMS micropumps. *Lab Chip*, 336-342.
- [23] W.Y. Zhang, G.S. Ferguson, S. Tatic-Lucic. “Elastomer-supported cold welding for room temperature wafer-level bonding.” *MEMS 2004 Technical Digest*, Maastricht, The Netherlands, January 25-29, 2004, 741-744
- [24] M. Kawabe, S. Tasaka, N. Inagaki, “Effects of surface modification by oxygen plasma on peel adhesion of pressure-sensitive adhesive tapes” *J. Appl. Polym. Sci.*, 78, p. 1392, 2000
- [25] H. Makamba, J. H. Kim, K. Lim, N. Park and J. H. Hahn, “Surface modification of poly (dimethylsiloxane) microchannels,” *Electrophoresis*, vol. 24(21), pp. 3607-3619, 2003.
- [26] K. Efimenko, W. E. Wallace and J. Genzer, “Surface modification of Sylgard-184 poly (dimethyl siloxane) networks by ultraviolet and ultraviolet/ozone treatment,” *Journal of Colloid and Interface Science*, vol. 254(2), pp. 306-315, 2002
- [27] S. Hu, X. Ren, M. Bachman, C. E. Sims, G. P. Li and N. L. Allbritton, “Tailoring the surface properties of poly (dimethylsiloxane) microfluidic devices,” *Langmuir*, vol. 20(13), pp. 5569-5574, 2004
- [28] S. Hu, X. Ren, M. Bachman, C. E. Sims, G. P. Li and N. Allbritton, “Surface modification of poly (dimethylsiloxane) microfluidic devices by ultraviolet polymer grafting,” *Analytical chemistry*, vol. 74(16), pp. 4117-4123, 2002.
- [29] R. Mukhopadhyay, “When PDMS isn't the best. What are its weaknesses, and which other polymers can researchers add to their toolboxes?” *Anal Chem.* 2007 May 1; 79(9):3248-53.
- [30] Z. Wu, K. Hjort, “Surface modification of PDMS by gradient-induced migration of embedded Pluronic” *Lab Chip*, 2009,9, 1500-1503